On the Determination of Hydrodynamic Coefficients for Real Time Ship Manoeuvring Simulation

Nicolaas Wilhelmus Teeuwen

Master of Science Thesis

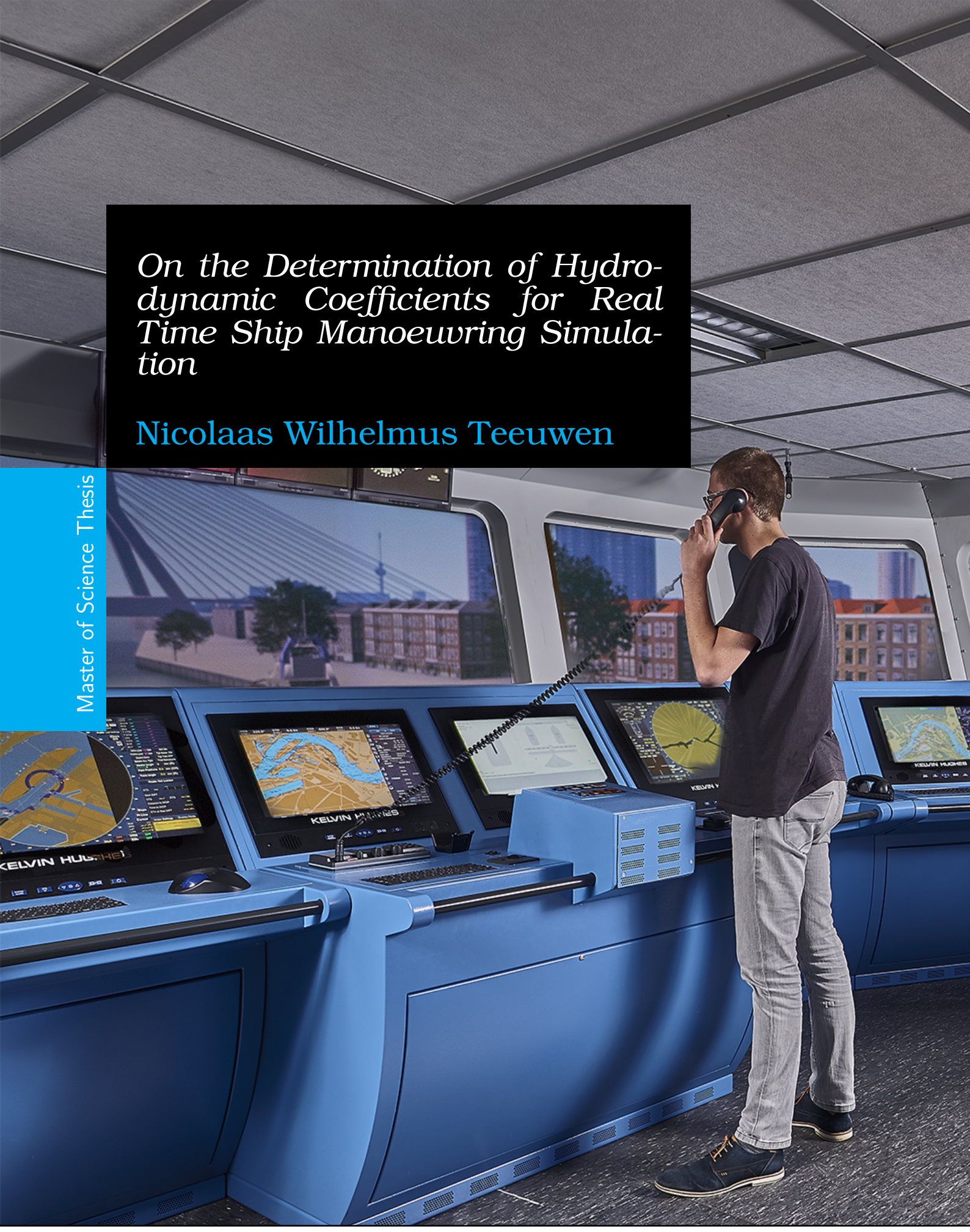

TU Delft Delft University of Technology

Thesis for the degree of MSc in Marine Technology in the specialization of Ship Hydromechanics

On the Determination of Hydrodynamic Coefficients for Real Time Ship Manoeuvring Simulation

By

Nicolaas Wilhelmus Teeuwen

Performed at

STC-Group

&

Faculty of Mechanical, Maritime and Materials Engineering, 3mE
Delft University of Technology
The Netherlands

15th January 2018

Abstract

The STC-group is an educational institution that among other things provides training in the maritime industry at their own simulator park. STC develops the Diomedea simulator in-house and also implements new vessels in the simulator. To speed up the process of implementing the physics of a vessel in the simulator, STC is looking for a different method to find the so-called hydrodynamic coefficients of a vessel. To eventually be able to determine the hydrodynamic coefficients from real ship data a method is developed to find hydrodynamic coefficients from ship manoeuvring data.

Equations of motion in the horizontal plane are used. Assuming that the only forces acting on the vessel are propeller forces, rudder forces and hydrodynamic forces, the hydrodynamic coefficients can be found when the velocities, accelerations, propeller forces and rudder forces are known.

To determine the velocities and accelerations of the vessel from the position data of a simulated track, numerical differentiation is used. The numerical differentiation method used is a form of Richardson extrapolation based on the central difference method. The propeller and rudder forces are estimated using a simple model as described by Yasukawa and Yoshimura [63]. The hydrodynamic forces are modelled after the coefficients derived from low aspect ratio lift theory.

It is shown that using numerical differentiation and Singular Value Decomposition, it is possible to find predefined sets of coefficients that are used to simulate manoeuvres. It is concluded that sets of coefficients can be found for manoeuvres in 1 degree of freedom, but also for manoeuvres with 3 degrees of freedom.

Finally the method is used on manoeuvres generated with the MMG method. It is concluded that the method is able to find coefficient sets based on low aspect ratio lift theory. It is concluded that the sets of coefficients determined using a zig-zag trial can recreate a turning circle and zig-zag trial accurately. Decomposing the hydrodynamic forces in the contributions by every

coefficient shows that some coefficients can not be determined accurately by only looking at straight sailing, turning circle manoeuvres and zig-zag trials. It is shown however that a set of coefficients can be found from position data using singular value decomposition. It is also shown that a set of coefficients based on low aspect ratio lift theory is sufficient for simulating straight sailing, turning circle manoeuvres and zig-zag trials.

Preface

It has been almost a year ago that I first set foot in a ship simulator at STC in Rotterdam. It almost felt like being part of a large video game, although it is used for much more serious purposes of course. Before starting this research project it never occurred to me that ship simulators are also part of maritime technology. This research project gave me the opportunity to learn more about manoeuvring, simulation and mathematical modelling while having a nice view over the river Maas.

I would like to thank Professor Rene Huijsmans and Henk de Koning Gans for their feedback, discussions and their sharing of knowledge about the subjects regarding my research. Secondly I owe a lot to my daily supervisor Wim Sinke from STC, who shared his experience on simulators, gave great feedback and helped me a lot by showing me different points of view on the subject. Next to that I like to thank Myrthe Koning for her helpful feedback on my report at different points in time. Finally I want to thank all the colleagues at STC for the enjoyable time. Special thanks to Erik Hogkamer for letting me use the picture on the cover.

I also need to thank Maarten Klapwijk for the valuable discussions about all kinds of subjects. Finally I want to thank my family, friends and all the people I might have forgotten.

Niek Teeuwen

Delft, October 26, 2017

Contents

List of Tables

List of Figures

Nomenclature

Symbol	Description	Unit
A_L	Lateral projected wind area	m^2
A_R	Profile area of rudder	m^2
A_T	Transverse projected wind area	m^2
B	Beam of the ship	m
C_D	Drag force coefficient	-
C_L	Lift force coefficient	-
C_N	Normal force coefficient	-
C_Q^*	Four quadrant torque coefficient	-
C_T^*	Four quadrant trust coefficient	-
C_T	Tangential force coefficient	-
C_{Xw}, C_{Yw}, C_{Nw}	wind load coefficients	-
D_P	Propeller drag force	N
D_R	Rudder drag force	N
D	Propeller diameter	m
F_N	Rudder normal force	N
I_{zG}	Mass moment of inertia around z-axis	kgm^2
I	Mass moment of inertia	kgm^2
J_P	Advance coefficient	-
J_z	Added mass moment of inertia around z-axis $J_z = -N_{\dot{r}}$	kgm^2
K, M, N	Moments in the ship fixed coordinate system	Nm
K_Q	Torque coefficient	-
K_T	Thrust coefficient	-
L_P	Propeller lift force	N
L_R	Rudder lift force	N
L_{pp}	Length between perpendiculars	m
L	Length of the ship	m
N_w	Steady horizontal wind moment	Nm
P	Propeller pitch	m
Q	Propeller torque	Nm
S	Wet surface of underwater ship	m^2

Symbol	Description	Unit
T_R	Tangential rudder force	N
T	Thrust force	N
U_R	Resultant inflow velocity on rudder	m/s
V_A	Velocity of advance	m/s
V_R	Relative water velocity	m/s
V_S	Ship speed	m/s
V_{rw}	Relative wind velocity	m/s
X, Y, Z	Forces in the ship fixed coordinate system	N
X_w, Y_w	Steady lateral and longitudinal wind forces	N
Δ	Displacement volume moulded	m^3
Λ	Rudder aspect ratio	-
α_P	Angle of attack at propeller blade	rad
α_R	Angle of attack at rudder	rad
α_{rw}	Relative wind direction	rad
β_H	Hydrodynamic pitch angle	rad
β_P	Geometrical inflow angle of the propeller	rad
β	Drift angle	rad
δ	Rudder angle	rad
λ	Aspect Ratio	-
ψ	Heading angle	rad
ρ_{air}	Density of air	kg/m^3
ρ	Density of seawater	kg/m^3
θ_P	Pitch angle of propeller	rad
$'$	Denotes a dimensionless quantity	-
a_H	Rudder force increase factor	-
d	Draught of the ship	m
m_x	Added mass in x-direction $m_x = -X_{\dot{u}}$	kg
m_y	Added mass in y-direction $m_y = -Y_{\dot{v}}$	kg
m	Mass of the ship	kg
n_P	Propeller rpm	s^{-1}
p	Roll velocity	rad/s
q	Pitch velocity	rad/s
r_P	Propeller radius	m
r	Yaw velocity	rad/s
t_P	Thrust deduction factor	-
t_R	Steering resistance deduction factor	-
u_R	Longitudinal component of inflow velocity on rudder	m/s
u	Longitudinal ship velocity	m/s

Symbol	**Description**	**Unit**
v_R	Lateral component of inflow velocity on rudder	m/s
v	Lateral ship velocity	m/s
w_{P0}	Wake fraction when sailing straight	-
w_P	Wake fraction	-
w	Vertical ship velocity	m/s
x, y, z	Ship fixed coordinates	m
x_0, y_0, z_0	Earth fixed coordinates	m
x_G, y_G, z_G	Location of center of gravity in ship fixed coordinate system	m
x_P	Longitudinal coordinate of the propeller position	rad
x_R, y_R, z_R	Location of acting point of rudder force in ship fixed coordinate system	m

Acronyms

ABS	American Bureau of Shipping.
CFD	Computational Fluid Dynamics.
CMT	Circular Motion Test.
DOF	Degrees of Freedom.
ECDIS	Electronic Chart Display and Information System.
FMB	Full Mission Bridge.
FPSO	Floating Production Storage and Offloading unit.
HBO	Hoger Beroepsonderwijs (Higher Professional Education).
IMO	International Maritime Organisation.
KVLCC2	KRISO Very Large Crude Carrier 2.
MARIN	Maritime Research Institute Netherlands.
MBO	Middelbaar Beroepsonderwijs (Senior Secondary Vocational Education).
MMG	Maneuvering Modeling Group.
NACA	National Advisory Committee for Aeronautics.
OTT	Oblique Towing Test.
PMM	Planar Motion Mechanism.
RANS	Reynolds Averaged Navier-Stokes.
RK4	Runge Kutta 4th order.
SMAP	Ship Maneuvering Assessment Program.

STC	Scheepvaart en Transport College.
SVD	Singular Value Decomposition.
SYMS	Soft Yoke Mooring System.
ULCC	Ultra Large Crude Carrier.
VLCC	Very Large Crude Carrier.
VMBO	Voorbereidend Middelbaar Beroepsonderwijs (Preparatory Vocational Education).

Chapter 1

Introduction

In the present day, much training and education on the operation of vehicles relies on the use of simulators. To have a good basis in the operation of a real ship it is necessary to have a realistic and representative simulation.

The STC-group is an educational institution that among other things provides training in the maritime industry at their own simulator park. STC develops the Diomedea simulator in-house and also implements new vessels in the simulator. Although there are some methods known to make a prediction about the manoeuvrability characteristics of a vessel based on generic ship parameters, it can still be very time consuming to get a realistic result.

To speed up the process of implementing the physics of a vessel in the simulator, STC is looking for a different method to find the so-called hydrodynamic coefficients of a vessel. Different methods have been proposed. Measuring manoeuvres aboard the real vessel and using an algorithm to find the coefficients as one of them. A method that finds the hydrodynamic coefficients on the basis of real ship motions was not available however.

In this report, a method is presented to determine the hydrodynamic coefficients for manoeuvring in real-time ship simulators using position data of a manoeuvre of a vessel. In chapter 2 information about the STC-Group is given followed by the problem description. In chapter 3 the objectives, limitations, and research questions for this study will be formulated. Chapter 4 provides an overview of the literature available on the subjects of manoeuvring an regression analysis. In chapter 5 the implementation and verification of the used simulation program is discussed. Chapter 6 describes the development of the method to find the hydrodynamic coefficients. In chapter 7 the verification of the predicion method is described and in chapter 8 the method is validated. The final conclusions and recommendations can be found in chapter 9.

Chapter 2

Problem Description

2.1 The STC-Group

The STC-Group is a worldwide operating educational and research institution for the shipping, logistics, transport and process industries. The STC-Group [52] consists of a private and a public part. The public part of STC-Group offers Voorbereidend Middelbaar Beroepsonderwijs (Preparatory Vocational Education) (VMBO), Middelbaar Beroepsonderwijs (Senior Secondary Vocational Education) (MBO), and Hoger Beroepsonderwijs (Higher Professional Education) (HBO).The private part provides education and training for different maritime related disciplines such as offshore, dredging and shipping. STC-Group has the role of one of the largest contract training institutes of the Netherlands and simulators play a large role in the training and education at STC-Group. The the STC-Group has a variety of training facilities, which consist of a simulator park, numerous training centres and training vessels. The core of the simulator park are the Full Mission Bridge (FMB) Simulators.

2.2 Diomedea simulator

The STC-Group is actively developing the Diomedea Simulator, which is used at several locations on the world. Next to the in-house development of the simulator, the visual databases and physical models are also developed in-house. This offers maximum flexibility to the customers and users of the simulator. The FMB Simulators are used for both training and research. The bridge simulators were for example, used to simulate the coupling of a Floating Production Storage and Offloading unit (FPSO) with a Soft Yoke Mooring System (SYMS) Wang et al. [61]. The simulator consists more or less of the following parts:

- Computers that run the simulation software.

- A replica of a ship's real bridge. To be able to simulate a full mission, the bridge is equipped with all the hardware that can be found on a real bridge such as steering equipment, radars, Electronic Chart Display and Information System (ECDIS), communication etc. In figure 2.1 the inside of a FMB simulator of the STC-Group is shown.
- Projectors or screens that show the simulated world outside of the bridge.
- Simulation software, that contains information about the appearance of the vessels and the environment, so-called visuals, and contains mathematical models to model the behaviour of the vessel, so-called physics.

Figure 2.1: Photograph of the inside of a FMB simulator at STC. Obtained from [26]

.

The physical implementation of the vessel consists of a large amount of coefficients which all represent properties of the vessel. These properties vary from mass of the vessel to the position of the rudder and also the manoeuvrability properties are implemented. The manoeuvrability properties are implemented using so-called hydrodynamic coefficients that represent the forces on the vessel due to the water it is sailing in.

2.3 Determining the hydrodynamic coefficients

Determining the hydrodynamic coefficients starts with a reference model, which is available in the database. In the past the STC-Group used a program, Ship Maneuvering Assessment Program (SMAP), that calculated the hydrodynamic coefficient based on generic ship parameters. As this proved to be less optimal than selecting one of the existing ships which was similar in size, one would often start with an other model as reference. With a working reference model, the data obtained from different sea trials is used to fine tune the model so that the ship is as close as possible to the real ship. The ship model is then tested with the personnel of the real ship that is familiar with the behaviour of the real ship. This often leads to small changes in the hydrodynamic model.

To speed up the process of comparing the model with available sea trials, an optimization algorithm was programmed. This program calculates the manoeuvres as done during trials of a real vessel such as turning circle test, zig-zag test, and acceleration test. The user of the program can specify which coefficient will be iterated and in which interval, in general the first iteration is done in an interval around the initial estimated value of the coefficient. In each iteration the program will calculate the specified manoeuvres and compares them to the trial data of the real vessel. In this way the best value for the coefficient can be found. When this is done the manoeuvring characteristics are tested again in the simulator together with people who have real-life experience on the vessel.
The iteration method still has disadvantages though:

- The trial data of the real vessel has to be available, which is not always the case.
- There could be no optimum in the specified interval. In this case the program returns a value on the boundary of the interval as optimum, so the interval has to be enlarged. When the best value for the coefficient is far away from the initial estimated value this can still be very time consuming.
- There could be more optima in the specified interval. Beforehand it is not known if the specified interval contains multiple optima. This means the program returns an optimum, but there might be a better solution in the same interval.
- Two or more different coefficients could interfere with each other. Every coefficient is an unknown in the same set of equations which means that optimization of a coefficient for the turning circle test for example could make the behaviour of the vessel in a zig-zag test worse.

- When a ship has to be modelled that is not very similar to any of the previously modelled vessels, the initial set of coefficients could be very different from the real values, which means a lot of iterations are needed to find an optimum value.
- From the iteration method it can not be concluded if a coefficient is missing in the simulator. If this is the case the simulator might not be able to simulate some manoeuvres that are requested by the user, while every coefficient is optimised. The iteration method does not show the absence of a coefficient.

The iteration method makes tuning of the coefficients faster because more sets of coefficients can be tested automatically. Improvements can be made however in the determination of the initial set of hydrodynamic coefficients. A new method with a better theoretical background could provide this. In an ideal situation, a set of hydrodynamic coefficients that gives the desired realism can be found directly.

Chapter 3

Study Definition

In this chapter the objectives of the study are defined. When the objectives are clarified the limitations of this study are discussed. Based on the objectives and limitations the research question will be formulated. The research question together with the formulated sub-questions will be the basis for the working plan which is discussed at the end of this chapter.

3.1 Objectives

This study has two main objectives, which are:

- Develop a method to determine the hydrodynamic coefficients which are used in a real-time ship simulator,
- verify and validate the method using synthetic data obtained from existing models.

The first objective is to develop a method for finding the hydrodynamic coefficients of a vessel using a path completed by the vessel and data about the controls of the vessel. Based on earlier work on ship manoeuvrability found in literature a mathematical model will be formed. Propeller forces and rudder forces will be implemented together with derived formulations of the hydrodynamic forces.

The second objective is the verification and validation of method developed, this will be done with generated synthetic data. This data will come from the current manoeuvring models used in the Diomedea Simulators of the STC-Group and an existing validated manoeuvring model. During the literature study, the manoeuvring model which will be used for validation is chosen.

3.2 Limitations

The limitations in this study are:

- Only ships with a conventional single propeller will be considered. This limitation will exclude a lot of vessels from the method. If the method works however, further research can be done to make the method also applicable to vessels with different propulsion.

- Only ships with a single rudder will be considered. The majority of all vessels with a single propeller will also have a single rudder, which makes this a reasonable limitation.

- Only ships which are symmetric in longitudinal direction will be considered. Since the majority of all vessels is symmetric in longitudinal direction this is a reasonable assumption.

- No forces due to wind will be taken into account. The hydrodynamic forces are considered to be much larger than the aerodynamic forces. For ships with a small lateral area above the waterline this assumption is reasonable.

- Only motions in the horizontal plane will be considered, which means only the motions surge, sway and yaw will be considered. In the case where ships make a turn with relatively large speed and relatively small turning radius, the vessel will get a roll angle due to centripetal acceleration. This means there is some coupling between yaw and roll, couplings like this will not be taken into account. For conventional merchant ships this coupling is assumed to be negligible.

- No limitations in the waterway are taken into account. This means canal width and water depth are neglected. When manoeuvring at sea is simulated this should not have a large impact. However, for simulations in smaller ports and inland waterways the influence of the limitations in the waterway could be large.

- No ship-to-ship interactions will be included in the study. When two ships sail close to each other, effects like suction between the vessels or interaction of the wave patterns can influence the manoeuvrability of the vessels. These effects are considered to be small in situations where two ships have about the same size and are not too close to each other. One could imagine situations where a vessel is assisted by a tug and both conditions are not satisfied, these situations will not be predicted accurately.

3.3 Research questions

Based on the objectives of the study a research question is formulated. The main question to be answered in this study is:

"How can a mathematical model, based on regression analysis, be made to derive the hydrodynamic coefficients from a selected path completed by a vessel to improve the accuracy of manoeuvring coefficients in a simulator?"

This question can be divided into sub-questions of which the answers will lay a path to find the answer on the main research question. To begin with, knowledge is needed on the subject of modelling of manoeuvring ships, leading to the question:

"What methods for the prediction and modelling of ship manoeuvring are available and which factors are most important?"

This question will be answered by doing a literature research on ship manoeuvring. The next sub-question relates to the regression analysis that will be used to develop a new method.

"What regression methods are available and which method is suited best for the application in a ship manoeuvring model?"

This question will be answered by doing literature research on regression analysis. After answering the two previous questions it should be possible to make a model which implements the important factors and the regression method found. When this model is completed it has to be tested to find out if the model really works. The question to be answered here is:

"What is the accuracy of a mathematical model based on manoeuvring models and regression analysis to determine the hydrodynamic coefficients?"

This will be tested using synthetic data generated using a simple manoeuvring model and an analytical solution. If this method proves to be accurate coefficient sets can be determined and compared with manoeuvres obtained from literature. The question to be answered here is:

"How do the results of the new method compare to the ship model obtained from literature?"

When this question is answered it should be possible to answer the main research question formulated at the top of this section.

3.4 Working Plan

Based on the research questions formulated a working plan is made, which is discussed in this section.

3.4.1 Literature study on ship manoeuvring

First a literature study on ship manoeuvring is carried out, in order to get a good understanding of the topic, and to get an overview on the different methods available. There is also some research done on the "known" forces that act on the ship such as thrust and rudder forces. The focus in this study will be on the modelling and calculation of hydrodynamic forces. The theoretical physical framework of the new model will be based on this literature study.

3.4.2 Literature study on regression methods

The next part of the study will consist of a literature study on regression analysis. This will be done to get insight in the different methods available and the advantages and disadvantages of each method. Also some insight will be gained in the calculation of errors and uncertainties of different regression methods. Based on this literature study the method most suitable for the application in the ship manoeuvring model will be determined.

3.4.3 Development of a new method

With the theoretical framework of the first literature study and the chosen regression method of the second literature study, a mathematical model will be made to extract the hydrodynamic coefficients from a path and the forces on rudder and propeller of a certain vessel. This part of the study also involves the programming of a manoeuvring prediction method, found during the literature study, which will later be used to generate synthetic data. This manoeuvring model should give a dataset, which at least contains the path of the vessel and information about rudder and propeller forces.

3.4.4 Validation and verification of the new method

When the new method is implemented it can be tested. This will be done with the synthetic data generated by the known manoeuvring model and with the data from the Diomedea Simulators owned by the STC-Group. For the verification of the developed method an existing verified manoeuvring model can be used. By using the predicted path of the manoeuvring model together with propeller and rudder forces as an input the method can be tested. When the method works, the output should be in the proximity of the coefficients predicted by the verified method. This can also say something about the uncertainty of the developed method. The models used by the simulators of STC-Group can also generate data sets, opposed to the most existing manoeuvring models, the simulator can also generate data sets for non-standard manoeuvres. This means that datasets generated by the

simulators can be used to test if the method also works for non-standard manoeuvres.

Chapter 4

Literature study

In this chapter the findings of the literature study are discussed. During the literature study the following subjects have been researched:

- manoeuvrability trials,
- establishing the equations of motions,
- rudder forces,
- propeller forces,
- hydrodynamic forces,
- influence of the environment on manoeuvring,
- regression analysis,
- validation cases.

4.1 Manoeuvrability trials

The manoeuvrability of a vessel is an important characteristic for the safety of ships. Butt et al. [8] found that still a significant part of the shipping accidents consists of collisions and groundings. Some of these incidents could have been avoided if the ship had better manoeuvrability characteristics. Because of the importance of manoeuvrability on the safety of ships the International Maritime Organisation (IMO) defined some standard trial manoeuvres to test if the manoeuvrability of the vessel is sufficient. These tests are:

- turning circle manoeuvre,
- zig-zag test,

- full astern stopping test.

To demonstrate compliance with the standards of IMO these manoeuvres should be carried out during the trials. Because these trials are obligatory for every vessel and have to be done in the same way, the data of these manoeuvres is often used to develop empirical formulations, or to validate manoeuvring models. These manoeuvres are currently also used to validate the model ships that are implemented in the Diomedea simulator.

4.1.1 Turning circle manoeuvre

The turning circle manoeuvre is a test where the ship initially sails a steady straight course, which means the ship does not yaw, at the test speed. IMO [29] defines the test speed as a speed of at least 90% of the ship's speed corresponding to 85% of the maximum engine output. When these conditions are satisfied the helmsman gives 35° rudder angle. This will make the ship turn in a circle as can be seen in figure 4.1.
From the trajectory of the vessel the tactical diameter (TD) and the advance (AD) can be determined. The advance is the distance travelled in the direction of the original course, from the position at which the rudder angle is given to the position where the heading has changed 90° from the original course IMO [29]. The tactical diameter is the distance travelled perpendicular to the original course, from the position the rudder angle is given to the position where the heading has changed 90° from the original course. The advance and tactical diameter are both displayed in figure 4.1.

The turning circle manoeuvre should be done for 35° to port and 35° to starboard because the advance and tactical diameter can be different in these two situations. IMO demands that the advance does not exceed 4.5 ship lengths and that the tactical diameter does not exceed 5 ship lengths.

4.1.2 Zig-zag test

The zig-zag manoeuvre is a test which is used to test the yaw abilities of a vessel. First the vessel has to sail a straight steady course at the test speed. When this is the case a rudder angle is ordered, 10° in case of the 10°/10° zig-zag manoeuvre and 20° in case of the 20°/20° zig-zag manoeuvre. When the heading angle is the same as the rudder angle ordered, the rudder will be ordered the same angle in opposite direction. This will be repeated and result in a winding path of the vessel. The rudder angle and heading angle can be plotted in a diagram as shown in figure 4.2. The overshoot angles as defined by IMO are also displayed.
IMO restricts the size of the overshoot angles, the exact rules are outside the scope of this research, but they can be found in IMO [29].

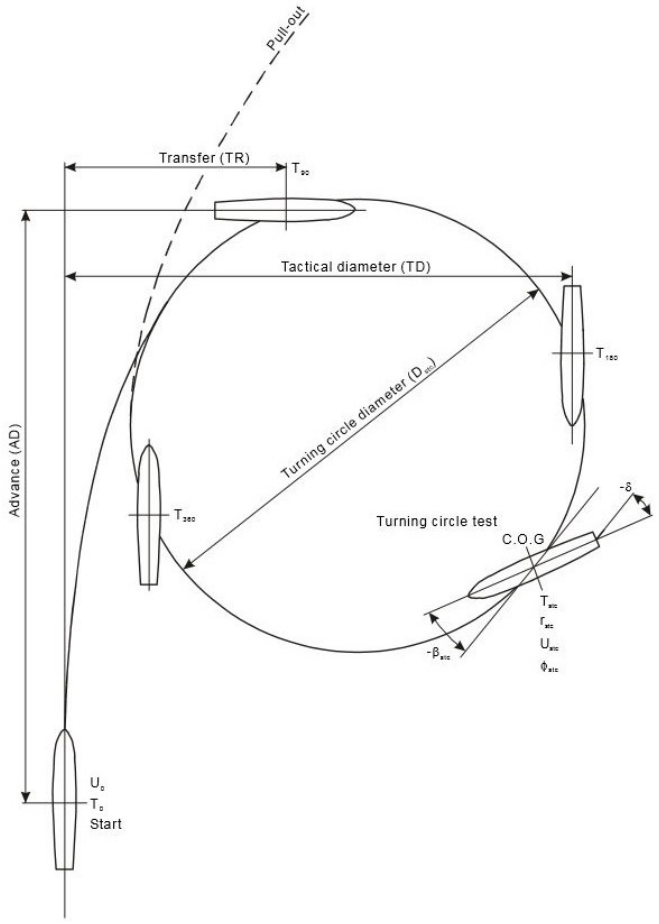

Figure 4.1: Schematic drawing of the turning circle manoeuvre and the distances used to determine manoeuvrability as defined by IMO. Obtained from Quadvlieg and van Coevorden [48].

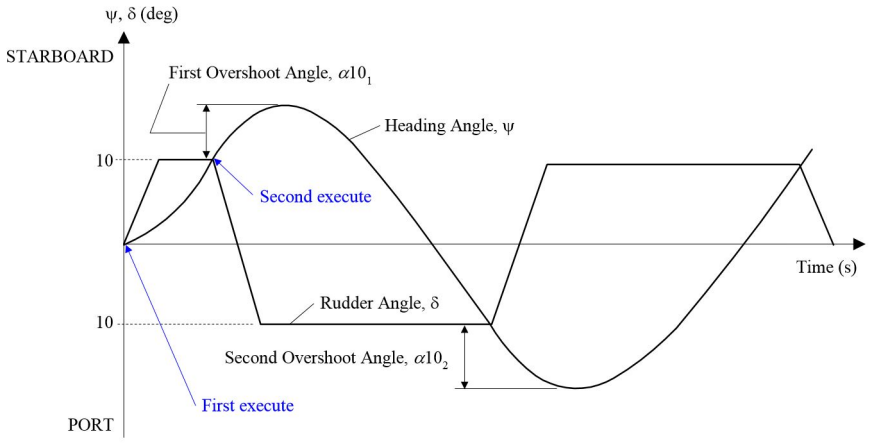

Figure 4.2: Plot of rudder and heading angle during zig-zag manoeuvre. Obtained from American Bureau of Shipping [3].

4.1.3 Full astern stopping test

The full astern stopping test is done to determine the stopping ability of the vessel. Here the vessel sails a steady straight course at the test speed and then orders full astern. This will make the ship stop, and also turn because of propeller effects. The ship will follow a path as sketched in figure 4.3. The path length of the vessel is called the track reach IMO [29]. The track reach is a measure of stopping ability. IMO specifies that the track reach should not exceed 15 ship lengths.

4.2 Equations of Motions

Almost every manoeuvrability model is based on the equations of motion as first derived by Euler [18], which are based on Newton's laws. In this section the equations of motion will be derived also using Newton's laws, but first the used coordinate systems will be defined.

4.2.1 Defining the Coordinate system

It is very convenient to define the velocities of a ship in a ship fixed coordinate system. In general a Cartesian coordinate system is used of which the origin is placed at the half length of the ship and half the beam of the vessel. The height of the coordinate system is in the vertical position of the center of gravity of the vessel. The x-axis is defined along the ship length with positive value towards the bow. The y-axis is defined perpendicular to the x-axis in the horizontal plane, with positive values towards starboard. The z-axis is defined perpendicular to the horizontal plane, pointing downwards

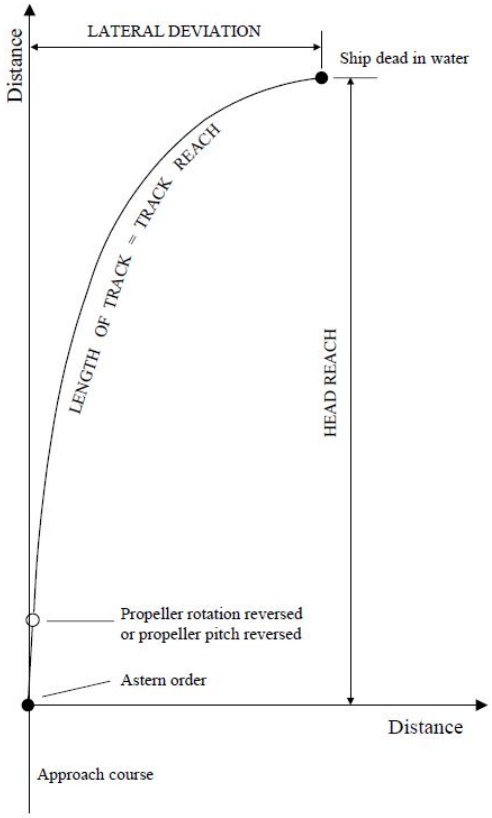

Figure 4.3: Schematic drawing of a full astern stopping test. Obtained from American Bureau of Shipping [3].

into the water. The coordinates x_0, y_0 and z_0 define the earth fixed coordinate system and the coordinates y, x and z define the ship fixed coordinate system Pinkster [46]. The earth fixed reference frame is assumed to be an inertial reference frame. A drawing of the coordinate system can be found in figure 4.4.
At first the choice of the coordinate system seems odd, because the y_0-axis points in the opposite direction of what is most commonly used, because the z_0-axis is chosen to point downwards into the water it is a right-handed coordinates system though. The reason for the choice of this coordinate system is purely historical, because the x_0, y_0, z_0 coordinate system now corresponds to the geological north-east-down coordinates system, which is used in navigation. This is convenient because heading and ship position as used during navigation can be converted to the coordinate system of the model without changes of sign.

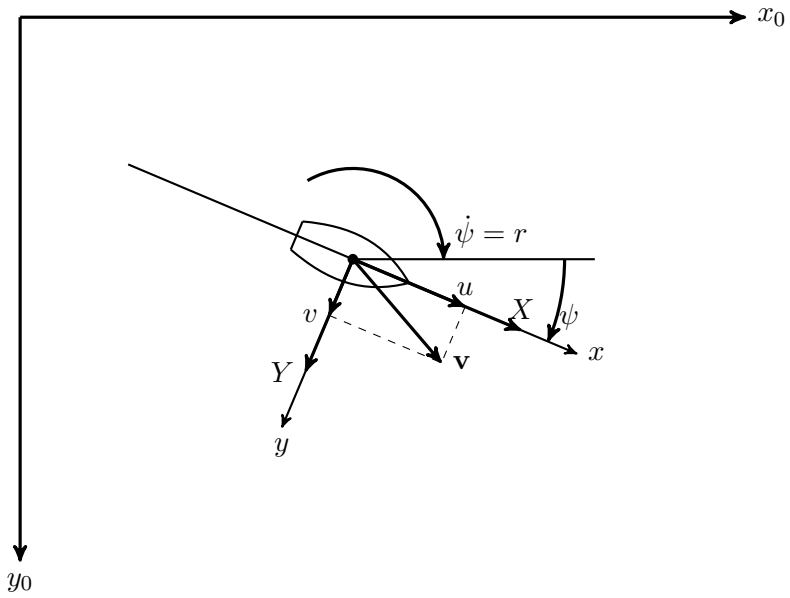

Figure 4.4: Definition of coordinate systems used. x_0,y_0 and z_0 are used to denote the earth fixed coordinate system, whereas x,y and z are used to denote the ship fixed coordinate system.

4.2.2 Inertia

The equations of motions are based on newton's second law and angular momentum. These laws result in the following equations

$$X = m(\dot{u} - vr) \tag{4.1}$$

$$Y = m(\dot{v} + ur) \tag{4.2}$$

$$N = I_z \dot{r}. \tag{4.3}$$

The additional terms $-vr$ and ur arise from the laws, because the velocities u, v and r are defined in the ship fixed coordinate system. The derivations of equations 4.1, 4.2 and 4.3 can be found in appendix C.

4.2.3 Rudder forces

Most ships make use of one or more rudders to steer, although more and more ships are equipped with azimuthing thrusters. The rudder has two functionalities, steering of the vessel and improving course-keeping stability. When the rudder stays in the middle of the ship the cours-keeping stability is improved, which is the same effect as the stabilizing effect of flights on a dart. When the rudder is placed under an angle the rudder causes the ship to turn [15], which is used to control the direction in which the ship is moving. Davidson and Schiff [15] investigated the influence of the propeller, rudder and fins on the course-keeping stability of a vessel. They also give a few analytic solutions to the linearised equations of motion and some criteria for the validity of these solutions. A rudder is a foil which is in general mounted at the stern of the vessel. A schematic picture of a foil with the forces exerted on it is presented in 4.5. The forces on a foil can be expressed

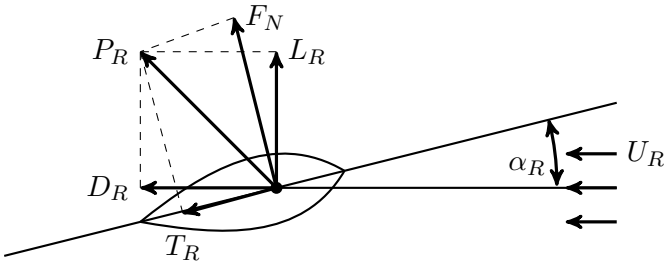

Figure 4.5: Schematic drawing of the forces acting on a rudder. The total force P_R on the rudder in a flow with velocity U_R is drawn, together with two different ways of decomposing P_R.

as

$$F_N = \frac{1}{2}\rho U_R^2 C_N A_R. \tag{4.4}$$

$$T_R = \frac{1}{2}\rho U_R^2 C_T A_R. \tag{4.5}$$

$$L_R = \frac{1}{2}\rho U_R^2 C_L A_R. \tag{4.6}$$

$$D_R = \frac{1}{2}\rho U_R^2 C_D A_R. \tag{4.7}$$

In general the lift and drag generated by a foil are of high interests. In the research on manoeuvring some methods use the normal force on the rudder

instead of the lift. These forces though all are strongly related to the angle of attack. According to Yasukawa and Yoshimura [63] the angle of attack of the rudder can be expressed as

$$\alpha_R = \delta - \tan^{-1}\left(\frac{v_R}{u_R}\right). \tag{4.8}$$

Lewandowski [38] directly relates the lift and drag forces to the rudder angle for a as

$$L_R = \frac{1}{2}\rho U_R^2 A_R \Lambda \delta \tag{4.9}$$

$$D_R = \frac{1}{2}\rho U_R^2 A_R \frac{\Lambda 2\delta^2}{\pi a_e}. \tag{4.10}$$

Where Λ is the lift curve slope and a_e is the effective aspect ratio of the rudder. According to Lewandowski [38], the rudder forces are in the standard coordinate system equal to

$$X_R = -D_R \tag{4.11}$$

$$Y_R = L_R \tag{4.12}$$

$$K_R = -L_R z_R \tag{4.13}$$

$$N = L_R x_R + D_R y_R. \tag{4.14}$$

where x_R , y_R and z_R is the location where the rudder forces act. In the case where one rudder is considered in the middle behind the propeller, y_R becomes 0. In general half of the length between perpendiculars is a good estimation for the longitudinal position of the rudder.
The normal force coefficent depends on the angle of attack α. Fuji and Tuda [19] found the following relation between angle of attack and normal force coefficient, which also depends on the aspect ratio of the rudder.

$$C_N = \frac{6.12\lambda}{\lambda + 2.25}\sin\alpha_R \tag{4.15}$$

Liu et al. [39] looked at this empirical formula using 2D Reynolds Averaged Navier-Stokes (RANS) simulations of different symmetric National Advisory Committee for Aeronautics (NACA) profiles and found that their results where quite close to the results of the empirical formula.
Shiba [51] already investigated the influence of rudder area on the manoeuvrability of ships. He also did some research on the influence of the propeller on the rudder forces and found that the normal force coefficient of the rudder reduces when the slip on the propeller increases.
Badoe et al. [4] researched the influence of the drift angle on the interaction between rudder hull and propeller. Badoe et al. [4] conclude that the drift angle influences the place where the lift force acts on the rudder. This shift is small compared to the ship length though.

4.2.4 Propeller forces

The propeller provides a thrust force which makes the ship move. The thrust force is generated by the blades of the propeller by generating a lift force. A schematic of a blade section with the velocities, forces and angles is shown in figure 4.6. The lift generated by the propeller blade depends on the angle

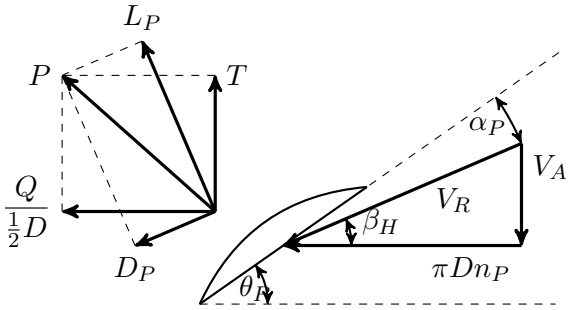

Figure 4.6: Velocities and forces on a section of a propeller blade. The total force P on the propeller blade section is drawn, together with two different ways of decomposing P.

of attack. As can be seen in figure 4.6 the angle of attack depends on the pitch angle θ_P and the hydrodynamic pitch angle β_H. When the propeller RPM is increased while the inflow velocity V_A remains constant, the angle of attack α_P increases, this results in an increase in lift, and therefore an increase in thrust. Notice that the lift is defined perpendicular to the flow along the blade. This means also the direction of the lift changes, when propeller RPM is increased. The thrust force can be made dimensionless in the following way

$$K_T = \frac{T}{\rho n_P^2 D^4}. \tag{4.16}$$

And the torque needed to drive the propeller can be made dimensionless as well

$$K_Q = \frac{Q}{\rho n_P^2 D^5}. \tag{4.17}$$

This means the thrust force can be written as

$$T = \rho n_P^2 D^4 K_T. \tag{4.18}$$

K_T depends on the advance coefficient J_P.

$$J_P = \frac{V_A}{n_P D} \tag{4.19}$$

Note that the advance coefficient differs from the tangent of V_R by a factor π. Because the inflow velocity of the propeller is not equal to the ship speed,

the wake fraction w_P is introduced, when the ship is sailing straight the wake fraction is denoted as w_{P0}. The wake fraction is defined as

$$w_P = \frac{V_S - V_a}{V_S}. \tag{4.20}$$

Now the advance coefficient can be expressed in the longitudinal ship velocity

$$J = \frac{V_S(1-w_P)}{n_P D} = \frac{u(1-w_P)}{n_P D}. \tag{4.21}$$

Yasukawa and Yoshimura [63] use a second order polynomial to approximate K_T

$$K_T(J) = k_2 J_P^2 + k_1 J_P + k_0. \tag{4.22}$$

Model tests are used to determine k_2,k_1 and k_0. More extensive tests were done by the Maritime Research Institute Netherlands (MARIN) with the Wageningen B-series propellers. MARIN used a systematic variation of number of blades, blade area ratio and pitch to find the influence on the thrust coefficient, torque coefficient and efficiency van Lammeren et al. [59]. They found the thrust coefficient could be approximated very well by

$$\begin{aligned} K_T =& A_{0,0} + A_{0,1}J_P + A_{0,2}J_P^2 + A_{0,3}J_P^3 + A_{1,0}\frac{P}{D} + A_{1,1}\frac{P}{D}J_P^3 \\ &+ A_{2,1}\left(\frac{P}{D}\right)^2 J_P + A_{6,0}\left(\frac{P}{D}\right)^6 + A_{6,1}\left(\frac{P}{D}\right)^6 J_P \end{aligned} \tag{4.23}$$

where $\frac{P}{D}$ is the pitch of the propeller. Barnitsas et al. [5] described the relations between K_T, K_Q and the advance ratios of the Wageningen B propeller series as polynomials. Barnitsas et al. [5] defined these polynomials as

$$K_T = \sum_{s,t,u,v} C^T_{s,t,u,v} J^s \left(\frac{P}{D}\right)^t \left(\frac{A_E}{A_0}\right)^u Z^v \tag{4.24}$$

and

$$K_Q = \sum_{s,t,u,v} C^Q_{s,t,u,v} J^s \left(\frac{P}{D}\right)^t \left(\frac{A_E}{A_0}\right)^u Z^v. \tag{4.25}$$

The values for c,s,t,u and v can be found in tables G.1 and G.2 in appendix G. The polynomials for the Wageningen B propeller series are only valid if the ship is moving forward and the propeller is generating a thrust force that pushes the ship forward. During manoeuvring it can also happen that the thrust and longitudinal velocity are not both the same direction. From figure 4.6 it can be seen that this influences the angle β_H. When this angle β_H is varied over a whole circle, a so-called four-quadrant measurement can be made, as is done by MARIN. In these tests van Lammeren et al. [59] used non dimensional thrust and torque coefficients

$$C_T^* = \frac{T}{\frac{1}{2}\rho\left(V_A^2 + (0.7\pi n_P D)^2\right)\frac{\pi}{4}D^2} \tag{4.26}$$

$$C_Q^* = \frac{Q}{\frac{1}{2}\rho\left(V_A^2 + (0.7\pi n_P D)^2\right)\frac{\pi}{4}D^3} \tag{4.27}$$

Fourier analysis was used to find an expression of C_T^* and C_Q^* as a function of hydrodynamic pitch angel β_H. van Lammeren et al. [59] have found that a fourier series of 20 terms already approximates the measured results very well.

So far only methods for ships sailing forwards are considered, turning of the vessel however influences the inflow velocity of the propeller. One of the differences on the thrust generation between manoeuvring and sailing straight is the occurrence of the flow straightening effect. When the ship is sailing under a drift angle, the flow into the propeller is oblique to centreline of the ship, and therefore has a different angle to the propeller shaft. The propeller itself pushes the flow in axial direction, which results in a difference between inflow angle and outflow angle. The definitions of the different quantities involved are shown in figure 4.7. This difference in angle influences

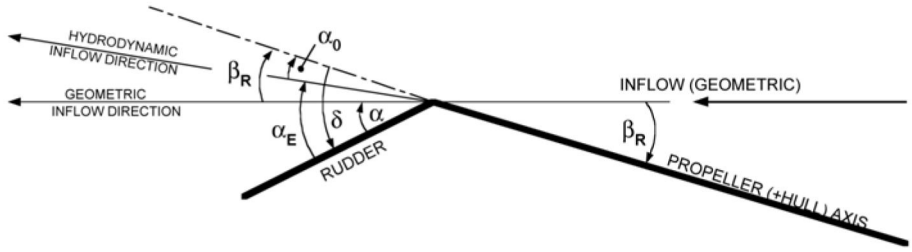

Figure 4.7: Schematic of the quantities involved in the flow straightening effect. Obtained from Molland and Turnock [41].

the direction of thrust and the amount of thrust generated. This means a lateral component of the thrust force develops and also that the inflow angle at the rudder is different. The difference in inflow at the rudder is considered to be more important though.

The difference in magnitude of the thrust force is taken into account by the change in wake of the hull. A few wake corrections are found in literature. Inoue et al. [30] use

$$w_P = w_{P0}e^{-4\beta_P^2} \tag{4.28}$$

where β_P is the geometrical inflow angle to the propeller, defined as

$$\beta_P = \beta - x'_P r'. \tag{4.29}$$

This method was based on model tests, that where carried out to investigate the flow straightening effect of propellers in oblique flows. Kose et al. [35]

use

$$(1 - w_P)/(1 - w_{P0}) = 1 + C_1(\beta_P + C_2\beta_P|\beta_P|)^2. \tag{4.30}$$

Where C_1 and C_2 are coefficients that have to be determined using regression, the physical meaning of C_1 and C_2 is not clear [63]. Yasukawa and Yoshimura [63] came up with the following expression

$$(1 - w_P)/(1 - w_{P0}) = 1 + (1 - \exp(-C_1|\beta_P|))(C_2 - 1). \tag{4.31}$$

4.2.5 Hydrodynamic forces

For the calculation of the hydrodynamic forces, there are two different methods that are commonly used, the approximation of the forces by a Taylor series and the approximation of the forces by considering the ship as a body that generates lift. In this section these two approaches are explained.

Taylor series

To model the hydrodynamic forces, some methods such as the method of Abkowitz [1] use a Taylor series expansion. A Taylor series expansion of a function that depends on only one function can be expressed as

$$f(x) = f(0) + \frac{\mathrm{d}}{\mathrm{d}x}f(0)x + \frac{1}{2!}\frac{\mathrm{d}^2}{\mathrm{d}x^2}f(0)x^2 + \frac{1}{3!}\frac{\mathrm{d}}{\mathrm{d}x}f(0)x^3 + \cdots \tag{4.32}$$

Stewart [53]. The more terms from the Taylor polynomial are taken into account the closer the polynomial approximates the original function around the point where the function is approximated. Care must be taken, because more terms can lead to a worse approximation further away from the point where the function is evaluated. The hydrodynamic forces are a function of velocities u and v, angular velocity r, accelerations $\dot{u}$ and $\dot{v}$, angular acceleration $\dot{r}$ and rudder angle δ when planar motion is considered. Assuming that the forces are continuously differentiable, and is infinitely differentiable, a Taylor series expansion for multiple variables can be used to approximate the forces around the initial value.

Because of symmetry some terms can be set equal to zero. This is shown for the longitudinal force when a Taylor series up to second order is chosen. When the hydrodynamic force X is approximated by a Taylor series up to the second order terms this results in equation 4.33. Because of port/starboard symmetry the center of gravity is located at $y = 0$ and the fluid force X will

not be depending on $\dot{r}$.

$$\begin{aligned} X(u,\dot{u},v,r,\delta) = {} & X_e + X_u u + X_{\dot{u}}\dot{u} + X_r r + X_\delta \delta + X_v v \\ & + X_{uu}u^2 + X_{uv}uv + X_{ur}ur + X_{u\delta}u\delta + X_{u\dot{u}}u\dot{u} \\ & + X_{\dot{u}\dot{u}}\dot{u}^2 + X_{\dot{u}u}\dot{u}u + X_{\dot{u}v}\dot{u}v + X_{\dot{u}r}\dot{u}r + X_{\dot{u}\delta}\dot{u}\delta \\ & + X_{vv}v^2 + X_{vu}vu + X_{v\dot{u}}v\dot{u} + X_{vr}vr + X_{v\delta}v\delta \\ & + X_{rr}r^2 + X_{ru}ru + X_{r\dot{u}}r\dot{u} + X_{rv}rv + X_{r\delta}r\delta \\ & + X_{\delta\delta}\delta^2 + X_{\delta u}\delta u + X_{\delta\dot{u}}\delta\dot{u} + X_{\delta v}\delta v + X_{\delta r}\delta r \end{aligned} \tag{4.33}$$

Because of three assumptions this expression can be simplified.

1. The first assumption, based on Newton's second law, is that the force is linear with acceleration. This means the second order acceleration term (coloured brown) is zero.

2. The second assumption is that there is no coupling between velocities and accelerations. So all the terms that invoke an acceleration and velocity term (coloured red) are zero.

3. The third assumption is that the ship has port-starboard symmetry. This leads to three conditions:

   (a) X is a symmetric function of v when $r = 0$ and $\delta = 0$. This implies $X_v = 0$; $X_{vu} = 0$ and $X_{uv} = 0$.

   (b) X is a symmetric function of r when $v = 0$ and $\delta = 0$. This implies $X_r = 0$; $X_{ru} = 0$ and $X_{ur} = 0$.

   (c) X is a symmetric function of δ when $v = 0$ and $r = 0$. This implies $X_\delta = 0$; $X_{\delta u} = 0$ and $X_{u\delta} = 0$.

   These terms are all coloured blue

This means 4.33 simplifies to

$$\begin{aligned} X(u,\dot{u},v,r,\delta) = {} & X_e + X_u u + X_{\dot{u}}\dot{u} + X_{uu}u^2 + X_{vv}v^2 \\ & + X_{vr}vr + X_{v\delta}v\delta + X_{rr}r^2 + X_{rv}rv + X_{r\delta}r\delta \\ & + X_{\delta\delta}\delta^2 + X_{\delta v}\delta v + X_{\delta r}\delta r \end{aligned} \tag{4.34}$$

The derivation for the force in lateral direction and the moment around the z-axis is derived in appendix B.

According to Triantafyllou and Hover [58] the Taylor series expansions for the hydrodynamic forces and moments up to third order terms become after

simplification

$$\begin{aligned} X = {} & X_e + X_{\dot{u}}\dot{u} + X_u u + X_{uu}u^2 + X_{uuu}u^3 + X_{vv}v^2 \\ & + X_{rr}r^2 + X_{\delta\delta}\delta^2 + X_{rv}rv + X_{r\delta}r\delta + X_{v\delta}v\delta \\ & + X_{vvu}v^2u + X_{rru}r^2u + X_{\delta\delta u}\delta^2 u + X_{r\delta u}r\delta u \\ & + X_{rvu}rvu + X_{v\delta u}v\delta u + X_{rv\delta}rv\delta \end{aligned} \tag{4.35}$$

$$\begin{aligned} Y = {} & Y_e + Y_u u + Y_{uu}u^2 + Y_{\dot{v}}\dot{v} + Y_{\dot{r}}\dot{r} + Y_v v + Y_r r \\ & + Y_\delta \delta + Y_{\delta u}\delta u + Y_{vu}vu + Y_{ru}ru + Y_{vuu}vu^2 \\ & + Y_{ruu}ru^2 + Y_{\delta uu}\delta u^2 + Y_{vvv}v^3 + Y_{rrr}r^3 + Y_{\delta\delta\delta}\delta^3 \\ & + Y_{rr\delta}r^2\delta + Y_{rrv}r^2v + Y_{vvr}v^2r + Y_{vv\delta}v^2\delta + Y_{vrd}vrd \\ & + Y_{\delta\delta r}\delta^2 r + Y_{\delta\delta v}\delta^2 v \end{aligned} \tag{4.36}$$

$$\begin{aligned} N = {} & N_e + N_u u + N_{uu}u^2 + N_{\dot{v}}\dot{v} + N_{\dot{r}}\dot{r} + N_v v + N_r r \\ & + N_\delta \delta + N_{\delta u}\delta u + N_{vu}vu + N_{ru}ru + N_{vuu}vu^2 \\ & + N_{ruu}ru^2 + N_{\delta uu}\delta u^2 + N_{vvv}v^3 + N_{rrr}r^3 + N_{\delta\delta\delta}\delta^3 \\ & + N_{rr\delta}r^2\delta + N_{rrv}r^2v + N_{vvr}v^2r + N_{vv\delta}v^2\delta + N_{vrd}vrd \\ & + N_{\delta\delta r}\delta^2 r + N_{\delta\delta v}\delta^2 v \end{aligned} \tag{4.37}$$

Although the quadratic terms in the Taylor series of the Y force become zero due to the symmetry of the vessel it is often argued that many of the non-linear forces and moments arise from a transverse drag force on the body and should be proportional to the square of the velocity Lewandowski [38]. This is why some methods include "square absolute" terms such as

$$Y_{|v|v} \tag{4.38}$$

to have an anti-symmetric term that depends on the square of the velocity. Hence $v|v|$ has the same magnitude as v^2 but the same sign as v. Note that terms like these can never arise from a Taylor series expansion because the absolute value function violates the condition that the function must be infinitely differentiable to apply a Taylor series expansion.Gertler and Hagen [22] implement 15 of these "square absolute" terms in their 6 equations of motions for submarine simulation which can be found in appendix C. Chislett and Strom-Tejsen [10] found that the port starboard symmetry in v was a good fit to the experimental data. He also found that a good representation of rudder forces and moments could be possible without even terms in δ. Inoue et al. [31] find that the approximation using up to third order terms is sufficiently accurate to analyse the ships manoeuvrability.

Low-aspect-ratio lift theory

Toxopeus [56] states that the forces and moments can be split up in a linear part and a non-linear part. The linear hull forces can be derived using slender body lift, the non-linear contributions then can be estimated using the cross-flow drag theory. Ross et al. [50] models the lift coefficient as proportional to the sine of the drift angle

$$C_L = C_{L\beta} \sin \beta. \tag{4.39}$$

He then treats the lift force as a function of longitudinal position, by expressing the sine of the drift angle as a ratio in velocities

$$C_L(x) = C_{L\beta} \frac{v + xr}{U(x)}. \tag{4.40}$$

Where $U(x) = \sqrt{u^2 + (v + xr)^2}$ By decomposing the lift force using the drift angle,Ross et al. [50] find the longitudinal force

$$X_L(x) = \frac{1}{2} \rho S C_{L\beta} (v + xr)^2. \tag{4.41}$$

By integrating over the length and taking together all the constants into hydrodynamic coefficients Ross et al. [50] find

$$X_L = X_{vv} v^2 + X_{rv} rv + X_{rr} r^2. \tag{4.42}$$

In a similar way the expression for the lateral force is found

$$Y_L = Y_{uv} uv + Y_{ur} ur. \tag{4.43}$$

Using the following expression for the drag coefficient Ross et al. [50]

$$C_D(x) = C_{D0} + C_{DU} U(x) + C_{D\beta\beta} \sin^2(\beta(x)) \tag{4.44}$$

find the total forces and moments

$$\begin{aligned} X_{LD} = {} & X_{uu} u^2 + X_{uuu} u^3 + X_{vv} v^2 + X_{rr} r^2 + X_{vr} vr + X_{uvv} uv^2 \\ & + X_{rvu} rvu + X_{urr} ur^2 \end{aligned} \tag{4.45}$$

$$\begin{aligned} Y_{LD} = {} & Y_{uv} uv + Y_{ur} ur + Y_{uur} u^2 r + Y_{uuv} u^2 v + Y_{vvv} v^3 + Y_{rrr} r^3 \\ & + Y_{rrv} r^2 v + Y_{vvr} v^2 r \end{aligned} \tag{4.46}$$

$$\begin{aligned} N_{LD} = Y_{LD} x_{cp} = {} & N_{uv} uv + N_{ur} ur + N_{uur} u^2 r + N_{uuv} u^2 v + N_{vvv} v^3 \\ & + N_{rrr} r^3 + N_{rrv} r^2 v + N_{vvr} v^2 r \end{aligned} \tag{4.47}$$

The non-linear lift can be used to derive the induced drag on the vessel. Norrbin [43] shows that the non-linear lateral force is approximately equal to

$$Y_{cf} = Y_{|v|v} |v| v + Y_{|r|v} |r| v + Y_{|v|r} |v| r + Y_{|r|r} |r| r \tag{4.48}$$

$$N_{cf} = N_{|v|v}|v|v + N_{|r|v}|r|v + N_{|v|r}|v|r + N_{|r|r}|r|r. \tag{4.49}$$

By experiments the lift coefficient and cross-flow drag coefficients can be determined, which provides an expression for the lateral force. Hooft [28] states that it is possible to predict the cross-flow drag coefficient for every drift angle when only the drag coefficient at $\beta = 90°$ is known.

4.3 Determining the hydrodynamic coefficients

In the previous section are two different methods explained to express the hydrodynamic forces as a sum of terms, all these terms are depending on their own hydrodynamic coefficient. In this section will be explained what different methods have been developed to determine these hydrodynamic coefficients.

4.3.1 Trial Data

Nomoto [42] uses a set of linear equations of motion and derives some methods to estimate the manoeuvring indices K and T from full-scale zig-zag data as proposed by Kempf [34]. Here K and T are coefficients that arise from the linear equations of motion.Journeé [32] has developed a method based on Nomoto's work to make the difference between calculated and measured data for yaw period and overshoot as small as possible.

4.3.2 Model tests

To find the hydrodynamic coefficients, often model tests are carried out. In Japan Ogawa et al. [44] developed the Maneuvering Modeling Group (MMG) standard method. This method uses a Taylor expansion up to the fourth order terms to approximate the hydrodynamic forces. Model tests are used to determine the unknown forces. Oblique Towing Test (OTT) and Circular Motion Test (CMT) are used to determine the hydrodynamic coefficients. Rudder force tests under different propeller loads, rudder force test in oblique towing and rudder force test in steady turning conditions are conducted to determine rudder forces. With this information the behaviour of the full-scale vessel can be predicted.

Panel H-10 of the Society of Navel Architects and Marine Engineers [45] uses a linear model and gives empirical formulas to estimate the hydrodynamic derivatives for a typical Very Large Crude Carrier (VLCC) and Ultra Large Crude Carrier (ULCC). The empirical formulations are based on typical dimensions of the vessel and are expressed in their non-dimensional form as

$$Y'_{\dot{v}} = -\pi \left(\frac{d}{L}\right)^2 \left(1.0 + 0.16 C_b \frac{B}{d} - 5.1 \left(\frac{B}{L}\right)^2\right) \tag{4.50}$$

$$Y'_{\dot{r}} = -\pi \left(\frac{d}{L}\right)^2 \left(0.67\frac{B}{L} - 0.33\left(\frac{B}{d}\right)^2\right) \tag{4.51}$$

$$N'_{\dot{v}} = -\pi \left(\frac{d}{L}\right)^2 \left(1.1\frac{B}{L} - 0.41\frac{B}{d}\right) \tag{4.52}$$

$$N'_{\dot{r}} = -\pi \left(\frac{d}{L}\right)^2 \left(\frac{1}{12} + 0.17C_b\frac{B}{d} - 0.33\frac{B}{L}\right) \tag{4.53}$$

$$Y'_v = -\pi \left(1.0 + 0.40C_b\frac{B}{d}\right) \tag{4.54}$$

$$Y'_r = -\pi \left(\frac{d}{L}\right)^2 \left(-0.5 + 2.2\frac{B}{L} - 0.08\frac{B}{d}\right) \tag{4.55}$$

$$N'_v = -\pi \left(\frac{d}{L}\right)^2 \left(0.5 + 2.40\frac{d}{L}\right) \tag{4.56}$$

$$N'_r = -\pi \left(\frac{d}{L}\right)^2 \left(0.25 + 0.039\frac{B}{d} - 0.56\frac{B}{L}\right). \tag{4.57}$$

Inoue et al. [31] have expanded this method by formulating empirical formulas to correct for a difference in trim of the vessel. Although the empirical formulas work, one must be cautious because the method is only tested for VLCC's and ULCC's.

4.3.3 Computational Fluid Dynamics

Instead of using regression to find the coefficients from experimental data, the hydrodynamic forces can also be calculated using Computational Fluid Dynamics (CFD). Fureby et al. [20] calculated the hydrodynamic forces of the KRISO Very Large Crude Carrier 2 (KVLCC2) for a drift angle of 0° , 12° and 30° . Disadvantage of this method is that it takes a large amount of computational time to calculate the forces in one situation, let alone, calculate the forces for a large series of drift angles. According to Toxopeus and Lee [55] the predictions using CFD were pretty disappointing when compared to model tests.

4.4 Regression methods

When the equations of motions are known, position and velocity data of a vessel at different points in time during a manoeuvre can be used to estimate the hydrodynamic coefficients of the vessel using a regression method. Multiple methods are available to carry out a regression analysis, part of them are discussed here.

Because the equation is linear in all of the coefficients, the system of equations can be written in the form

$$A\mathbf{x} = \mathbf{b}. \tag{4.58}$$

Here $\mathbf{x}$ is the vector with coefficients, A is a matrix with all the velocities and accelerations that the hydrodynamic forces depend on, and $\mathbf{b}$ is a vector with "known" forces. It is expected that this linear system of equations which has to be solved to find the coefficients, can not be solved directly. This is very likely since errors will occur in the measurements of the path, rudder angle and rpm of the propeller. Therefore a regression method will be used to find the coefficients that are closest to the solution. The regression methods that are discussed in this section are

- least square method,
- singular value decomposition,
- ridge regression.

4.4.1 Least squares method

The least square method minimises the sum of the squares of the residuals. The residuals are the distances between the observed values and the regression line. When a function $f(x, \boldsymbol{\beta})$, where $\boldsymbol{\beta}$ is a vector with the adjustable variables , has to be fitted on a set of data points (x_i, y_i) the residual can be defined as

$$r_i = y_i - f(x_i, \boldsymbol{\beta}). \tag{4.59}$$

The least square method then minimizes the sum of the squares of these residuals

$$S = \sum_{i=1}^{n} r_i^2 = \sum_{i=1}^{n} (y_i - f(x_i, \boldsymbol{\beta}))^2. \tag{4.60}$$

When a linear model function is chosen this can be written as [16]

$$S = \sum_{i=1}^{n} |y_i - \sum_{j=1}^{n} x_{ij}\hat{\beta}_j|^2 = ||\mathbf{y} - X\boldsymbol{\beta}||^2. \tag{4.61}$$

Minimizing S is the same as solving the normal equation

$$(X^T X)\hat{\boldsymbol{\beta}} = X^T \mathbf{y} \tag{4.62}$$

in the case of linear function $f(x, \boldsymbol{\beta})$. For the equation

$$A\mathbf{x} = \mathbf{b} \tag{4.63}$$

the least squares solution is given by Lay [36]

$$\hat{\mathbf{x}} = (A^T A)^{-1} A^T \mathbf{b}. \tag{4.64}$$

The type of least squares method that is applied depends on the model function $f(x, \boldsymbol{\beta})$, when the model function is linear, for example, the linear least squares method is applied. In the Taylor series expansion all the coefficients could be considered as adjustable variables. For the hydrodynamic forces the adjustable coefficients always occur as linear, so a linear least squares method can be applied. This has the advantage that the linear least square method has just one unique solution, while the non-linear least squares method has multiple solutions. In the case of the example, only one independent variable x is considered. When this method has to be applied on the hydrodynamic forces, more independent variables have to be taken into account.

4.4.2 Singular value decomposition

The problem of solving the linear least squares problem is the same as finding the pseudo inverse of the matrix A and multiplying it with $\mathbf{b}$.

$$A^+ = (A^T A)^{-1} A^T. \tag{4.65}$$

One way to do this is by finding the singular value decomposition of A. The singular value decomposition, is a method where the matrix is decomposed in three different matrices

$$A = U \Sigma V^T. \tag{4.66}$$

When A is a $m \times n$ matrix U is a $m \times m$ orthogonal matrix and V is $n \times n$ orthogonal matrix and Σ is a $m \times n$ "diagonal" matrix Lay [36]. The pseudoinverse now can be found by calculating

$$A^+ = V \Sigma^+ U^T. \tag{4.67}$$

According to Lay [36], computing $A^T A$ should be avoided in practice , because errors in the entries of matrix A are squared in the entries of $A^T A$. The singular values and singular vectors of A can be calculated accurately to many decimal places because of the existence of fast iterating algorithms. This also increases the accuracy in computing the pseudoinverse of A.
According to Press [47] singular value decomposition can also be used when the matrix A is singular or almost singular.

Condition number

To determine whether the problem is well-posed or ill-posed the condition number of the matrix A can be calculated. This condition number can be found using

$$\kappa(A) = \frac{\sigma_{max}(A)}{\sigma_{min}(A)}. \tag{4.68}$$

where $\sigma_{max}(A)$ is the largest singular value of A and $\sigma_{min}(A)$ is the smallest singular value of A. When the condition number is infinite, the problem is ill-posed, which means that no unique solution to the problem can be found. When the condition number is large, the matrix is said to be ill-conditioned. This means that the matrix A is not invertible and the problem does not posses a unique well-defined solution [6]. According to Cheney and Kincaid [9], the condition is a measurement of the transfer of error from A and $\mathbf{b}$ to solution $\mathbf{x}$, one can expect to lose at least k digits of precison in solving a linear system when

$$\kappa(A) = 10^k. \tag{4.69}$$

4.4.3 Ridge regression

In the case of the use of an arbitrary path it could be the case that there are more solutions to the same set of equations, it could be the case that different sets of coefficients lead to the same manoeuvre. This means a so-called ill-posed problem has to be solved. The linear least squares method is not able to solve ill-posed problems. However ridge regression or Tikhonov regularization can be used to find a solution to an ill-posed problem. Tikhonov regularization is very similar to ordinary least squares. To give preference to certain solution a regulation term is added however Tikhonov et al. [54]. This means the minimum of

$$||A\mathbf{x} - \mathbf{b}||^2 + ||\Gamma\mathbf{x}||^2 \tag{4.70}$$

is sought. This leads to the solution

$$\hat{\mathbf{x}} = (A^T A + \Gamma^T \Gamma)^{-1} A^T \mathbf{b}. \tag{4.71}$$

For Ridge regression a regulation matrix $\Gamma = kI$ is used where $k \leq 0$ McDonald [40]. Hoerl and Kennard [25] state that when ridge regression is used, always a better estimate can be made than by using linear least squares, because the mean square error is lower than for linear least squares. Conniffe and Stone [13] confirm this for the case k is known, but they are also critical about the applicability of ridge regression because k is estimated. To estimate the value of k Hoerl and Kennard [25] plot the solutions for different values of k and choose a value of k if the signs of the coefficients are correct, if the coefficients are reasonable, if the residual sum of squares is not unreasonable and if the system stabilizes. Conniffe and Stone [13] state these arguments are too vague to make an estimate of k and require more knowledge about the system than is probably known by the researcher. Conniffe and Stone [13] also state that when the matrix is ill-conditioned the data may be inadequate, which can be solved by collecting more data points, or the variables in the model are too dependent on each other which needs revision of the model. Rong and Mou [49] used ridge regression to determine

the manoeuvring indices for Nomoto's first order model from AIS Data. Although the AIS Data contain some errors they found a reliable method for one reference ship. This shows ridge regression has its applications regarding manoeuvring.

4.5 Validation Cases

The manoeuvring model has to be validated. This can be done using experimental data or existing manoeuvring models. In this section these validation cases will be discussed.

4.5.1 Experimental data

To validate a manoeuvring model, often experimental data is used. These data can be obtained by performing model tests or by performing sea trials. Not very much data on sea trials can be found in literature however.

Exceptions are the trials performed with the VLCC Esso Osaka that where performed by Exxon international [14]. Trials performed where turning circle manoeuvre, zig-zag test, spiral test and full astern stopping manoeuvre. Similar tests were done for the Esso Benicia [11], although these data are not used as much as those of the Esso Osaka. Abkowitz [2] used the trial data of the Esso Osaka to determine hydrodynamic coefficients. The data of these trials can also be used to be compared with predicted manoeuvres of a manoeuvring model, to validate the model.

Model tests that are used extensively, are the tests performed by INSEAN on the KVLCC1 and KVLCC2 models. Toxopeus and Lee [55] used these model test data to compare different manoeuvring prediction programs. The KVLCC1 and KVLCC2 where also used to perform CFD calculations to compare them with model test data. The KVLCC1 and KVLCC2 where tested using the Planar Motion Mechanism (PMM) manoeuvring test. A picture of the hull geometry of KVLCC2 can be found in 4.8. The main dimensions of the KVLCC2 can be found in 4.1.

4.5.2 Manoeuvring model

The manoeuvring model can also be validated by comparing it with a manoeuvring model that is already validated. Yoshimura et al. [64] verified and validated the MMG model, which is developed in Japan. This model was validated by using the KVLCC2 model tests. The results of the prediction method were compared with both full-scale and model-scale results. From the validation process is it was concluded that the method can describe the manoeuvring motions and is useful for manoeuvring predictions in full scale

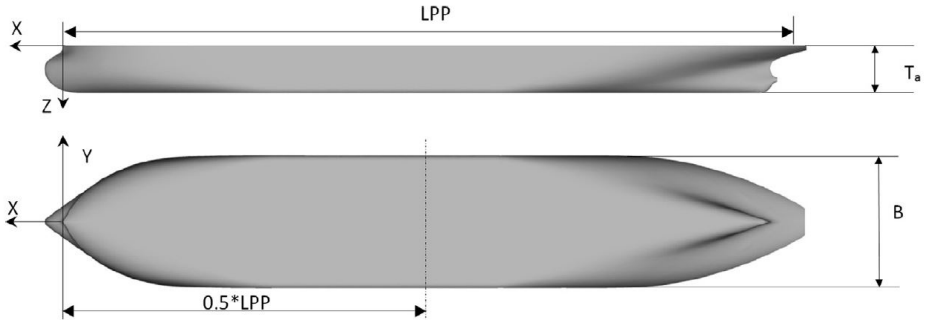

Figure 4.8: Render of the hull geometry of the KVLCC2. Obtained from Fureby et al. [20].

Table 4.1: Main dimensions of the KVLCC2. Obtained from Toxopeus et al. [57].

Descripton	Symbol	Magnitude		Unit
		Ship	Model	
Length between perpendiculars	L_{pp}	320	7.00	m
Moulded breadth	B	58	1.269	m
Moulded draught	d	20.8	0.455	m
Displacement volume moulded	Δ	312635	3.237	m^3
Wetted surface area bare hull	S_{wa}	27197	13.01	m^2
Potition center of buoyancy forward of midship	x_B	3.50	0.077	m

[63]. A comparison between the results for the model and the prediction for the turning circle test are shown in figure 4.9.

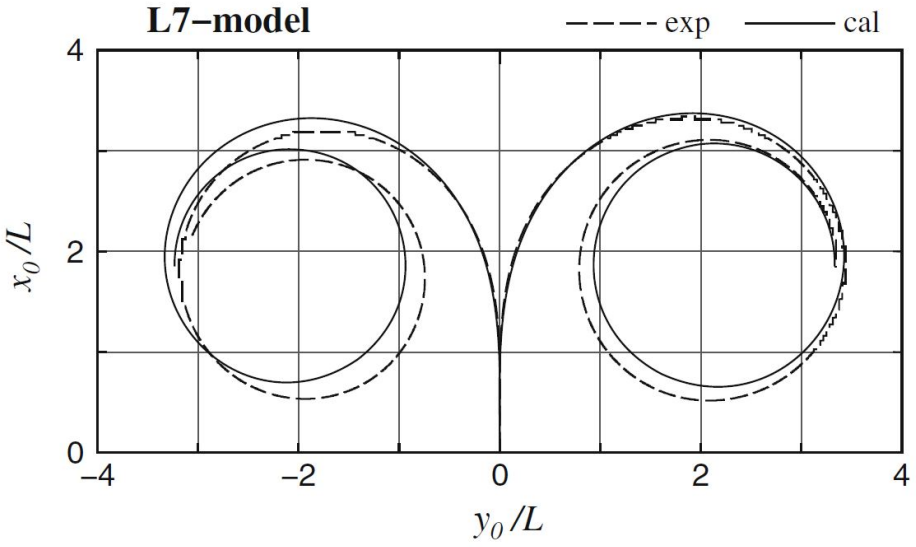

Figure 4.9: Comparison of the calculated and experimental turning circle manoeuvres. Obtained from Yasukawa and Yoshimura [63].

The MMG method uses a polynomial upto the fourth order to estimate the hydrodynamic forces, a second order polynomial to estimate the thrust coefficient and estimates the rudder forces using the method of Fuji and Tuda [19]. The MMG method also takes interaction between propeller and rudder into account by correcting the inflow velocity. The difference in thrust due to manoeuvring of the vessel is taken into account by correcting the wake fraction.

An other model that predicts the manoeuvrability of ULCC's and VLCC's is the model adopted by Panel H-10 of the Society of Navel Architects and Marine Engineers [45]. This method is not validated for a very large range of vessels, but the ships where it is validated for could be used to validate the developed method. The coefficients that are calculated are only coefficients for terms that are linear with acceleration and velocity. The expressions for these coefficients can be found in section 4.3.2.

4.6 Conclusions drawn from literature

Based on the literature study a framework is defined in which the rest of the study will be carried out. In this chapter a summary is given of the conclusions based on the literature study.

4.6.1 Modelling assumptions

To simplify the problem, the ship will be assumed to sail in "trial conditions". This implies that the vessel sails in conditions where the environmental influences, such as wind, waves and current are negligible. When the environmental influences are not negligible, the forces due to the environmental forces have to be estimated and added to the known forces in the method.

Forces that will be taken into account are, rudder, propeller and hydrodynamic forces. The interaction forces between hull, propeller and rudder will not be taken into account. The forces on the rudder are modelled after the method of Yasukawa and Yoshimura [63].

The thrust force of the propeller will be implemented in the model by use of the thrust coefficient. The thrust coefficient will be approximated by the use of a quadratic approximation adapted from Yasukawa and Yoshimura [63].

The modelling of the hydrodynamic forces is based on the low-aspect-ratio lift theory, Ross et al. [50] found that the results of this method came closer to the results of Planar Motion Mechanism tests than the results obtained with a model based on a Taylor series. For this reason the set of coefficients based on low-aspect-ratio lift theory will be implemented. Although the approach is totally different for both methods, it can be seen that both results share a large part of the coefficients. The coefficients found with the low-aspect-ratio lift theory are all based on physical principles, while the origin of the coefficients obtained with a Taylor series is purely mathematical. The Taylor series approach does also find coefficients that show dependency of the accelerations, so-called added mass. Terms like this are expected to have an influence as well, and are therefore also implemented in the model. The coefficients that will be implemented are $X_{\dot{u}}$, X_{uu}, X_{uuu}, X_{vv}, X_{rr}, X_{vr}, X_{uvv}, X_{rvu}, X_{urr}, $Y_{\dot{v}}$, Y_{uv}, Y_{ur}, Y_{uur}, Y_{uuv}, Y_{vvv}, Y_{rrr}, Y_{rrv}, Y_{vvr}, $Y_{|v|v}$, $Y_{|r|v}$, $Y_{|v|r}$, $Y_{|r|r}$, $N_{\dot{r}}$, N_{uv}, N_{ur}, N_{uur}, N_{uuv}, N_{vvv}, N_{rrr}, N_{rrv}, N_{vvr}, $N_{|v|v}$, $N_{|r|v}$, $N_{|v|r}$, $N_{|r|r}$.
The quantities that are input for the method are $\dot{u}$, u, $\dot{v}$, v, r, $\dot{r}$, n_p, δ.

4.6.2 Regression method

The model that is chosen is linear dependent on the coefficients that need to be estimated. This means a linear regression method is suitable for this application. When the matrix with data is ill-conditioned Hoerl and Kennard [25] claim that the residual sum of squares is too large when ordinary linear least squares method is used and ridge regression should be used. When

using ridge regression, a regulation factor k is introduced which has to be estimated. Conniffe and Stone [13] explained that an ill-conditioned matrix could also indicate that too little data points are taken into account or that the model has to be revised. To be sure that results can be found even when the matrix is ill-conditioned, the linear least squares problem will be solved by using singular value decomposition.

Table 4.2: Test scheme for validation using MMG model.

Input	Predict
10/10 zig-zag	20/20 zig-zag
10/10 zig-zag	turning circle
20/20 zig-zag	10/10 zig-zag
20/20 zig-zag	turning circle
turning circle	10/10 zig-zag
turning circle	20/20 zig-zag

4.6.3 Validation

The model will be validated using the MMG model. The MMG method will be used to find the hydrodynamic coefficients of the KVLCC2 with the developed method. Then the hydrodynamic coefficients will be compared with the hydrodynamic coefficients used in the MMG model. This can be done for the turning circle manoeuvre and the zig-zag that are predicted for the KVLCC2 in [63]. The MMG model is programmed in MATLAB, this program is verified using the results of Yasukawa and Yoshimura [63], to be sure that the program is working correctly. When this is done the programmed MMG method can be used to generate the path of a vessel. This will be the input to test the newly developed method. By predicting a manoeuvre with the coefficients obtained from an other manoeuvre, the extend to which the set of coefficients is able to mimic the behaviour of the vessel can be determined. A overview of the different combinations for the input and the predictions done using the determined coefficients is displayed in table 4.2.

Chapter 5

Implementing simulation program

To generate test input for the developed model and for validation purposes, a simulation program is implemented in MATLAB. The basis for the implementation is the paper of Yasukawa and Yoshimura [63], which discusses the MMG method. In this chapter the theory behind the simulation program and the MMG model will be explained and after that the implementation in MATLAB will be discussed. The program is implemented in such a way that different models for forces can be changed very easily.

5.1 Theory behind the MMG model

The MMG model is a model developed in Japan bij the MMG. One of the most important assumptions made in this model is that the problem of manoeuvring is considered to be a quasi-steady problem. This means that the longitudinal component of the velocity is considered to be almost constant an only small differences in longitudinal velocity occur due to propeller and rudder forces.

5.1.1 Equations of motion

The equations of motion used by Yasukawa and Yoshimura [63] are

$$(m + m_x)\dot{u} - (m + m_y)v_m r - x_G m r^2 = X \tag{5.1}$$

$$(m + m_y)\dot{v}_m + (m + m_x)ur + x_G m\dot{r} = Y \tag{5.2}$$

$$(I_{zG} + x_G^2 m + J_z)\dot{r} + x_G m(\dot{v}_m + ur) = N_m. \tag{5.3}$$

The right-hand sides of equations 5.1, 5.2 and 5.3 consist of propeller forces, rudder forces and hydrodynamic forces. Yasukawa and Yoshimura [63] express these right hand sides as

$$X = X_H + X_R + X_P \tag{5.4}$$

$$Y = Y_H + Y_R \tag{5.5}$$

$$N_m = N_H + N_R. \tag{5.6}$$

Yasukawa and Yoshimura [63] non-dimensionalize the hydrodynamic forces X_H and Y_H by dividing by $\frac{1}{2}\rho L_{pp} d U^2$. The hydrodynamic moment N_H is non-dimensionalized by dividing by $\frac{1}{2}\rho L_{pp}^2 d U^2$. Because Yasukawa and Yoshimura [63] assume the forces acting on the vessel to be quasi-steady, the hydrodynamic forces and moments are considered to be independent of u. The lateral velocity v_m and the angular velocity r can be non-dimensionalized by dividing by U and $\frac{U}{L_{pp}}$ respectively. Non-dimensional quantities are denoted with a prime $'$.

5.1.2 Hydrodynamic forces

The hydrodynamic forces are modelled by Yasukawa and Yoshimura [63] as nondimensional forces

$$X'_H = -R'_0 + X'_{vv} v'_m + X'_{vr} v'_m r' + X'_{rr} r'^2 + X'^4_{vvvv} \tag{5.7}$$

$$Y'_H = Y'_v v'_m + Y'_r r' + Y'_{vvv} v'^3_m + Y'_{vvr} v'^2_m r' + Y'_{vrr} v'_m r'^2 + Y'_{rrr} r'^3 \tag{5.8}$$

$$N'_H = N'_v v'_m + N'_r r' + N'_{vvv} v'^3_m + N'_{vvr} v'^2_m r' + N'_{vrr} v'_m r'^2 + N'_{rrr} r'^3. \tag{5.9}$$

Note here that R'_0 is a constant here, this is because u is assumed to be almost constant due to the quasi-steady case. When u varies to much this assumption is not valid any more and terms that are dependent on u have to be included instead of R'_0 .

5.1.3 Propeller forces

Yasukawa and Yoshimura [63] only take thrust force into account when considering propeller forces. Due to hull interaction, the force that the vessel actually "feels" is less than the thrust generated by the propeller, this can be taken into account with the thrust deduction factor t_P

$$X_P = (1 - t_P)T. \tag{5.10}$$

Because of the quasi-steady assumption, the thrust deduction factor is assumed to be constant. Propeller thrust force can be expressed as

$$T = \rho n_p^2 D_4^4 K_T(J_P). \tag{5.11}$$

Yasukawa and Yoshimura [63] approximate the K_T characteristic as a polynomial of second order of the advance ratio

$$K_T(J_P) = k_2 J_P^2 + k_1 J_P + k_0. \tag{5.12}$$

Th advance coefficient can be found using

$$J_P = \frac{(1 - w_P)u}{n_P D_P} \tag{5.13}$$

To correct the wake fraction w_P for the manoeuvring motion of the vessel Yasukawa and Yoshimura [63] use a formula based on the geometrical inflow angle

$$\beta_P = \beta - x'_P r'. \tag{5.14}$$

The correction formula is

$$\frac{1 - w_P}{1 - w_{P0}} = 1 + (1 - e^{-C_1|\beta_P|})(C_2 - 1). \tag{5.15}$$

Because of the asymmetric characteristic of of the wake, Yasukawa and Yoshimura [63] use different values for C_1 and C_2 for different signs of β_P.

5.1.4 Rudder forces

For the rudder forces, Yasukawa and Yoshimura [63] only take the normal force on the rudder into account. The tangential influences are modeled as a correction in the flow velocity. The normal force on the rudder can be decomposed in a longitudinal and a lateral part, as is shown in figure 5.1.

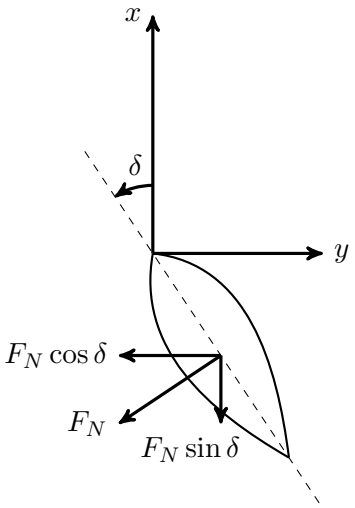

Figure 5.1: Schematic drawing of a rudder and the decomposition of its normal force.

Yasukawa and Yoshimura [63] correct these components of the normal force for the interaction between hull and rudder. These correction factors are measured during model tests. By measuring the hydrodynamic forces when

the ship model is sailing straight with different rudder angles, these correction factors can be determined. The longitudinal component of the rudder normal force is corrected by the steering resistance deduction factor t_R which is defined in a similar manner as the thrust deduction factor. This leads to the expression for longitudinal component of the rudder force

$$X_R = -(1 - t_R)F_N \sin\delta \tag{5.16}$$

as defined by Yasukawa and Yoshimura [63]. The lateral component of the rudder normal force is corrected by the rudder force increase factor a_H [63]. This factor represents the factor between total lateral force induced by a rudder angle and the lateral component of the rudder normal force. Yasukawa and Yoshimura [63] thus define the lateral component of the rudder force as

$$Y_R = -(1 + a_H)F_N \cos\delta. \tag{5.17}$$

The lateral component of the rudder also induces a moment on the vessel, this moment is corrected for the position where the force acts with a factor x_H. Yasukawa and Yoshimura [63] define the moment induced by the rudder as

$$N_R = -(x_R + a_H x_H)F_N \cos\delta. \tag{5.18}$$

Yasukawa and Yoshimura [63] calculate the normal force of the rudder using

$$F_N = \frac{1}{2}\rho A_R U_R^2 f_\alpha \sin\alpha_R. \tag{5.19}$$

where

$$f_\alpha = \frac{6.13\Lambda}{\Lambda + 2.25} \tag{5.20}$$

as found by Fuji and Tuda [19]. The total velocity at the rudder can be determined by using Pythagoras' theorem

$$U_R = \sqrt{u_R^2 + v_R^2}. \tag{5.21}$$

The angle of attack can be expressed as

$$\alpha_R = \delta - \tan^{-1}\left(\frac{v_R}{u_R}\right). \tag{5.22}$$

5.1.5 Flow velocity at rudder position

The velocity of the water that reaches the rudder is influenced by a few different factors however.

- hull of the ship
- acceleration by propeller

- flow straightening effect of the propeller
- rotation of the hull.

Yasukawa and Yoshimura [63] suggest that the velocity at the rudder can be considered to be an weighted averaged velocity between the velocity on the part of the rudder that is in the slipstream of the propeller and the velocity on the part of the rudder that is not in the slipstream. A schematic drawing of the different velocities aft of the vessel is found in figure 5.2.

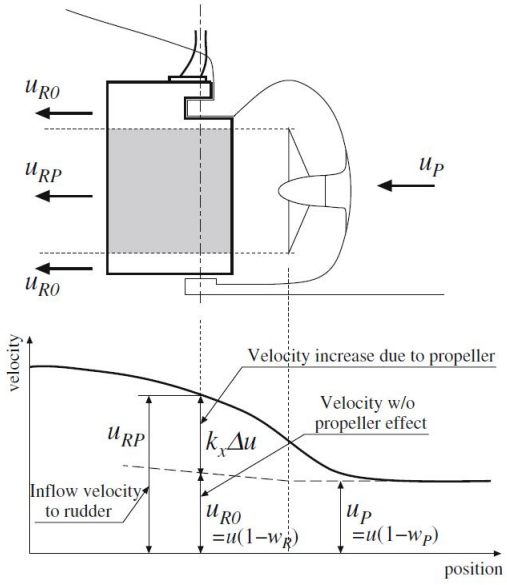

Figure 5.2: Schematic of the relation between ship velocity and inflow velocity on the rudder. Obtained from Yasukawa and Yoshimura [63].

The area of the rudder that is in the slipstream is denoted A_{RP}, the area of the rudder that is not in the slipstream is denoted A_{R0}. Together they make up the total rudder area

$$A_R = A_{R0} + A_{RP}. \tag{5.23}$$

The weighted average of the longitudinal velocity at the rudder can now be calculated as

$$u_R = \sqrt{\frac{A_{RP}}{A_R} u_{RP}^2 + \frac{A_{R0}}{A_R} u_{R0}^2} = \sqrt{\eta u_{RP}^2 + (1-\eta) u_{R0}^2}, \tag{5.24}$$

where

$$\eta = \frac{A_{RP}}{A_R}. \tag{5.25}$$

It is convenient to express both velocities in terms of the inflow velocity of the propeller. For the flow velocity outside the slipstream of the propeller a

factor similar to the wake fraction w_R can be considered to express the flow velocity in terms of the ship velocity

$$u_{R0} = (1 - w_R)u. \tag{5.26}$$

Now by use of the wake fraction the velocity u_{R0} can be expressed in terms of the propeller velocity

$$u_p = (1 - w_P)u \tag{5.27}$$

$$u_{R0} = \frac{1 - w_R}{1 - w_P} u_P. \tag{5.28}$$

This ratio of wake fraction at propeller and rudder positions is denoted by Yasukawa and Yoshimura [63] as

$$\epsilon = \frac{1 - w_R}{1 - w_P}. \tag{5.29}$$

According to [63] velocity at the part of the rudder that is inside of the slipstream can be approximated by the velocity outside of the slipstream plus a velocity increase due to the propeller

$$u_{RP} = u_{R0} + k_x \Delta u. \tag{5.30}$$

The velocity increase due to the propeller is assumed to be proportional to the increase in velocity obtained from actuator disk theory

$$\Delta u = u_\infty - u_P. \tag{5.31}$$

From actuator disk theory the ratio between u_∞ and u_P can be derived

$$\frac{u_\infty}{u_P} = \sqrt{1 + \frac{8K_T}{\pi J_P^2}} \tag{5.32}$$

This derivation is carried out in appendix F. The velocity at the rudder in the propeller slipstream can now be represented by

$$u_{RP} = \epsilon u_P + k_x \left(\sqrt{1 + \frac{8K_T}{\pi J_P^2}} - 1 \right) u_P \tag{5.33}$$

$$u_{RP} = \epsilon u_P \left(1 + \kappa \left(\sqrt{1 + \frac{8K_T}{\pi J_P^2}} - 1 \right) \right), \tag{5.34}$$

where

$$\kappa = \frac{k_x}{\epsilon}. \tag{5.35}$$

Substitution in equation 5.24 of both u_{r0} and u_{RP} results in

$$u_R = \epsilon u_P \sqrt{\eta \left(1 + \kappa \left(\sqrt{1 + \frac{8K_T}{\pi J_P^2}} - 1 \right) \right)^2 + 1 - \eta} \tag{5.36}$$

which is equal to

$$u_R = \epsilon(1 - w_P)u\sqrt{\eta\left(1 + \kappa\left(\sqrt{1 + \frac{8K_T}{\pi J_P^2}} - 1\right)\right)^2 + 1 - \eta}. \tag{5.37}$$

For the lateral component of the flow velocity at rudder position, a different method is used.

5.1.6 Finding new velocities

After calculating all the forces these can be substituted in equations 5.1, 5.2 and 5.3. Now these equations can be solved for $\dot{u}$, $\dot{v}$ and $\dot{r}$, which yields

$$\dot{u} = \frac{X + (m + m_y)v_m r + x_G m r^2}{m + m_x} \tag{5.38}$$

$$\dot{v}_m = \frac{Y - (m + m_x)ur - x_G m\dot{r}}{m + m_y} \tag{5.39}$$

$$\dot{r} = \frac{N_m - x_G m(v_m + ur)}{I_{zG} + x_G^2 m + J_z}. \tag{5.40}$$

These accelerations can be integrated with respect to time to get to velocities

$$u = \int \dot{u}\ \mathrm{d}t \tag{5.41}$$

$$v = \int \dot{v}\ \mathrm{d}t \tag{5.42}$$

$$r = \int \dot{r}\ \mathrm{d}t. \tag{5.43}$$

5.2 Implementation of the MMG model

With the theoretical basis of the MMG model known, the model is implemented in MATLAB. The input of for the MMG model consists of properties of the vessel, in this case the KVLCC2. These properties consist of geometric properties of the vessel and rudder, correction factors for rudder forces and hydrodynamic coefficients. Other inputs that should be defined are the size of integration time-step, the simulation time, rudder angles and propeller RPM.

The calculations for all forces are defined in different subroutines, which are used to calculate the accelerations using the equations of motion. For the integration of the accelerations to update the velocity components, a numerical integration method is used. The Euler method and Runge Kutta 4th order (RK4) will be compared to determine which method is most suitable for this situation. A schematic diagram of the working of the whole program can be found in figure 5.3.

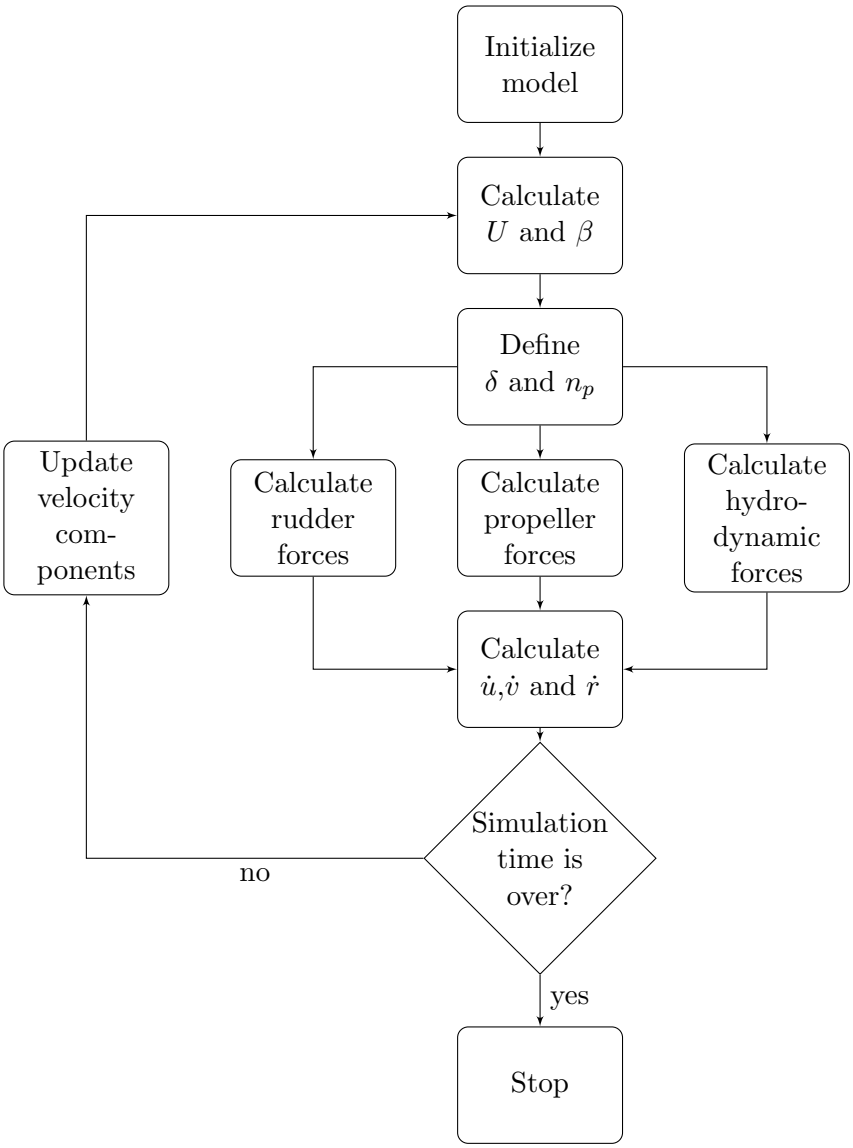

Figure 5.3: Diagram of running the manoeuvring simulation.

5.3 Verification Simulation

In this section the simulation program is verified. First the cases that are used for verification will be defined.

5.3.1 Verification Cases

The different cases that are tested are displayed in table 5.1, the coefficients used in the simulation are also displayed. The vessel used in the simulation is the KVLCC2, which is also used to validate the MMG method. The mass of the vessel is $m = 320415000$ kg. For verification 4 cases for straight sailing are simulated. These cases differ in the external forces that are applied on the vessel. The first case is a decelerating case as the result of constant external force, in the second case also a sinusoidal force is added to the constant force. In the third case the vessel accelerates due to application of a constant force and in the last case a sinusoidal force is added to this constant force.

Table 5.1: Verification Cases.

Case	$X_{\dot{u}}$ [kg]	X_u [kg/s]	F_0 [N]	F_A [N]
1.	-1000000	-200000	1000000	0
2.	-1000000	-200000	1000000	700000
3.	-1000000	-200000	10000000	0
4.	-1000000	-200000	10000000	7000000

All four cases in table 5.1 only include the hydrodynamic coefficients $X_{\dot{u}}$ and X_u because this results in an equation of motion which can be solved analytically. The analytical solution can be used to compare with the numerical integration methods to verify them.

5.3.2 Verifying numerical integration

The errors that occur in the coefficients can arise from numerical errors in the simulation or they can be a result of the developed method. To differentiate between these two kind of errors, the following case is considered. When straight sailing is considered with only coefficients X_u and $X_{\dot{u}}$, the equation of motion becomes

$$(m - X_{\dot{u}})\dot{u} - X_u u = F_{ext}. \tag{5.44}$$

When the external forces on the vessel are set to be equal to a constant force and a sinusoidal force, the equation becomes

$$(m - X_{\dot{u}})\dot{u} - X_u u = F_0 + F_A \sin \omega t, \tag{5.45}$$

which has an analytic solution. This analytic solution is

$$\begin{aligned} u(t) = c_1 e^{\frac{X_u}{m - X_{\dot{u}}} t} - \frac{F_A X_u}{(m - X_{\dot{u}})^2 \omega^2 + X_u^2} \sin \omega t \\ - \frac{(m - X_{\dot{u}}) \omega F_A}{(m - X_{\dot{u}})^2 \omega^2 + X_u^2} \cos \omega t - \frac{F_0}{X_u}. \end{aligned} \tag{5.46}$$

The derivation of the analytic solution can be found in appendix H. The simulation program solves the equation of motion numerically. Lewandowski [38] gives the Euler integration method as the simplest method, the disadvantage of this method is that to increase accuracy a smaller time step is needed, which increases the amount of calculations that has to be done. Another problem that Lewandowski [38] calls is that of numerical stability. The Euler method becomes unstable when time steps are taken to large, which also is a reason to reduce time steps. According to Lewandowski [38] a popular alternative is the RK4 method, which is more accurate and more stable when a larger time step is used, a disadvantage however is that the acceleration has to be evaluated 4 times during each time step. To verify whether the Euler method is sufficiently accurate or not, the RK4, the Euler method and the analytical solution are compared. According to Vuik et al. [60] the stability range for the RK4 method is larger than for the Euler method. [60] also mentions that the local truncation error for the euler method is of order $O(\Delta t)$ while the local truncation error for RK4 is of order $O(\Delta t^4)$. In figure 5.4 it can be seen that both integration methods approximate the analytical result very well for the acceleration. In the velocity plot however, it can be seen that the Euler method deviates much more from the analytical solution than the 4th order Runge-Kutta method. In this case the known forces do not depend on the velocity of the vessel. In the case when propeller force and rudder force are used, the known forces do depend on the velocity of the vessel and a deviation in the velocity is of much higher influence on the solution in the next time step.

Error estimation numerical integration

Because the analytical solution is known, the global truncation error can be calculated. In figure 5.5 the relative truncation error at $t = 4000$ is shown for the 4 different verification cases. The time $t = 4000$ is chosen because the length of the manoeuvres that later will be tested could be of the order of an hour. The relative truncation error is defined as

$$\epsilon_{n+1} = \frac{y_{n+1} - w_{n+1}}{y_{n+1}}, \tag{5.47}$$

where y is the analytical solution and w is the numerical solution. In figure 5.5a and 5.5c it can be seen that the error for the Euler method is linear with respect to the step size, this is in accordance with the theory that states that

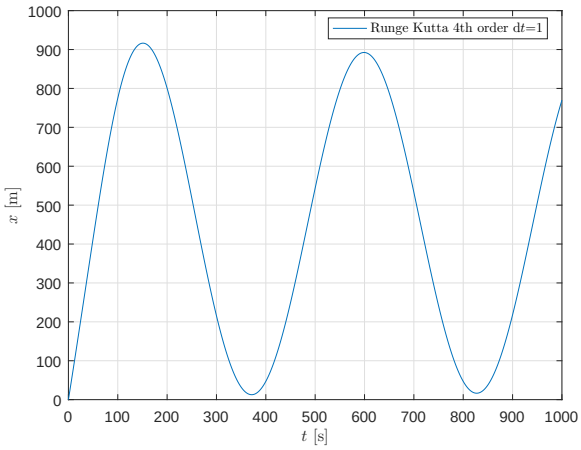

(a) Comparison of solutions of position.

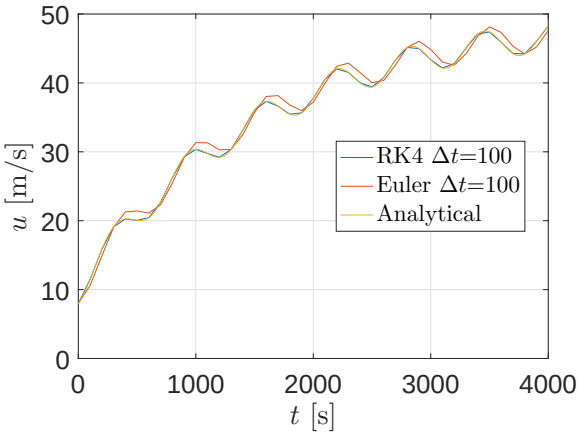

(b) Comparison of solutions of velocity.

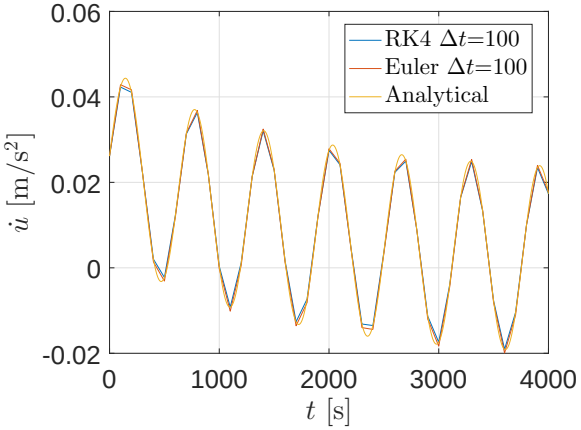

(c) Comparison of solutions of position.

Figure 5.4: Comparison of numerical integration methods.

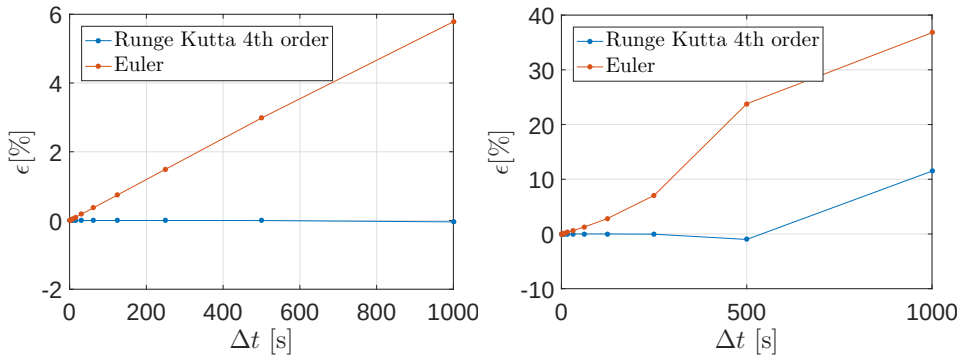

(a) Case 1.

(b) Case 2.

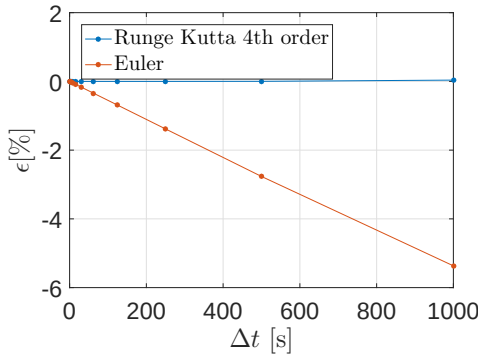

(c) Case 3.

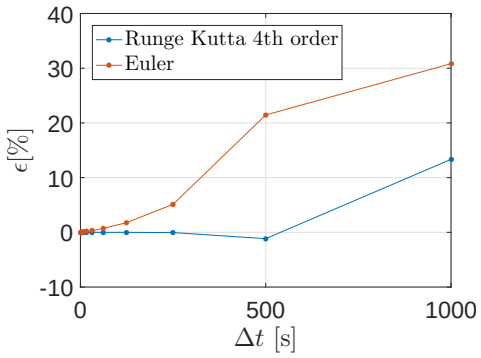

(d) Case 4.

Figure 5.5: Relative global truncation error of longitudinal velocity for different time steps a $t = 4000$.

the Euler method has a truncation error of order $O(\Delta t)$ [60]. In figure 5.5b and 5.5d the Euler method does not show such a linear relation ship, this is probably because of the sinusoidal behaviour of the solution, which lets the local truncation error fluctuate over time. In all four plots it is shown that the Runge-Kutta method converges much faster to the analytical solution as Δt approaches zero than the Euler method. For this reason the Runge-Kutta 4th order method is implemented in the simulation program.

Chapter 6

Development of the prediction method

In this chapter the theoretical background for the method is formulated, and the prediction method is set up. First is explained how based on literature research, the equations of motions are set up and from these equations the hydrodymanic coefficients can be found using singular value decomposition. Secondly the method to derive velocities and accelerations from the position of the vessel is explained. Lastly some implications of manoeuvres will be discussed based on the mathematical model that is used to find the coefficients.

6.1 From equations of motion to coefficients

In literature different sets of coefficients were found to model the hydrodynamic forces on the vessel. When these coefficients are known they can be plugged into the equations of motion, which can be solved to find accelerations, velocities, position and heading. When the velocities and accelerations of the vessel are known at different time steps however, together with rudder and propeller forces, the hydrodynamic coefficients can be considered as unknowns. The velocities and accelerations can be plugged in into the three equations of motions. The three remaining equations are linear in each coefficient and they are also uncoupled because every coefficient occurs in only one equation of motion. These equations can now be solved using Singular Value Decomposition (SVD) to find the least squares approximation of the coefficients. As discussed earlier, the set of coefficients based on low-aspect-ratio lift theory will be used in the prediction method, this results in the use of the following equations of motion

In longitudinal direction the equation of motion becomes:

$$\begin{aligned} &X_{\dot{u}}\dot{u} + X_{uu}u^2 + X_{uuu}u^3 + X_{vv}v^2 + X_{rr}r^2 + X_{vr}vr \\ &+X_{uvv}uv^2 + X_{rvu}rvu + X_{urr}ur^2 + X_P + X_R = m(\dot{u} - rv). \end{aligned} \tag{6.1}$$

In lateral direction the equation of motion becomes:

$$\begin{aligned} &Y_{\dot{v}}\dot{v} + Y_{uv}uv + Y_{ur}ur + Y_{uur}u^2r + Y_{uuv}u^2v + Y_{vvv}v^3 + Y_{rrr}r^3 \\ &+Y_{rrv}r^2v + Y_{vvr}v^2r + Y_{|v|v}|v|v + Y_{|r|v}|r|v + Y_{|v|r}|v|r + Y_{|r|r}|r|r \\ &+Y_P + Y_R = m(\dot{v} + ru). \end{aligned} \tag{6.2}$$

The equation of motion for rotation around the z-axis becomes:

$$\begin{aligned} &N_{\dot{r}}\dot{r} + N_{uv}uv + N_{ur}ur + N_{uur}u^2r + +N_{uuv}u^2v + N_{vvv}v^3 + N_{rrr}r^3 \\ &+N_{rrv}r^2v + N_{vvr}v^2r + N_{|v|v}|v|v + N_{|r|v}|r|v + N_{|v|r}|v|r + N_{|r|r}|r|r \\ &+N_P + N_R = I_z\dot{r} \end{aligned} \tag{6.3}$$

For simplicity, the following simple longitudinal equation of motion is considered as an example

$$X_{\dot{u}}\dot{u} + X_{uu}u^2 + X_P + X_R = m(\dot{u} - rv). \tag{6.4}$$

Note that when the total motion of the vessel needs to be solved, all three coupled equations of motion are needed. When the velocities, accelerations, propeller forces and rudder forces on n points in time are known, this can be written as a set of n linear equations

$$X_{\dot{u}}\dot{u}_i + X_{uu}u_i^2 + X_{P,i} + X_{R,i} = m(\dot{u}_i - r_iv_i) \quad 1 \geq i \geq n. \tag{6.5}$$

Putting all known forces at the right hand side and writing it in matrix form yields

$$\begin{bmatrix} \dot{u}_1 & u_1^2 \\ \vdots & \vdots \\ \vdots & \vdots \\ \dot{u}_n & u_n^2 \end{bmatrix} \begin{bmatrix} X_{\dot{u}} \\ X_{uu} \end{bmatrix} = \begin{bmatrix} m(\dot{u}_1 - r_1v_1) - X_{P,1} - X_{R,1} \\ \vdots \\ \vdots \\ m(\dot{u}_n - r_nv_n) - X_{P,n} - X_{R,n} \end{bmatrix}. \tag{6.6}$$

This equation can be written shorter as

$$A_X\mathbf{X} = \mathbf{b}_X. \tag{6.7}$$

Here we will call A_X the velocity matrix for longitudinal direction, $\mathbf{X}$ the longitudinal coefficient vector and $\mathbf{b_X}$ the known forces vector for longitudinal direction. In the same way the equations for sway and yaw can be rewritten. Despite the fact that the three equations are uncoupled, one

could still write these three equations as one matrix equation, but solving this one matrix equation involves inverting a matrix that is much larger, which will require more computational effort.
A linear least square estimate of the solution can now be made to find using singular value decomposition

$$\mathbf{X} = V\Sigma^{+}U^{T}\mathbf{b}_{X}. \tag{6.8}$$

In the same way this can be done for equations 6.1,6.2 and 6.3.

6.2 Finding velocities and accelerations

To find the hydrodynamic coefficients in the equation of motions, the velocities and accelerations of the vessel need to be known. These quantities need to be derived from the path that the vessel has sailed. The position of the vessel is described by a x-coordinate, y-coordinate and a heading angle. When these quantities are measured on a real vessel, the position will be measured at different steps in time.

Consider two moments in time t_1 and t_2 for which the position and heading of the vessel is known. This is illustrated in figure 6.1. The difference in time between these moments can be defined as

$$\Delta t = t_2 - t_1. \tag{6.9}$$

In the same way differences between heading, x-coordinate and y-coordinate can be defined as

$$\Delta\psi = \psi_2 - \psi_1 \tag{6.10}$$

$$\Delta x = x_2 - x_1 \tag{6.11}$$

$$\Delta y = y_2 - y_1 \tag{6.12}$$

From classical mechanics it is known that a velocity can be defined as a derivative of position with respect to a certain reference frame

$$V = \lim_{\Delta t \to 0} \frac{\Delta s}{\Delta t}. \tag{6.13}$$

In the same way a velocity in the x-direction and the y-direction of the earth fixed coordinate system can be defined

$$\dot{x}_0 = \lim_{\Delta t \to 0} \frac{\Delta x}{\Delta t} \tag{6.14}$$

$$\dot{y}_0 = \lim_{\Delta t \to 0} \frac{\Delta y}{\Delta t}. \tag{6.15}$$

The angular velocity can be defined as

$$r = \lim_{\Delta t \to 0} \frac{\Delta \psi}{\Delta t}. \tag{6.16}$$

Using goniometric relations the velocities in the ship fixed reference frame can be found

$$u = \dot{x}_0 \cos\psi + \dot{y}_0 \sin\psi \tag{6.17}$$

$$v = -\dot{x}_0 \sin\psi + \dot{y}_0 \cos\psi \tag{6.18}$$

$$r = \dot{\psi}. \tag{6.19}$$

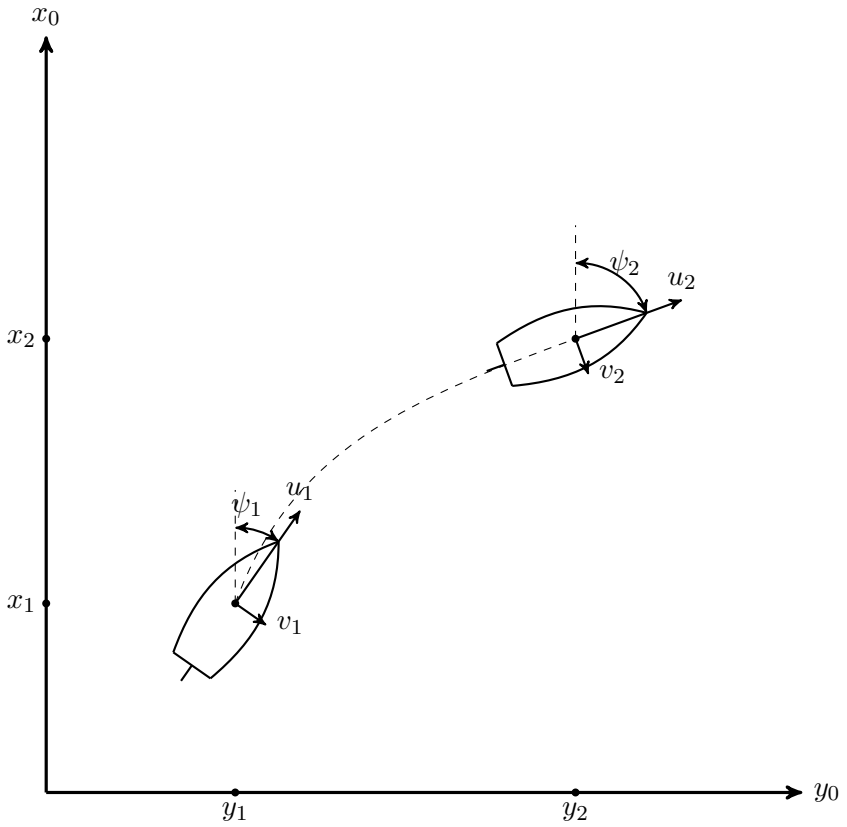

Figure 6.1: Schematic display of a vessel during two different time steps.

Because the change in reference frame is only a change in the xy-plane, the rotation r remains the same for the ship fixed reference frame. In a similar manner the accelerations can be calculated, by differentiating the velocities

$$\dot{u} = \ddot{x}_0 \cos\psi - \dot{x}_0 r \sin\psi + \ddot{y}_0 \sin\psi + \dot{y}_0 r \cos\psi \tag{6.20}$$

$$\dot{v} = -\ddot{x}_0 \sin\psi - \dot{x}_0 r \cos\psi + \ddot{y}_0 \cos\psi - \dot{y}_0 r \sin\psi \tag{6.21}$$

$$\dot{r} = \ddot{\psi}. \tag{6.22}$$

In reality it is impossible to measure time en position continuously, so the limit for $\Delta t \to 0$ can never be reached. Because of this it is needed to approximate the derivative numerically.

6.2.1 Numerical Differentiation

Numerical differentiation uses function values to approximate the rate of change of the function. Over the years many different methods of numerical differentiation have been developed. The accuracy and stability of a method does highly depend on the interval Δt over which the rate of change is determined. A so called truncation error of the differentiation method can be estimated by using a Taylor series expansion. In most cases the truncation error increases as the step size Δt increases [60].

Finite difference methods

The easiest examples of numerical differentiation are the forward difference and backward difference methods. These methods basically use the definition of the derivative, but use a finite difference instead of taking the limit of the difference to zero. The forward difference method becomes

$$f'(x) \approx \frac{f(x+h) - f(x)}{h} \text{ for } h > 0, \tag{6.23}$$

and the backward difference method is

$$f'(x) \approx \frac{f(x) - f(x-h)}{h} \text{ for } h > 0. \tag{6.24}$$

According to [21], the truncation error can be reduced to order $O(h^2)$ by taking the average of both methods, which results in the central difference method

$$f'(x) \approx \frac{f(x+h) - f(x-h)}{2h}. \tag{6.25}$$

This corresponds to the slope of a straight line between the two adjacent points, where the slope is evaluated, as drawn in figure 6.2. To derive the accelerations of the vessel, it is necessary to differentiate the position of the vessel twice. By introducing points at $x + \frac{h}{2}$ and $x - \frac{h}{2}$, the central difference method can be applied twice to find

$$f'' \approx \frac{f(x+h) - 2f(x) + f(x-h)}{h^2}. \tag{6.26}$$

The advantage of approximating the second derivative using the function original function values, over differentiating the first derivative again is that the error is smaller.

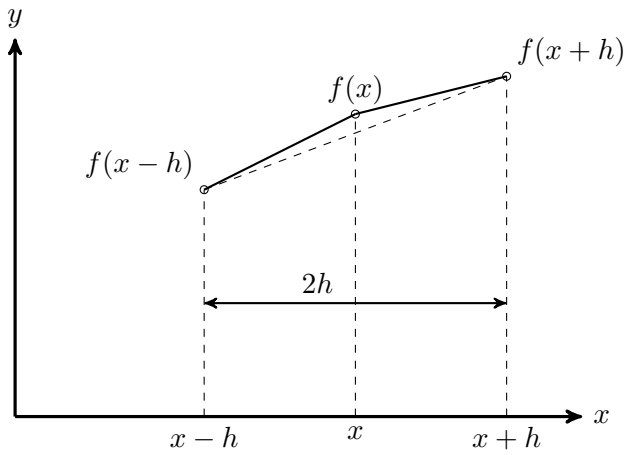

Figure 6.2: Approximation of derivative in $f(x)$ with central difference method.

Richardson Extrapolation

According to Grasselli and Pelinovsky [23], the accuracy of the numerical differentiation can be improved by a method called Richardson extrapolation. Using Richardson extrapolation a better multipoint approximation can be made by cancellation of the truncation error of previous multipoint approximation. Using the central difference method as a basis in the Richardson extrapolation, we find

$$f' \approx \frac{-f(x+2h) + 8f(x+h) - 8f(x-h) - f(x-2h)}{12h}, \tag{6.27}$$

which has a truncation error of order $O(h^4)$. In a similar way, Richardson extrapolation can be used to make a better approximation can be made of the second derivative

$$f'' \approx \frac{-f(x+2h) + 16f(x+h) - 30f(x) + 16f(x-h) - f(x-2h)}{12h^2}, \tag{6.28}$$

which also has a truncation error of order $O(h^4)$. The same principle can be used for the forward and backwards difference methods. These methods are slightly less accurate, but they can be used on the edge of the interval. The expressions found are

$$f' \approx \frac{f(x+4h) - 12f(x+2h) + 32f(x+h) - 21f(x)}{12h} \tag{6.29}$$

$$f'' \approx \frac{-f(x+4h) + 10f(x+2h) - 16f(x+h) + 7f(x)}{4h^2}. \tag{6.30}$$

Both approximations on the edge have truncation errors of $O(h^3)$.

6.2.2 Moving-average filter

The data that is used to determine the accelerations and velocities may contain noise and steps. To reduce the noise, and to be sure that a differentiation can be carried out, a filter is used. Because steps in the data that cause peaks in the derivatives are the main problem, a filter that smooths the data is needed. For this purpose a moving average is used. The moving average filter uses the data in a specified window to calculate the average [12]. When the window is 5 for example, the moving average filtered data become

$$g(x) = \frac{f(x-2) + f(x-1) + f(x) + f(x+1) + f(x+2)}{5}. \tag{6.31}$$

6.3 Implications of certain paths

Although the method is able to find coefficients from a manoeuvre executed by the vessel, not every manoeuvre is suitable to find all coefficients that are sought after. This has to do with the implicit assumption that $\dot{u}$, $\dot{v}$, $\dot{r}$, u,v and r all will vary during the executed manoeuvre. In this section the implications of situation where this is not the case will be discussed. Although not every situation is equally likely to occur, it is important to realize that these situations can take place.

6.3.1 Longitudinal acceleration is zero

When the longitudinal acceleration $\dot{u}$ is zero, the longitudinal velocity u is a constant velocity u_0. This means that no distinction can be made between coefficients that only define a relation between longitudinal force and u. When this situation is substituted in 6.1 this leads to

$$\begin{aligned}&(X_{uu}u_0^2 + X_{uuu}u_0^3) + (X_{vr} + X_{rvu}u_0)vr + (X_{vv} + X_{uvv}u_0)v^2 \\ &+(X_{urr}u_0 + X_{rr})r^2 + X_P + X_R = -mvr.\end{aligned} \tag{6.32}$$

Because the longitudinal velocity remains constant, the expressions between brackets are constant as well. This means no distinction can be made between the different coefficients between brackets. In this situation no distinction can be made between X_{uu} and X_{uuu}, which means they can not be determined in this situation. The same problem arises for X_{vr} and X_{rvu}, X_{vv} and X_{uvv} and X_{urr} and X_{rr}. The added mass $X_{\dot{u}}$ can not be determined because the acceleration $\dot{u}$ is zero, which makes the term vanish from the equation. When the same substitution is done for 6.2 this leads to

$$\begin{aligned}&(Y_{uv}u_0 + Y_{uuv}u_0^2)v + (Y_{ur}u_0 + Y_{uur}u_0^2)r + Y_{\dot{v}}\dot{v} + Y_{vvv}v^3 \\ &+Y_{rrr}r^3 + Y_{rrv}r^2v + Y_{vvr}v^2r + Y_{|v|v}|v|v + Y_{|r|v}|r|v + Y_{|v|r}|v|r \\ &+Y_{|r|r}|r|r + Y_p + Y_R = m(\dot{v} + ru_0).\end{aligned} \tag{6.33}$$

In equation 6.33 it can be seen that no distinction can be made between Y_{uv} and Y_{uuv}, the same applies to Y_{ur} and Y_{uur}.

$$\begin{aligned}&(N_{ur}u_0 + N_{uur}u_0^2)r + (N_{uv}u_0 + N_{uuv})v + N_{\dot{r}}\dot{r} + N_{vvv}v^3\\ &+N_{rrr}r^3 + N_{rrv}r^2v + N_{vvr}v^2r + N_{|v|v}|v|v + N_{|r|v}|r|v + N_{|v|r}|v|r\\ &+N_{|r|r}|r|r + N_P + N_R = I_z\dot{r}\end{aligned} \tag{6.34}$$

In the same way equation 6.34 can be found after substitution of $u = u_0$ in 6.3. From this equation it can be concluded that N_{uv} and N_{uuv} indistinguishable, which is also the case for N_{ur} and N_{uur}.

6.3.2 Lateral acceleration is zero

The lateral acceleration $\dot{v}$ is zero when the lateral velocity v is constant. When a constant velocity v_0 is substituted in equation, this results in 6.1

$$\begin{aligned}&X_{\dot{u}}\dot{u} + (X_{uu} + X_{uuv}v_0)u^2 + X_{vv}v_0^2 + X_{vr}v_0r + X_{rvu}rv_0u\\ &+X_{uuu}u^3 + X_{rr}r^2 + X_{urr}ur^2 + X_P + X_R = m(\dot{u} - rv_0).\end{aligned} \tag{6.35}$$

In this case, due to the constant velocity, X_{uu} and X_{uuv} will not be distinguishable. When the constant lateral velocity v_0 is substituted in equation 6.2, this will result in

$$\begin{aligned}&Y_{uv}uv_0 + Y_{ur}ur + Y_{uur}u^2r + Y_{uuv}u^2v_0 + Y_{vvv}v_0^3\\ &+Y_{rrr}r^3 + Y_{rrv}v_0r^2 + Y_{vvr}v_0^2r + Y_{|v|v}|v_0|v_0 + Y_{|r|v}|r|v_0 + Y_{|v|r}|v_0|r\\ &+Y_{|r|r}|r|r + Y_P + Y_R = mru.\end{aligned} \tag{6.36}$$

The added mass term becomes zero, due to the acceleration being zero. The rest of the coefficients can still be calculated as long as there are positive and negative values of v and r during the path of the vessel, this is explained in section 6.3.7. The equation of motion for the rotation about the z-axis in this situation is

$$\begin{aligned}&N_{\dot{r}}\dot{r} + N_{uv}v_0u + N_{ur}ur + N_{uur}u^2r + N_{uuv}u^2v_0 + N_{vvv}v_0^3\\ &+N_{rrr}r^3 + N_{rrv}v_0r^2 + N_{vvr}v_0^2r + N_{|v|v}|v_0|v_0 + N_{|r|v}|r|v_0 + N_{|v|r}|v_0|r\\ &+N_{|r|r}|r|r + N_P + N_R = I_z\dot{r}.\end{aligned} \tag{6.37}$$

Because no terms show the same dependencies and no term depends on $\dot{v}$, all coefficients in this equation can be determined.

6.3.3 Rotational acceleration is zero

If the vessel is rotating with a constant angular velocity r_0, the rotational acceleration $\dot{r}$ is zero. Substituting the constant angular velocity in equations

6.1 en 6.2 yields

$$\begin{aligned} &X_{\dot{u}}\dot{u} + X_{uu}u^2 + X_{uuv}vu^2 + X_{vv}v^2 + X_{vr}vr_0 + X_{rvu}r_0vu \\ &+X_{uuu}u^3 + X_{rr}r_0^2 + X_{urr}ur_0^2 + X_P + X_R = m(\dot{u} - r_0v) \end{aligned} \tag{6.38}$$

and

$$\begin{aligned} &Y_{\dot{v}}\dot{v} + Y_{uv}uv + Y_{ur}ur_0 + Y_{uur}u^2r_0 + Y_{uuv}u^2v + Y_{vvv}v^3 \\ &+Y_{rrr}r_0^3 + Y_{rrv}r_0^2v + Y_{vvr}r_0v^2 + Y_{|v|v}|v|v + Y_{|r|v}|r_0|v + Y_{|v|r_0}|v|r_0 \\ &+Y_{|r|r}|r_0|r + Y_P + Y_R = m(\dot{v} + r_0u). \end{aligned} \tag{6.39}$$

From equation 6.38 it can be concluded that every coefficient for the hydrodynamic forces in x-direction can be determined if the rotational acceleration is zero. Because the hydrodynamic forces in y-direction contains square absolute terms, all coefficients of the hydrodynamic forces in y-direction can only be determined when either r_0 or v contains negative values, this is explained in section 6.3.7. The equation of motion for rotation around the z-axis becomes

$$\begin{aligned} &N_{uv}vu + N_{ur}ur_0 + N_{uur}u^2r_0 + N_{uuv}u^2v + N_{vvv}v^3 \\ &+N_{rrr}r_0^3 + N_{rrv}r_0^2v + N_{vvr}v^2r_0 + N_{|v|v}|v|v + N_{|r|v}|r_0|v + N_{|v|r_0}|v|r_0 \\ &+N_{|r|r}|r_0|r + N_P + N_R = 0. \end{aligned} \tag{6.40}$$

Because the angular velocity is zero, the added mass moment of inertia has no influence and can not be determined. So $N_{\dot{r}}$ can not be found when the rotational acceleration is zero.

6.3.4 Longitudinal velocity is zero

When not only the longitudinal acceleration is zero, but the longitudinal velocity u is zero, a lot more terms cancel from the equation of motion in x-direction:

$$X_{vv}v^2 + X_{vr}vr + X_{rr}r^2 + X_P + X_R = mrv. \tag{6.41}$$

This means it is not possible to determine $X_{\dot{u}}$, X_{uu}, X_{uuu}, X_{uvv}, X_{rvu} and X_{urr} when u is zero. When $u = 0$ is substituted in equation 6.2, the equation becomes

$$\begin{aligned} &Y_{\dot{v}}\dot{v} + Y_{vvv}v^3 + Y_{rrr}r^3 + Y_{rrv}r^2v + Y_{vvr}v^2r + Y_{|v|v}|v|v + Y_{|r|v}|r|v \\ &+Y_{|v|r}|v|r + Y_{|r|r}|r|r + Y_P + Y_R = m\dot{v}. \end{aligned} \tag{6.42}$$

Equation 6.42 shows less terms than the original equation, because the terms involving u are cancelled. It can be concluded that the coefficients Y_{uv}, Y_{ur}, Y_{uur}, Y_{uuv} can not be obtained when the longitudinal velocity is zero. When

a longitudinal velocity of zero is substituted in the moment equation around the z-axis 6.3, the equation becomes

$$\begin{aligned} &N_{\dot{r}}\dot{r} + N_{vvv}v^3 + N_{rrr}r^3 + N_{rrv}r^2v + N_{vvr}v^2r + N_{|v|v}|v|v + N_{|r|v}|r|v \\ &+N_{|v|r}|v|r + N_{|r|r}|r|r + N_P + N_R = I_z\dot{r}. \end{aligned} \tag{6.43}$$

The terms N_{uv}, N_{ur}, N_{uur} and N_{uuv} have dropped out of the equation, which means they cannot be determined in this situation.

6.3.5 Lateral velocity is zero

When the lateral velocity v is zero equation 6.1 becomes

$$X_{\dot{u}}\dot{u} + X_{uu}u^2 + X_{uuu}u^3 + X_{rr}r^2 + X_{urr}ur^2 + X_P + X_R = m\dot{u}. \tag{6.44}$$

The coefficients X_{vv}, X_{vr}, X_{uuv} and X_{rvu} cannot be determined, because they dropped out of the equation.

$$Y_{ur}ur + Y_{uur}u^2r + Y_{rrr}r^3 + Y_{|r|r}|r|r + Y_P + Y_R = mru. \tag{6.45}$$

$$N_{\dot{r}}\dot{r} + N_{ur}ur + N_{uur}u^2r + N_{rrr}r^3 + N_{|r|r}|r|r + N_P + N_R = I_z\dot{r}. \tag{6.46}$$

6.3.6 Rotational velocity is zero

$$X_{\dot{u}}\dot{u} + X_{uu}u^2 + X_{uuu}u^3 + X_{vv}v^2 + X_{uvv}uv^2 + X_P + X_R = m\dot{u}. \tag{6.47}$$

$$Y_{\dot{v}}\dot{v} + Y_{uv}uv + Y_{uuv}u^2v + Y_{vvv}v^3 + Y_{|v|v}|v|v + Y_P + Y_R = m\dot{v}. \tag{6.48}$$

$$N_{uv}uv + N_{uuv}u^2v + N_{vvv}v^3 + N_{|v|v}|v|v + N_P + N_R = 0. \tag{6.49}$$

6.3.7 Lateral and Rotational velocity are both positive

Because some terms of the lateral force balance include square absolute terms, no distinction can be made between some coefficients when both lateral and rotational velocity remain constant along the entire path. When this is the case, $Y_{|r|v}$ and $Y_{|v|r}$ will play the same role, because $|v| = v$ and $|r| = r$. This means the equation of motion in lateral direction in this situation can be written as:

$$\begin{aligned} &Y_{\dot{v}}\dot{v} + Y_{uv}uv + Y_{ur}ur + Y_{uur}u^2r + Y_{uuv}u^2v + Y_{vvv}v^3 + Y_{rrr}r^3 \\ &+Y_{rrv}r^2v + Y_{vvr}v^2r + Y_{|v|v}|v|v + (Y_{|r|v} + Y_{|v|r})vr + Y_{|r|r}|r|r \\ &+Y_P + Y_R = m(\dot{v} + ru) \end{aligned} \tag{6.50}$$

$$\begin{aligned} &N_{\dot{r}}\dot{r} + N_{uv}uv + N_{ur}ur + N_{uur}u^2r + N_{uuv}u^2v + N_{vvv}v^3 + N_{rrr}r^3 \\ &+N_{rrv}r^2v + N_{vvr}v^2r + N_{|v|v}|v|v + (N_{|r|v} + N_{|v|r})vr + N_{|r|r}|r|r \\ &+N_P + N_R = I_z\dot{r}. \end{aligned} \tag{6.51}$$

Chapter 7

Verification prediction method

To find out whether it is possible to find a set of manoeuvring coefficients by using the method developed around singular value decomposition, it is needed to verify the method. This means it is needed to test if the method is able to return a set of coefficients that is already known. This can be done in the following way:

- Select a known set of coefficients,
- Apply known external forces to simulate a track,
- Use the developed method to find the same set of coefficients,
- Determine the error of the found coefficients to verify the developed method.

7.1 Verification plan

7.1.1 Known set of coefficients

To start verifying the method, a known set of coefficients has to be chosen. To begin with, a small set of coefficients is preferable because it makes computations and debugging less complex. The set also needs to be a valid set of coefficients itself to be sure that the manoeuvres simulated are valid. The coefficients are chosen form the set of coefficients derived from low-aspect-ratio lift theory, these coefficients can be found in table 7.1. Because

7.1.2 Apply known forces to simulate a track

To move the vessel forces have to be applied on the ship. IN reality this is done by the use of rudders and propellers. To be sure that errors in the

Table 7.1: Coefficients derived from low-aspect-ratio lift theory.

X coefficients	**Y coefficients**	**N coefficients**
$X_{\dot{u}}$	$Y_{\dot{v}}$	$N_{\dot{r}}$
X_{uu}	Y_{uv}	N_{uv}
X_{uuu}	Y_{ur}	N_{ur}
X_{vv}	Y_{uur}	N_{uur}
X_{rr}	Y_{uuv}	N_{uuv}
X_{vr}	Y_{vvv}	N_{vvv}
X_{uvv}	Y_{rrr}	N_{rrr}
X_{rvu}	Y_{rrv}	N_{rrv}
X_{urr}	Y_{vvr}	N_{vvr}
	$Y_{\|v\|v}$	$N_{\|v\|v}$
	$Y_{\|r\|v}$	$N_{\|r\|v}$
	$Y_{\|v\|r}$	$N_{\|v\|r}$
	$Y_{\|r\|r}$	$N_{\|r\|r}$

method are not caused by errors in the propeller and rudder forces, known forces and moments are applied. To start verification as easy as possible, it is convenient to start with simulations of motions in 1 Degrees of Freedom (DOF), which can be done by applying a force or moment in 1 DOF.

7.1.3 Determining the coefficients

Using the developed method and the selected tracks, the coefficients can be determined. The known forces used to generate the manoeuvres are used as known forces in this method as well. The coefficients that arise from the method should be the same or close to the original set. To measure how close the coefficients approximate the behaviour of the vessel, the variance can be calculated. The sampling time can also be varied to research what the influence is on the results and the condition number of the matrices that need to be decomposed in the singular value decomposition. The condition number can be used as a measure of the sensitivity of the solution to errors in the entries of the matrix.

7.2 Verification of numerical differentiation

To verify whether the chosen numerical differentiation method based on Richardson extrapolation is implemented correctly, the derivative can be compared with the analytical solution. The error can also be estimated to see if the order of the error is in accordance with the theory. To test whether any complications arise in the numerical differentiation Vuik et al. [60] advises to verify the order of the error. According to Vuik et al. [60],

the order of the truncation error p can be estimated using

$$\frac{Q(2h) - Q(4h)}{Q(h) - Q(2h)} = 2^p. \tag{7.1}$$

In this formula $Q(h)$ is the numerical derivative found with a step size of h. To use this method, the analytical solutions of the verification cases described in table 5.1 are used. The analytical solution of the position is then used as input to find the velocity and acceleration by numerical differentiation. Because the analytical solution is known, the error can also be calculated by calculating the difference between the numerical derivative and the analytical derivative.

7.2.1 Numerical differentiation at edges of the interval

At the edges of the interval a form of Richardson extrapolation is used that is based on the forward difference method at the left edge and the backwards difference method at the right edge. The formula that is used is displayed in equation 6.29. In figure 7.1 the truncation errors at t=0 are displayed that are determined by calculating the difference between the numerical derivative and the analytical derivative. It can be seen that the error converges to 0 as Δt goes to 0 in all four cases, which means that the method is stable. In figures 7.1b and 7.1d the error shows a different behaviour for Δt larger than 128 seconds, this is due to the fact that the time step becomes too large to model the sinusoidal behaviour of the solution.

To estimate the order of the truncation error, the method of Vuik et al. [60] is used, which is displayed in Equation 7.1, to find the order p. The results are displayed in table 7.2. In table 7.2 it can be seen that for most cases the

Table 7.2: Estimation of the order of the truncation error for numerical differentiation at the beginning of the interval.

Δt [s]	p case 1	p case 2	p case 3	p case 4
125	2.936	-0.699	2.936	-0.062
62.5	2.973	0.943 - 4.532i	2.973	1.033 - 4.532i
31.25	2.987	2.906	2.987	2.905
15.625	2.994	3.691	2.994	3.702
7.8125	2.997	3.785	2.997	3.805
3.9063	2.999	3.701	2.999	3.732
1.9531	2.999	3.549	2.999	3.588
0.9766	3.000	3.381	3.001	3.419
0.4883	2.993	3.239	2.988	3.265

truncation error at the ends of the interval have a truncation error of order

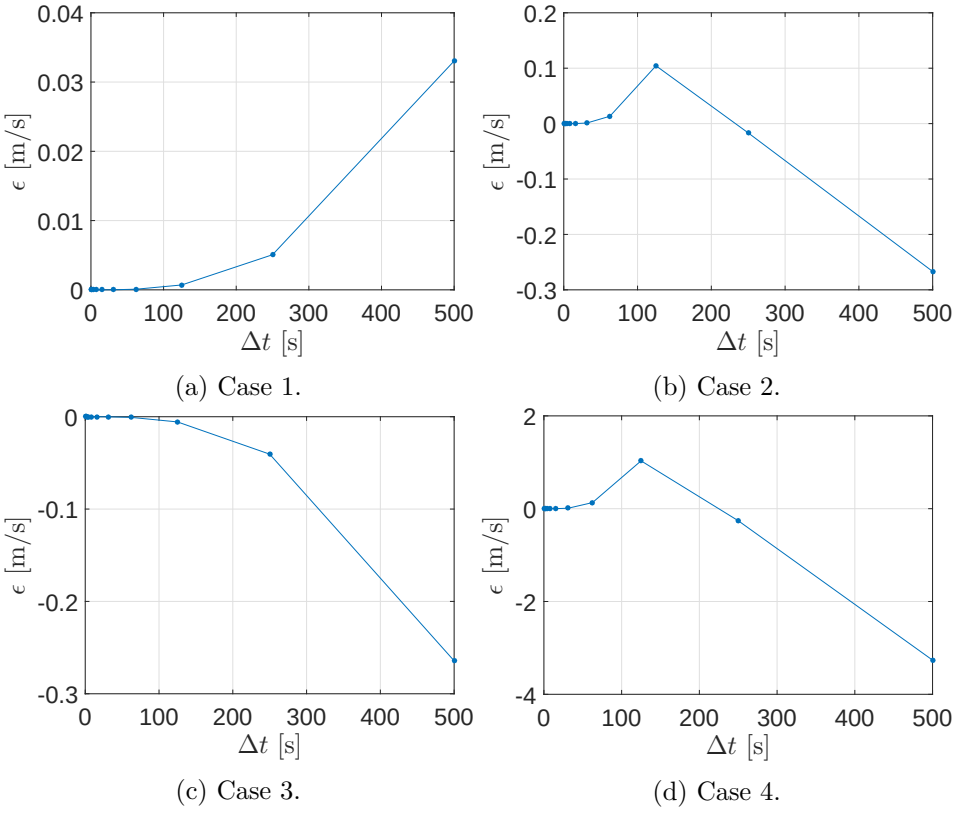

(a) Case 1.

(b) Case 2.

(c) Case 3.

(d) Case 4.

Figure 7.1: Truncation error at $u(t = 0)$ due to numerical differentiation for different step sizes using Richardson extrapolation.

$O(h^3)$, this is in accordance with the theoretical order of the truncation error, as mentioned in 6.2.1 which means that the method is verified. In case 2 and 4, where a sinusoidal behaviour is differentiated, the p-value is not 3 or even negative or complex for large step sizes. This behaviour occurs, because the step size is too large to approximate the sinusoidal behaviour, a phenomenon called aliasing.

7.2.2 Numerical differentiation in the middle of the interval

In the middle of the interval a form of Richardson extrapolation is used that is based on the central difference method. The formula for this numerical differentiation method can be found in equation 6.27. To test this method, the same analytical solution is used, but now the situation at $t = 2000$ is used. In figure 7.2 the errors in the numerical differentiation compared to the analytical solution are displayed. In figure 7.2 it can be seen that the

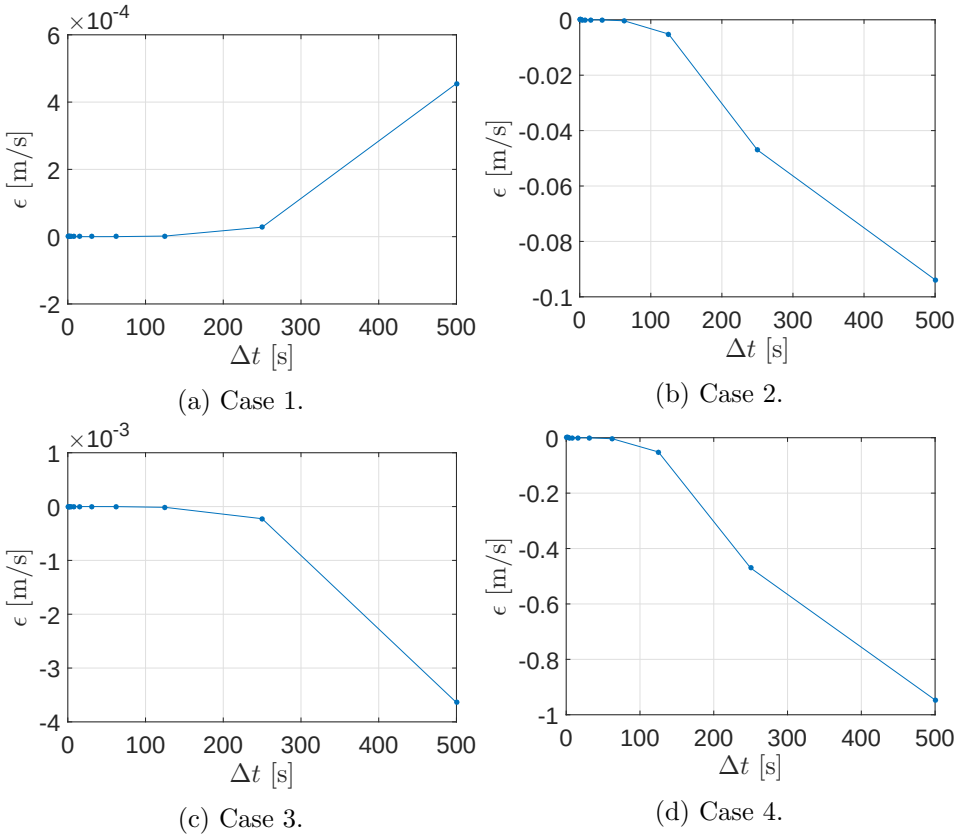

(a) Case 1.

(b) Case 2.

(c) Case 3.

(d) Case 4.

Figure 7.2: Truncation error at $u(t = 2000)$ due to numerical differentiation for different step sizes using Richardson extrapolation..

error converges to 0 when Δt goes to 0. It can also be noticed that the errors

are smaller compared to the errors for the differentiation method that is used at the edges of the interval.

In table 7.3 the truncation error is displayed that is calculated using equation 7.1. It can be seen that the truncation error for most cases is of the order $O(h^4)$, which also followed from theory. In case 2 and case 4, the order of the error is less than 4 for Δt =125, this is due to the sinusoidal behaviour of the motion. In these 2 cases the time step is too large to model the sinusoidal behaviour of the velocity. For the time steps smaller than 2 second, case 1 and 3 show errors smaller than the order of 4. This is because the truncation errors are very small and are in the order of magnitude of the rounding error.

Table 7.3: Estimation of the truncation error for numerical differentiation in the middle of the interval.

h [s]	p case 1	p case 2	p case 3	p case 4
125	4.013	0.163	4.013	0.185
62.5	4.003	3.131	4.003	3.132
31.25	4.001	3.787	4.001	3.787
15.625	4.000	3.947	4.000	3.947
7.8125	4.000	3.987	4.000	3.987
3.9063	3.993	3.997	3.993	3.997
1.9531	4.703	3.999	4.703	3.999
0.9766	1.059	3.997	1.059	4.002
0.4883	-1.876	4.083	-1.876	3.977

It can be concluded that the Richardson Extrapolation is implemented correctly, because the method shows the truncation errors as expected from theory.

7.3 Verifying SVD using Analytical solution

If the prediction method works it should be able to give back the coefficients that where used to simulate the track in the first place. When an analytical solution is used to generate a data set, this data set does not contain any numerical errors. Every error that will occur in the predicted coefficients thus has to be a result of the prediction method itself. To be sure that the singular value decomposition is implemented correctly, the singular value decomposition can be verified using the analytical solution to equation 5.45. To do this, a dataset consisting of u,$\dot{u}$ and the known force $F_{known} = F_0 + F_A \sin \omega t$ at different points in time is generated from the analytical solution.

The equation that the single value decomposition needs to solve is

$$\begin{bmatrix} \dot{u}_1 & u_1 \\ \vdots & \vdots \\ \vdots & \vdots \\ \dot{u}_n & u_n \end{bmatrix} \begin{bmatrix} X_{\dot{u}} \\ X_u \end{bmatrix} = \begin{bmatrix} F_{known,1} \\ \vdots \\ \vdots \\ F_{known,n} \end{bmatrix}. \tag{7.2}$$

Because every data point in the dataset is part of the analytical solution to the equation of motion, the singular value decomposition has to find the exact same $X_{\dot{u}}$ and X_u when implemented correctly, independently of the amount of data points n. Using the verification cases displayed in 5.1, the found values of $X_{\dot{u}}$ and X_u indeed match the input values. From this it can be concluded that the singular value decomposition is implemented correctly.

7.4 Testing coefficient sets in straight sailing

In the prediction method it is needed to specify the set of coefficients that need to be sought after. When the same set of coefficients is specified in the prediction method as is used to simulate the manoeuvre, the method should find the values of these coefficients with a slight error due to the truncation error of numerical integration and numerical differentiation. To test whether the combined method of differentiation and singular value decomposition is able to find the coefficients, the situation is considered where the ship is only sailing straight forward. For the motions pure sway and pure yaw, the exact same method can be used. The results for sway and yaw can be found in appendix J.

7.5 Testing the same set as used in simulation

The basis for this test is verification case 4, which includes only the hydrodynamic coefficients $X_{\dot{u}}$ and X_u. This case will be tested and then more coefficients will be added. The input values for the known forces are displayed in table 7.4.

Table 7.4: Input values for known forces in case 4.

F_0 [N]	F_A [N]	ω [rad/s]	m [kg]
10000000	7000000	0.01	320415000

The initial conditions are displayed in table 7.5.
The sets that are tested go up to third order. Because only longitudinal motion is considered, no coupling terms are included, because they would

Table 7.5: Initial conditions used in the simulation.

u_0 [m/s]	v_0 [m/s]	r_0 [rad/s]
7.9739	0	0

not have any influence. The sets of coefficients that are tested are displayed in table 7.6.

Table 7.6: Values of the coefficients that are used for testing in straight sailing.

Set	$X_{\dot{u}}$ [kg]	X_u [kg/s]	X_{uu} [kg/m]	X_{uuu} [kg s/m^2]
1	−1 000 000.00	−200 000.00	-	-
2	−100 000.00	−20 000.00	−10 000.00	-
3	−100 000.00	−20 000.00	−8 000.00	−500.00

Note that the coefficients in sets 2 and 3 with dashes are not used in the calculation. When the calculations are carried out, data sets are generated that can be used to find the coefficients. For finding these coefficient different time step sizes Δt for differentiation can be used. In table 7.7 the coefficients found with the prediction method for a differentiation time step of $\Delta t = 1$ are displayed. The found coefficients are close to the original input values. This can also be seen by calculating the relative errors, which are displayed in table 7.8

Table 7.7: Predicted coefficients for differentiation time step $\Delta t = 1$.

Set	$X_{\dot{u}}$ [kg]	X_u [kg/s]	X_{uu} [kg/m]	X_{uuu} [kg s/m^2]
1	−999 990.96	−199 999.99	-	-
2	−99 982.29	−20 000.09	−1 000 0.00	-
3	−99 998.55	−19 998.83	−8 000.12	−500.00

From the error calculation it can be concluded that the error for the added mass coefficient $X_{\dot{u}}$ is small but much larger than for the other coefficients calculated. This larger error is caused by rounding errors, because the acceleration is smaller than the velocity relatively more information is lost with the same amount of decimal places. A time step of 1 second was used to be sure that the truncation error is small. To show the influence of differentiation time step, the coefficients are also calculated using a differentiation time step of $\Delta t = 10$. These coefficients are displayed in 7.9.
Table 7.10 shows the errors when a differentiation time step of 10 seconds is used. It can be seen that the errors are much larger than when a timestep of 1 second is used. This is due to the truncation error of the numerical differentiation, which increases with increasing time steps.

Table 7.8: Relative error of predicted coefficients for differentiation time step $\Delta t = 1$.

Set	$\epsilon_{X_{\dot{u}}}$ [%]	ϵ_{X_u} [%]	$\epsilon_{X_{uu}}$ [%]	$\epsilon_{X_{uuu}}$ [%]
1	$-0.000\,9$	$-4.266\,7 \cdot 10^{-06}$	-	-
2	$-0.017\,7$	$0.000\,5$	$-3.459\,5 \cdot 10^{-05}$	-
3	$-0.001\,4$	$-0.005\,9$	$0.001\,5$	$-0.000\,6$

Table 7.9: Predicted coefficients for differentiation time step $\Delta t = 10$.

Set	$X_{\dot{u}}$ [kg]	X_u [kg/s]	X_{uu} [kg/m]	X_{uuu} [kg s/m^2]
1	$-984\,426.36$	$-199\,990.94$	-	-
2	$-74\,497.08$	$-20\,092.43$	$-9\,996.50$	-
3	$-99\,044.36$	$-18\,473.14$	$-8\,153.52$	-496.18

In table 7.10 it shown that the relative errors can be up to 25 % when a step size of 10 seconds is used. For this reason it can be concluded that it is better to use a time step of 1 second.

7.5.1 Testing when coefficients are 0 in straight sailing

It is shown that the prediction method can find the coefficients that are used to simulate a path of a ship, when the same set of coefficients is specified in the prediction method. When a coefficient is not used for simulation however, the prediction method should find that this coefficient has no influence and this coefficient should therefore be close to zero. To test if this is the case, the prediction method is used on set 1 and 2 from table 7.6 while specifying larger sets of coefficients in the prediction method. The coefficients predicted using data set 1 with different coefficients specified in the prediction method can be found in table 7.11. Because only motion in longitudinal direction is simulated, only coefficients that depend on u and $\dot{u}$ are considered.
To create data set 1, only coefficients $X_{\dot{u}}$ and X_u where used. In table 7.11 it can be seen that the other coefficients are indeed small and negligible compared to the size of $X_{\dot{u}}$ and X_u, while $X_{\dot{u}}$ and X_u still have values close

Table 7.10: Relative error of predicted coefficients for differentiation time step $\Delta t = 10$.

Set	$\epsilon_{X_{\dot{u}}}$ [%]	ϵ_{X_u} [%]	$\epsilon_{X_{uu}}$ [%]	$\epsilon_{X_{uuu}}$ [%]
1	$-1.557\,4$	$-0.004\,5$	-	-
2	$-25.502\,9$	$0.462\,2$	$-0.035\,0$	-
3	$-0.955\,6$	$-7.634\,3$	$1.919\,0$	$-0.764\,6$

Table 7.11: Coefficients predicted from data set 1 with different coefficient sets.

Set	$X_{\dot{u}}$ [kg]	X_u [kg/s]	X_{uu} [kg/m]	X_{uuu} [kg s/m^2]
Constant	−999 990.97	−199 999.99	-	-
Quadratic	−999 977.08	−200 000.09	0.00	-
Cubic	−999 988.13	−199 999.76	−0.02	0.00

to the original coefficients. In table 7.12 the coefficients calculated using data set 2 can be found.

Table 7.12: Coefficients predicted from data set 2 with different coefficient sets.

Set	$X_{\dot{u}}$ [kg]	X_u [kg/s]	X_{uu} [kg/m]	X_{uuu} [kg s/m^2]
Quadratic	−99 982.29	−20 000.09	−1 000 0.00	-
Cubic	−99 990.06	−19 999.69	−10 000.03	0.00

In this case the values of the coefficients used for the simulation also remain close to the original values, the added coefficient X_{uuu} is very small when compared to the values of the original set.

From these tests it can be concluded that the singular value decomposition returns coefficients close to zero when they have no influence on the manoeuvre.

7.6 Finding coefficients in 3 DOF

The prediction method is verified for straight sailing. Of course the goal is to find the hydrodynamic coefficients for planar motion, which means that coefficients for 3 DOF need to be found. To verify if the prediction method works for planar motion the coefficients are split up in 2 types. Hydrodynamic forces that depend on motions in another DOF than the force acts, such as X_{vv} ,Y_{uvv} and N_{ur} are called *coupled*. Hydrodynamic forces that only depend on motions in the same DOF as the force acts, such as X_u, Y_v and $N_r r$ are called *uncoupled*. Note that the 3 equations of motions are coupled, due to the inertial terms ur and vr in equation C.18.

7.6.1 Verification uncoupled coefficients in 3 DOF

First a set of uncoupled coefficients is tested. The initial conditions and the known forces used for simulation are displayed in table 7.13. Coefficients up to third order are used. The input values used for simulation are displayed

in table 7.14 together with the predicted coefficients for a differentiation step of 1 second.

Table 7.13: Initial conditions and known forces used for verification 3 DOF prediction.

u_0	7.9739	m/s
v_0	0	m/s
r_0	0.1	rad/s
$\dot{u}_0$	0	m/s^2
$\dot{v}_0$	0	m/s^2
$\dot{r}_0$	0	rad/s^2
x_0	0	m
y_0	0	m
ψ_0	0	rad
ω	0.01	rad/s
X_0	0	N
X_A	0	N
Y_0	0	N
Y_A	0	N
N_0	100000000	Nm
N_A	700000	Nm
$\mathrm{d}t$	1	s

In table 7.14 the error of the predicted coefficients is displayed. The errors are small compared to the size of the coefficients. This error is due to the truncation error of the used numerical differentiation method. When the quantity which needs to be multiplied with a coefficient is small, the rounding error is relatively larger, this is why the errors of $X_{\dot{u}}$, $Y_{\dot{v}}$, N_{rr} and N_{rrr} is of a different order of magnitude.
In table 7.15 the predicted coefficients and relative errors for with a differentiation time step of 10 seconds are displayed. The errors are much larger compared to the values in table 7.14. This is in accordance with the theory, which states that the truncation error of the differentiation method is of order $O(h^4)$.

7.6.2 Verification coupled coefficients in 3 DOF

It has been showed that the method is able to find coefficients in the case the only coupling between the DOF consists of the inertia term. From theory it is also found that coupling exists due to the hydrodynamic forces. To test if the method is able to find these *coupled* coefficients a set of coefficients based on low aspect ratio lift theory is used. The input values for the simulation and the output form the prediction method van be found in table 7.16 together

Table 7.14: Input and output values of a set uncoupled coefficients, with differentiation step Δt=1 s.

Coefficients	**Input**	**Output**	ϵ [%]
$X_{\dot{u}}$	−100 000.00	−102 865.95	2.87
X_u	−20 000.00	−20 163.55	0.82
X_{uu}	−8 000.00	−7 999.97	0.00
X_{uuu}	−500.00	−497.11	0.58
$Y_{\dot{v}}$	−100 000.00	−102 762.79	2.76
Y_v	−20 000.00	−20 068.92	0.34
Y_{vv}	−8 000.00	−7 994.59	0.07
Y_{vvv}	−500.00	−498.79	0.24
$N_{\dot{r}}$	$-1.00 \cdot 10^{+12}$	$-1\,0.00 \cdot 10^{+11}$	0.00
N_r	−10 000 000.00	−10 014 806.99	0.15
N_{rr}	−8 000 000.00	−7 909 224.52	1.13
N_{rrr}	−7 000 000.00	−7 179 149.01	2.56

Table 7.15: Input and output values of a set uncoupled coefficients, with differentiation step Δt=10 s.

Coefficients	**Input**	**Output**	ϵ [%]
$X_{\dot{u}}$	−100 000.00	−103 317.24	3.32
X_u	−20 000.00	−48 350.61	141.75
X_{uu}	−8 000.00	−6 606.73	17.42
X_{uuu}	−500.00	231.14	146.23
$Y_{\dot{v}}$	−100 000.00	−157 989.72	57.99
Y_v	−20 000.00	−20 526.94	2.63
Y_{vv}	−8 000.00	−8 666.61	8.33
Y_{vvv}	−500.00	−526.27	5.25
$N_{\dot{r}}$	$-1.00 \cdot 10^{+12}$	$-1.00 \cdot 10^{+12}$	0.01
N_r	−10 000 000.00	−9 927 675.65	0.72
N_{rr}	−8 000 000.00	−8 532 645.62	6.66
N_{rrr}	−7 000 000.00	−5 760 207.24	17.71

with the calculated relative errors.

Table 7.16: Input and output values of a test in 3 DOF with coupled coefficients.

Coefficients	**Input**	**Output**	ϵ [%]
$X_{\dot{u}}$	−100 000.00	−104 344.24	4.34
X_{uu}	−20 000.00	−19 998.46	0.01
X_{vv}	−8 000.00	−8 000.66	0.01
X_{rr}	−500.00	27 685.77	5 637.15
X_{vr}	−100 000.00	−95 714.82	4.29
$Y_{\dot{v}}$	−20 000.00	38 053.11	290.27
Y_{uv}	−8 000.00	−7 998.29	0.02
Y_{ur}	−500.00	57 733.71	11 646.74
Y_{uur}	−2 000.00	−2 007.62	0.38
Y_{vvr}	−2 000.00	−2 001.71	0.09
$N_{\dot{r}}$	$-1.00 \cdot 10^{+12}$	$-1.00 \cdot 10^{+12}$	0.02
N_{uv}	−10 000 000.00	−10 000 781.52	0.01
N_{ur}	−8 000 000.00	−8 016 022.25	0.20
N_{uur}	−7 000 000.00	−6 996 731.38	0.05
N_{vvr}	−7 000 000.00	−6 999 767.06	0.00

When looking at the errors in table 7.16 it is noticeable that the coefficients X_{rr}, $Y_{\dot{v}}$ and Y_{ur} have very large errors. The fact that the rest of the coefficients are predicted pretty accurately shows that the influence of the coefficients with large errors are small. Looking at X_{rr} it can be seen that this coefficient is rather small in comparison to other coefficients that express a longitudinal component of the hydrodynamic force. Note that also the values for r are very small compared to u and v, which makes $X_{rr}r^2$ a very small force. The fact that the coefficient has a small influence makes it hard to predict the value of the coefficient. To verify that this is the case, the same test is done again byt know the value of X_{rr} is increased. The results of this test are displayed in table 7.17 The influence of X_{rr} is now much larger, which makes it easier to find the value of the coefficient which is why the error of X_{rr} is much smaller in this test.

7.7 Using multiple paths for coefficient prediction

When the results of section 7.4 and section 7.6.2 are compared it can be seen that the errors of the coefficients are smaller in straight sailing. Because of this the question arises if the determination of the coefficients can become more accurate when more paths are used in the determination. This can be done in two ways:

Table 7.17: Input and output values of a test in 3 DOF with coupled coefficients.

Coefficients	**Input**	**Output**	ϵ [%]
$X_{\dot{u}}$	−100 000.00	−95 496.00	4.50
X_{uu}	−20 000.00	−20 002.00	0.01
X_{vv}	−8 000.00	−8 004.00	0.05
X_{rr}	−5 000 000.00	−4 975 715.00	0.49
X_{vr}	−100 000.00	−104 720.00	4.72
$Y_{\dot{v}}$	−2 000 000.00	−1 684 443.00	15.78
Y_{uv}	−8 000.00	−7 992.00	0.10
Y_{ur}	−500 000.00	−185 674.00	62.87
Y_{uur}	−2 000.00	−2 032.00	1.61
Y_{vvr}	−2 000.00	−2 011.00	0.56
$N_{\dot{r}}$	$-1.00 \cdot 10^{+12}$	$-1.00 \cdot 10^{+12}$	0.05
N_{uv}	−10 000 000.00	−9 998 221.00	0.02
N_{ur}	−8 000 000.00	−7 973 915.00	0.33
N_{uur}	−7 000 000.00	−7 006 357.00	0.09
N_{vvr}	−7 000 000.00	−7 000 762.00	0.01

- Use one manoeuvre to predict a part of the set of coefficients and use these as 'known' forces when using the other manoeuvre.

- Create one dataset, which consists of both manoeuvres and use the prediction method to find the coefficients.

7.7.1 Predict part of set

In this case the same set of coefficients is used as in table 7.17, but know 2 manoeuvres will be simulated. The same manoeuvre as used in section 7.6.2 will be simulated together with a straight path where the ship accelerates. When sailing straight only the coefficients $X_{\dot{u}}$ and X_{uu} have their influence, which then can be predicted pretty accurately as showed in section 7.4. With these coefficients known this part of the hydrodynamic forces can be calculated and subtracted in the second manoeuvre. In this way it is possible to increase the accuracy of $X_{\dot{u}}$ and X_{uu}. Because X_{vr} is also an inertial contribution just like $X_{\dot{u}}$, the accuracy of this coefficient will increase too. In table 7.18 the results are displayed when first a straight path is used to predict $X_{\dot{u}}$ and X_{uu}. It can be seen that the values for the coefficients in x-direction are much closer to the original than the coefficients found in table 7.17. Especially the inertial coefficient $X_{\dot{u}}$ is predicted better when only straight sailing is considered, which also makes the predicted value of X_{vr} much closer to the input value. To improve the values of the Y-coefficients

Table 7.18: Input and output values of a test in 3 DOF with coupled coefficients, where 2 paths are used.

Coefficients	**Input**	**Output**	ϵ [%]
$X_{\dot{u}}$	−100 000.00	−99 994.00	0.01
X_{uu}	−20 000.00	−20 000.00	0.00
X_{vv}	−8 000.00	−8 002.00	0.03
X_{rr}	−5 000 000.00	−4 974 226.00	0.52
X_{vr}	−100 000.00	−100 204.00	0.20
$Y_{\dot{v}}$	−2 000 000.00	−1 684 443.00	15.78
Y_{uv}	−8 000.00	−7 992.00	0.10
Y_{ur}	−500 000.00	−185 674.00	62.87
Y_{uur}	−2 000.00	−2 032.00	1.61
Y_{vvr}	−2 000.00	−2 011.00	0.56
$N_{\dot{r}}$	$-1.00 \cdot 10^{+12}$	−999 458 929 786.00	0.05
N_{uv}	−10 000 000.00	−9 998 221.00	0.02
N_{ur}	−8 000 000.00	−7 973 915.00	0.33
N_{uur}	−7 000 000.00	−7 006 357.00	0.09
N_{vvr}	−7 000 000.00	−7 000 762.00	0.01

a motion with only a v-component can be used, although it is much less realistic to perform a manoeuvre with only sway.

7.7.2 Create data set from 2 manoeuvres

Instead of using the first manoeuvre to calculate more of the known forces, the two manoeuvres can also be used in one dataset to get more points for the coefficient determination. Notice that it is needed to differentiate first and then join the two manoeuvres in one dataset, because the data will be discontinuous at the boundary between the two manoeuvres. After differentiation the velocity vectors, acceleration and force vectors of the two manoeuvres are merged into 1 new set of velocity, acceleration and force vectors. Now the singular value decomposition can be applied to find the coefficients. The resulting set of found coefficients is displayed in table 7.19 It can be seen that the values for the coefficients in x-direction are much closer to the original than the coefficients found in table 7.17. The coefficients predicted found in 7.18 are even closer though. The reason for this is that data that is less suitable for predicting added mass, namely the 3 DOF manoeuvre is also used for predicting added mass, which increases the error. The reason that the 3 DOF manoeuvre is less suitable for finding the added mass $X_{\dot{u}}$ is the fact that the total inertial part of the equation of motion in x-direction is: $(m + X_{\dot{u}})\dot{u} + (-m + X_{vr})vr$. When a motion in 3 DOF is considered, the term that depends on vr is not zero. This means that

Table 7.19: Input and output values of a test in 3 DOF with coupled coefficients, where 2 paths are used and merged into 1 dataset.

Coefficients	**Input**	**Output**	ϵ [%]
$X_{\dot{u}}$	−100 000.00	−99 653.00	0.35
X_{uu}	−20 000.00	−20 000.00	0.00
X_{vv}	−8 000.00	−8 003.00	0.03
X_{rr}	−5 000 000.00	−4 975 058.00	0.50
X_{vr}	−100 000.00	−100 546.00	0.55
$Y_{\dot{v}}$	−2 000 000.00	−1 684 443.00	15.78
Y_{uv}	−8 000.00	−7 992.00	0.10
Y_{ur}	−500 000.00	−185 674.00	62.87
Y_{uur}	−2 000.00	−2 032.00	1.61
Y_{vvr}	−2 000.00	−2 011.00	0.56
$N_{\dot{r}}$	$-1.00 \cdot 10^{+12}$	$-1.00 \cdot 10^{+12}$	0.05
N_{uv}	−10 000 000.00	−9 998 221.00	0.02
N_{ur}	−8 000 000.00	−7 973 915.00	0.33
N_{uur}	−7 000 000.00	−7 006 357.00	0.09
N_{vvr}	−7 000 000.00	−7 000 762.00	0.01

the error of both v and r cause an extra error in the coefficient $X_{\dot{u}}$ which is relatively large due to multiplication of both quantities.

From these tests it can be concluded that a more accurate result can be obtained when more different manoeuvres are used. The best result can be obtained by cleverly selecting multiple manoeuvres, such that a subset of the total set of coefficients can be found accurately, this subset can then be used to subtract part of the hydrodynamic forces in the other manoeuvre(s) which increases the accuracy for the other coefficients. This method is shown to be accurate for determining added mass. The method where multiple different manoeuvres are used to create one data set is much faster however. A second advantage of this method is that more manoeuvres can be used to determine a set of coefficients, which may be needed when one manoeuvre does not contain enough information to determine a (sub)set of coefficients.

Chapter 8

Model validation

In this chapter the validation of the prediction method is discussed. In the first paragraph simulations using coefficient sets based on a single manoeuvre are compared with results of the MMG method. In the second paragraph the hydrodynamic forces during a simulated manoeuvre are discussed. In the last paragraph the results of the prediction method are discussed when more manoeuvres are used to find a set of coefficients.

8.1 Comparing manoeuvres with MMG data

To make sure that the results of the implemented method are valid, the method needs to be validated. To determine whether the developed method is able to give a set of manoeuvring coefficients which can reproduce the manoeuvring behaviour of the vessel, the method is tested using manoeuvres calculated with the MMG method. To validate the method, different manoeuvres are simulated using the MMG model, these manoeuvres are then used to determine the manoeuvring coefficients. In this chapter the coefficients are made non-dimensional to be able to compare them to MMG results. The method of non-dimensionalization is given in appendix K, dimension-full coefficients can be found in L. To check if the a valid solution is found, the same manoeuvre is simulated using the found coefficients. To check how much influence every single coefficient has, every component of the hydrodynamic force can be plotted against time to give insight in the magnitude of every component.

Because trial data are often available at STC when a ship model is implemented, standard trials are used to validate the method. The sets of manoeuvring coefficients found can then be used to simulate the same manoeuvre to find how close the behaviour is to that of the MMG model. The found set can also be used tot predict a different manoeuvre. The total set of validation cases can be found in table 8.1.

Table 8.1: Test scheme for validation using MMG model.

Input	Predict
straight sailing	straight sailing
10/10 zig-zag	10/10 zig-zag
10/10 zig-zag	20/20 zig-zag
10/10 zig-zag	turning circle
20/20 zig-zag	20/20 zig-zag
20/20 zig-zag	10/10 zig-zag
20/20 zig-zag	turning circle
turning circle	turning circle
turning circle	10/10 zig-zag
turning circle	20/20 zig-zag

8.1.1 Validation of resistance

First the predicted coefficients in straight sailing are validated. This is equivalent to validation of the resistance. The coefficients found by the prediction method are displayed in table L.1. These coefficients can be used tot simulate the ship in straight sailing again. Note that a large part of the coefficients is zero. These coefficients play no role in this manoeuvre and therefore cannot be determined, the SVD algorithm sets these coefficients equal to zero. When the condition numbers of the velocity matrices are calculated, they are all three found to be equal to infinity. This means that the problem is ill-posed and that the solution is not unique. This is caused by the coefficients that cannot be determined because their corresponding velocities and accerations are zero. Every coefficient that cannot be determined makes one of the singular values equal to zero. When the coefficients that have no influence are excluded from the prediction method, exactly the same values for $X_{\dot{u}}$, X_{uu} and X_{uuu} are found, and the value for the condition number is $\kappa(A_X) = 1464143.378$, which is finite and thus a unique solution. It should be noted that the coefficient $X_{\dot{u}}$ in table 8.2 is very close to the original value of the MMG method, which has a value of 0.022. From this it can be concluded that accelerating in a straight line is a good manoeuvre to determine the added mass accurately. In figure 8.1 the velocity of the vessel using found coefficient is displayed together with the velocity found using the MMG coefficients.

8.1.2 Validation using 10/10 zig-zag trial

One of the manoeuvres which is calculated using the MMG method is the 10/10 zig-zag manoeuvre. When the prediction method is used on this manoeuvre, the coefficients in table 8.3 are found. Because this manoeuvre involves motions in all 3 DOF considered, a value is found for all coefficients.

Table 8.2: Table of al the dimensionless coefficients based on low aspect ratio lift theory found in straight sailing.

$X'_{\dot{u}}$	$-0.022\,001$	$Y'_{\dot{v}}$	$0.000\,000$	$N'_{\dot{r}}$	$0.000\,000$
X'_{uu}	$-0.022\,000$	Y'_{uv}	$0.000\,000$	N'_{uv}	$0.000\,000$
X'_{uuu}	$-4.996\,520 \cdot 10^{-10}$	Y'_{ur}	$0.000\,000$	N'_{ur}	$0.000\,000$
X'_{vv}	$0.000\,000$	Y'_{uur}	$0.000\,000$	N'_{uur}	$0.000\,000$
X'_{rr}	$0.000\,000$	Y'_{uuv}	$0.000\,000$	N'_{uuv}	$0.000\,000$
X'_{vr}	$0.000\,000$	Y'_{vvv}	$0.000\,000$	N'_{vvv}	$0.000\,000$
X'_{uvv}	$0.000\,000$	Y'_{rrr}	$0.000\,000$	N'_{rrr}	$0.000\,000$
X'_{rvu}	$0.000\,000$	Y'_{rrv}	$0.000\,000$	N'_{rrv}	$0.000\,000$
X'_{urr}	$0.000\,000$	Y'_{vvr}	$0.000\,000$	N'_{vvr}	$0.000\,000$
		$Y'_{v\|v\|}$	$0.000\,000$	$N'_{v\|v\|}$	$0.000\,000$
		$Y'_{r\|v\|}$	$0.000\,000$	$N'_{r\|v\|}$	$0.000\,000$
		$Y'_{v\|r\|}$	$0.000\,000$	$N'_{v\|r\|}$	$0.000\,000$
		$Y'_{r\|r\|}$	$0.000\,000$	$N'_{r\|r\|}$	$0.000\,000$

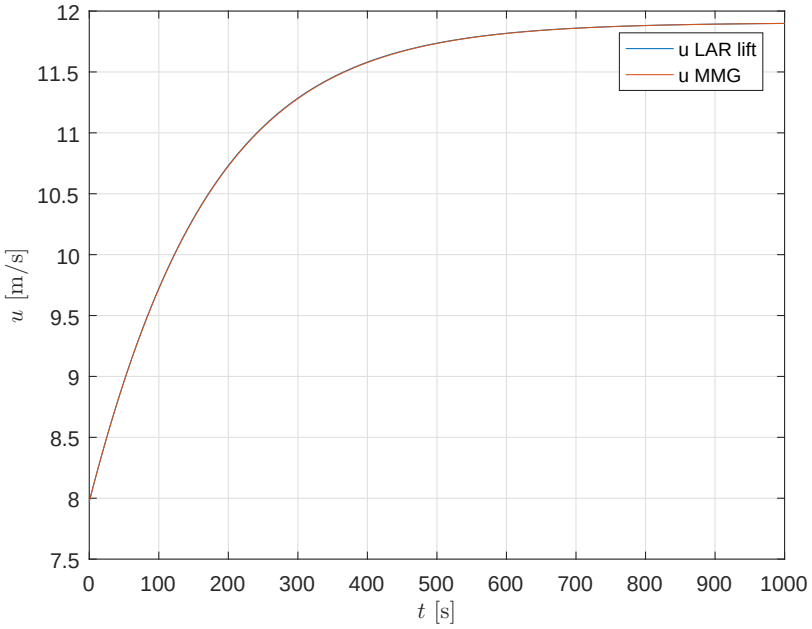

Figure 8.1: Plot of the velocity in straight sailing calculated with third order coefficients.

Because the ship is the same as when straight sailing was simulated, it is expected that the coefficients involved in both manoeuvres should be the same. It can be seen that the coefficients $X_{\dot{u}}$ and X_{uu} are in the same order of magnitude as found from straight sailing. X_{uuu} is approximately 2000 times bigger however.

Table 8.3: Table of al the dimensionless coefficients based on low aspect ratio lift theory found with 10/10 zig-zag manoeuvre.

$X'_{\dot{u}}$	−0.020 314	$Y'_{\dot{v}}$	−0.254 329	$N'_{\dot{r}}$	−0.012 812
X'_{uu}	−0.022 361	Y'_{uv}	−0.485 691	N'_{uv}	−0.093 928
X'_{uuu}	0.000 001	Y'_{ur}	0.008 202	N'_{ur}	−0.029 157
X'_{vv}	−0.505 162	Y'_{uur}	0.027 523	N'_{uur}	−0.009 919
X'_{rr}	−0.055 075	Y'_{uuv}	0.077 980	N'_{uuv}	−0.024 508
X'_{vr}	−0.358 526	Y'_{vvv}	18.424 394	N'_{vvv}	−7.618 022
X'_{uvv}	0.254 096	Y'_{rrr}	2.075 088	N'_{rrr}	−0.807 732
X'_{rvu}	0.179 115	Y'_{rrv}	13.072 945	N'_{rrv}	−5.075 244
X'_{urr}	0.026 726	Y'_{vvr}	28.343 265	N'_{vvr}	−10.935 739
		$Y'_{v\|v\|}$	−0.249 748	$N'_{v\|v\|}$	0.079 871
		$Y'_{r\|v\|}$	0.071 865	$N'_{r\|v\|}$	−0.020 759
		$Y'_{v\|r\|}$	−0.056 236	$N'_{v\|r\|}$	0.016 771
		$Y'_{r\|r\|}$	0.054 895	$N'_{r\|r\|}$	−0.016 340

To compare the manoeuvring behaviour of the vessel, the predicted coefficients are used to simulate a 10/10 zig-zag manoeuvre. To simulate the manoeuvres the same external forces are used, as where used in the MMG simulation. In figure 8.2 the track of the 10/10 zig-zag manoeuvre is displayed as simulated using the MMG coefficients and the low aspect ratio lift coefficients as predicted from the MMG track.
The same coefficents can be used to simulate a 20/20 zig-zag trial, the resulting track is displayed in figure 8.3 together with the 20/20 zig-zag manoeuvre that is calculated using the MMG Model.

8.1.3 Validation using 20/20 zig-zag trial

In figure 8.5 the track of the 20/20 zig-zag manoeuvre is displayed as found from the MMG method and the low aspect ratio lift coefficients.
The coefficient for lateral added mass $Y'_{\dot{v}}$ in table 8.4 is close to the value found in the MMG method which is equal to -0.223. The coefficient for added mass moment of inertia is close to the value -0.011 found in MMG method.
In figure 8.5 it can be seen that the coefficients derived from a zig-zag manoeuvre leads to a track that resembles the results of the MMG method. From the picture it can also be concluded that the deviation from the ori-

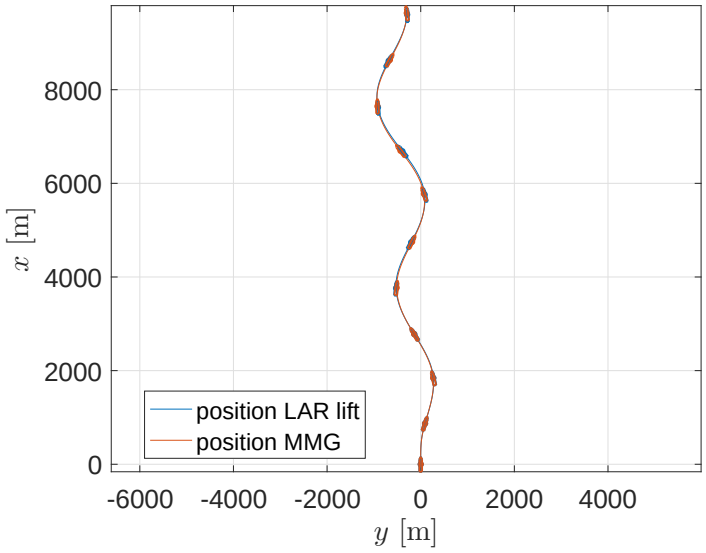

Figure 8.2: Plot of the position of the 10/10 zig-zag trial calculated with Low aspect ratio lift coefficients. Every 100 seconds a contour of the ship is plotted.

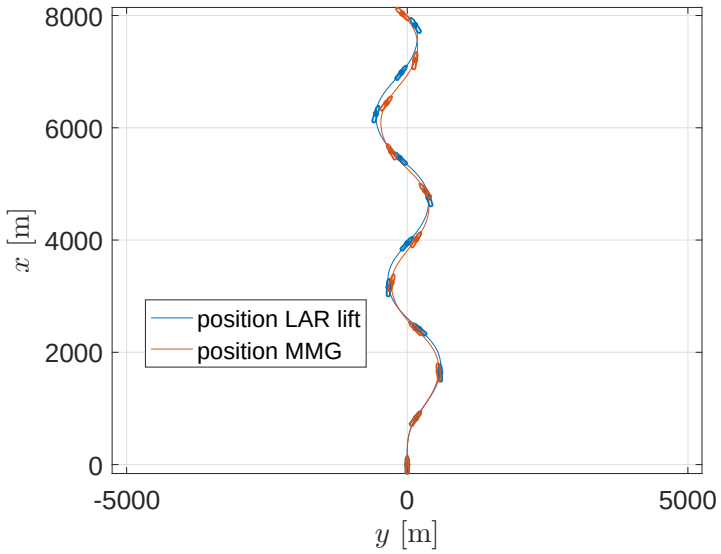

Figure 8.3: Plot of the position of the 20/20 zig-zag trial calculated with third order coefficients, predicted with a 10/10 zig-zag trial. Every 100 seconds a contour of the ship is plotted.

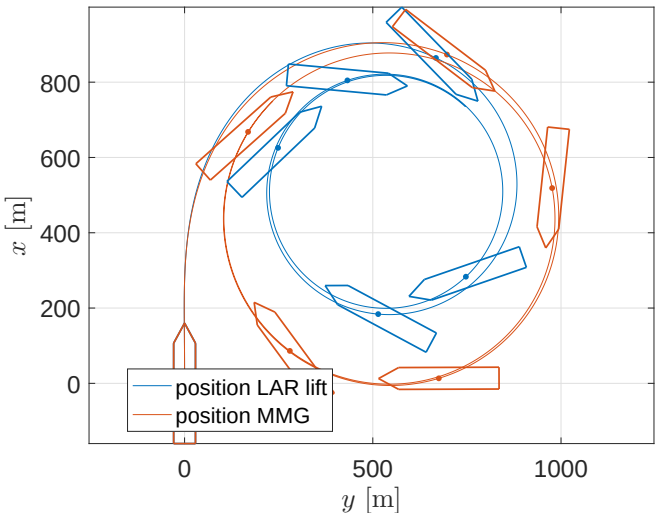

Figure 8.4: Plot of the position of a turning circle manoeuvre calculated with third order coefficients, predicted with a 10/10 zig-zag trial. Every 175 seconds a contour of the ship is plotted.

Table 8.4: Table of al the dimensionless coefficients based on low aspect ratio lift theory found with 20/20 zig-zag manoeuvre.

$X'_{\dot{u}}$	−0.017 133	$Y'_{\dot{v}}$	−0.265 278	$N'_{\dot{r}}$	−0.013 291
X'_{uu}	−0.022 526	Y'_{uv}	−0.751 567	N'_{uv}	−0.039 710
X'_{uuu}	0.000 001	Y'_{ur}	−0.066 293	N'_{ur}	−0.014 690
X'_{vv}	−2.060 707	Y'_{uur}	0.081 841	N'_{uur}	−0.021 871
X'_{rr}	−0.340 434	Y'_{uuv}	0.289 300	N'_{uuv}	−0.070 054
X'_{vr}	−1.719 814	Y'_{vvv}	7.560 649	N'_{vvv}	−3.329 158
X'_{uvv}	1.743 434	Y'_{rrr}	0.897 192	N'_{rrr}	−0.331 147
X'_{rvu}	1.461 417	Y'_{rrv}	5.470 483	N'_{rrv}	−1.988 940
X'_{urr}	0.295 301	Y'_{vvr}	12.842 578	N'_{vvr}	−4.623 796
		$Y'_{v\|v\|}$	−0.071 729	$N'_{v\|v\|}$	0.041 892
		$Y'_{r\|v\|}$	−0.007 264	$N'_{r\|v\|}$	0.014 482
		$Y'_{v\|r\|}$	0.003 822	$N'_{v\|r\|}$	0.010 536
		$Y'_{r\|r\|}$	0.011 647	$N'_{r\|r\|}$	0.000 826

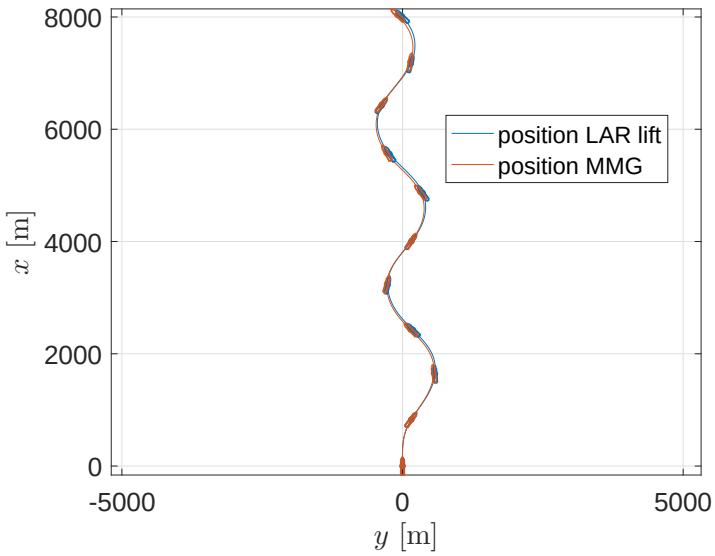

Figure 8.5: Plot of the position of the 20/20 zig-zag trial calculated with third order coefficients predicted using 20/20 MMG zig-zag manoeuvre. Every 100 seconds a contour of the ship is plotted.

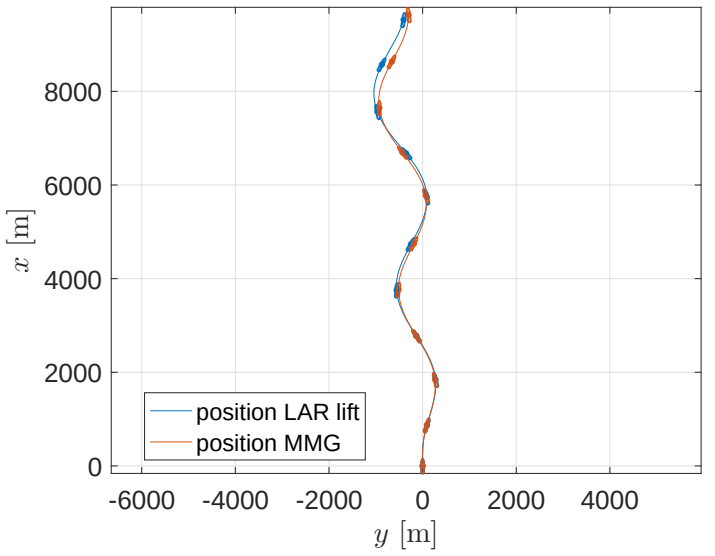

Figure 8.6: Plot of the position of the 10/10 zig-zag trial calculated with third order coefficients, predicted with a 20/20 zig-zag trial. Every 100 seconds a contour of the ship is plotted.

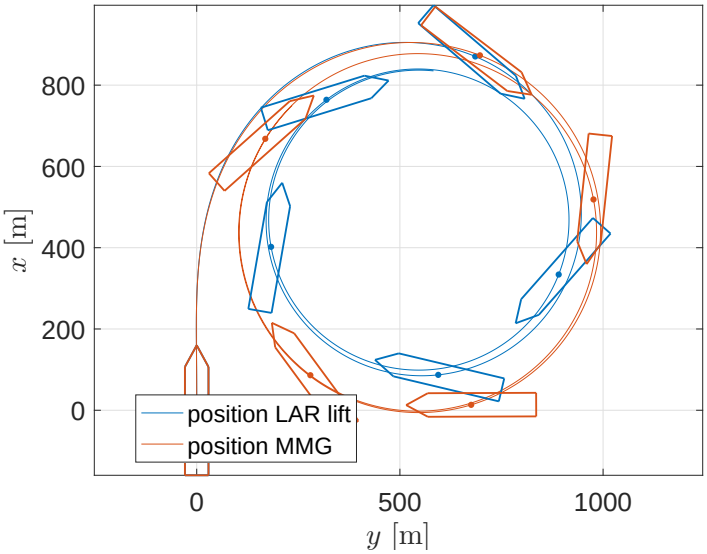

Figure 8.7: Plot of the position of the turning circle manoeuvre calculated with third order coefficients, predicted with a 20/20 zig-zag trial. Every 175 seconds a contour of the ship is plotted.

ginal track increases over time. This is caused by the accumulation of errors over time, which are caused by uncertainties in the predicted coefficients. In figure 8.7 a turning circle is simulated using the coefficients obtained from the 20/20 zig-zag manoeuvre. The figure shows that the tracks almost coincide for the first 175 seconds, behind this point however the two tracks start to deviate from each other, resulting in an underestimated tactical diameter.

8.1.4 Validation using Turning circle

In figure 8.8 the turning circle manoeuvre simulated with the coefficients in table 8.5 is compared with the turning circle manoeuvre as simulated using the MMG method. The manoeuvre calculated with low aspect ratio lift theory is plotted till $t = 206$, because at this time the lateral velocity starts to explode, eventually resulting in infinite velocities. This is caused by the square absolute terms, which will be discussed further in sectio 8.2.

It can be concluded that that the set of coefficients based on low aspect ratio lift theory determined with singular value decomposition is able to recreate a zig-zag manoeuvre. In the case of a turning circle the method is only able to recreate the beginning of the manoeuvre. The coefficients obtained from a zig-zag manoeuvre however are able to recreate a turning circle manoeuvre although the turning circle diameter is underestimated.

Table 8.5: Table of al the dimensionless coefficients based on low aspect ratio lift theory found with turning circle manoeuvre.

$X'_{\dot{u}}$	-0.013386	$Y'_{\dot{v}}$	-0.351591	$N'_{\dot{r}}$	-0.018038
X'_{uu}	-0.061373	Y'_{uv}	0.892320	N'_{uv}	-0.258894
X'_{uuu}	0.000120	Y'_{ur}	2.701388	N'_{ur}	-0.817982
X'_{vv}	-1.626419	Y'_{uur}	-3.666798	N'_{uur}	1.096488
X'_{rr}	-0.371995	Y'_{uuv}	-6.415128	N'_{uuv}	1.807939
X'_{vr}	-1.775817	Y'_{vvv}	54.938818	N'_{vvv}	-14.126234
X'_{uvv}	1.323957	Y'_{rrr}	1.617930	N'_{rrr}	-0.491884
X'_{rvu}	1.470504	Y'_{rrv}	5.380216	N'_{rrv}	-0.972883
X'_{urr}	0.312051	Y'_{vvr}	32.890340	N'_{vvr}	-8.026087
		$Y'_{v\|v\|}$	-28.808766	$N'_{v\|v\|}$	8.327702
		$Y'_{r\|v\|}$	12.624785	$N'_{r\|v\|}$	-4.008834
		$Y'_{v\|r\|}$	-12.624785	$N'_{v\|r\|}$	4.008834
		$Y'_{r\|r\|}$	3.303865	$N'_{r\|r\|}$	-1.071149

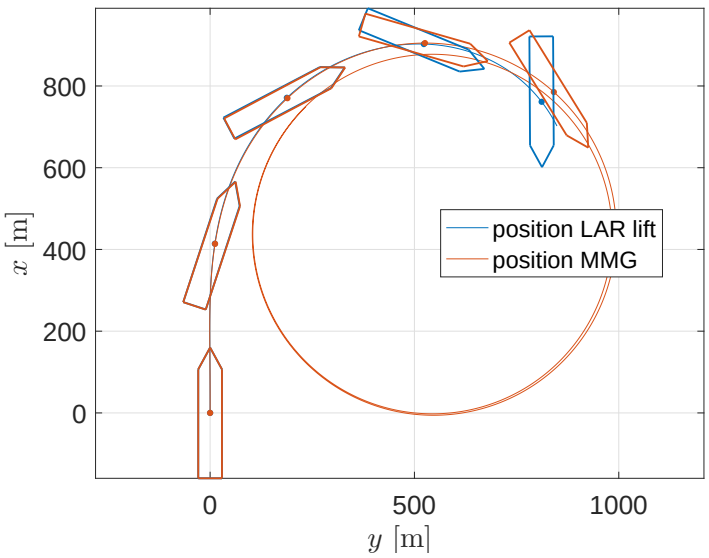

Figure 8.8: Plot of the position of the turning circle manoeuvre calculated with Low aspect ratio lift coefficients. Every 50 seconds a contour of the ship is plotted.

8.2 Comparing coefficient influences

It is shown that the coefficients based on low aspect ratio can be used to simulate straight sailing, zig-zag manoeuvres and turning circle manoeuvres. In this section it will be shown which coefficients of the set are the most important for the simulation of these manoeuvres. Because the MMG-method is only validated for turning circle and 20/20 zig/zag manoeuvres, only these manoeuvres are discussed in this section.

8.2.1 Hydrodynamic force components during 20/20 zig-zag manoeuvre

To get insight in the influence of each coefficient on the total hydrodynamic force, the contribution to the total force of each coefficient is plotted together with the total force.

Longitudinal hydrodynamic force

In figure 8.9 the contribution of each coefficient to the longitudinal hydrodynamic force is plotted.

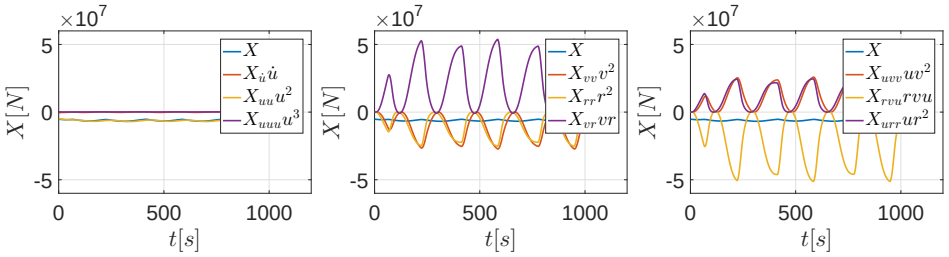

(a) (b) (c)

Figure 8.9: Comparison of longitudinal force components during 20°/20° zig-zag trial.

In figure 8.9 it is noticable that the influence of X_{uu} only, approximates the total longitudinal hydrodynamic force X already very well. Although every single contribution of X_{vv}, X_{rr}, X_{vr}, X_{uvv}, X_{rvu} and X_{urr} is much larger, they don't seem to contribute much to the total longitudinal force X. The contributions of these coefficients however almost cancel each other out. This could be the result of the small longitudinal acceleration, which could lead to approximately the same behaviour as caused by a longitudinal acceleration of zero. In section 6.3.1 it is explained why no distinction can be made when the longitudinal acceleration is zero. When this is indeed caused by the effect described, we should find the following relationship between

pairs of coefficients:

$$\frac{X_{vv}}{X_{uvv}} \approx -u, \ \frac{X_{rr}}{X_{urr}} \approx -u, \ \frac{X_{vr}}{X_{rvu}} \approx -u. \tag{8.1}$$

Using the coefficients found, which are displayed in table L.3, the ratios become

$$\frac{X_{vv}}{X_{uvv}} = -9.4249, \ \frac{X_{rr}}{X_{urr}} = -9.1929, \ \frac{X_{vr}}{X_{rvu}} = -9.3837. \tag{8.2}$$

When these values are compared with the longitudinal velocity profile in figure 8.11a, it can be seen that these values indeed approximate the longitudinal velocity during the zig-zag trial. Therefore it can be concluded that the longitudinal velocity does not vary enough during a 20°/20° zig-zag trial to make a distinction between X_{vr} and X_{rvu}, X_{vv} and X_{uvv} and X_{urr} and X_{rr}. In this case it might be better to fit the a set of coefficients without the third order terms to get a better estimate of X_{vr} ,X_{vv} and X_{rr}. To determine the third order coefficients it could be better to use manoeuvre in which the longitudinal velocity u varies more. The cancellation of components of the hydrodynamic force show that a set consisting of less coefficients could model the same behaviour.

In figure 8.9 it can also be seen that X_{uuu} almost doesn't contribute to the total longitudinal hydrodynamic force. This shows that the longitudinal hydrodynamic force behaves mainly quadratic with respect to longitudinal velocity as can be expected from the theory of resistance.

Lateral hydrodynamic force

In figure 8.10 the contributions of the coefficients to the lateral hydrodynamic force are plotted. It is noticeable that in this case there are sets of components that seem to cancel the influence of each other on the total force. The contributions of the coefficients Y_{ur} and Y_{uur} almost cancel each other because of the small changes in u, a more detailed explanation about this phenomenon can be found in section 6.3.1. The coefficients in figure 8.10b also show a behaviour of cancellation, although this originates from a different cause. In this case the cancellation of the coefficients is not caused a velocity coefficient being so small that 2 coefficient can not be distinguished. Still Y_{vvr} and Y_{rvv} almost cancel each other and also Y_{vvv} and Y_{rrr} seem to cancel each other. The only way this can be the case is when there is a linear relationship between v and r.
When v and r are compared for a 20°/20° zig-zag trial, as is done in figure 8.11, it can be seen that v and r show an almost linear relationship. Because of this the singular value decomposition results in a set of coefficients that makes a good fit on the original track, by almost cancelling 2 large forces.

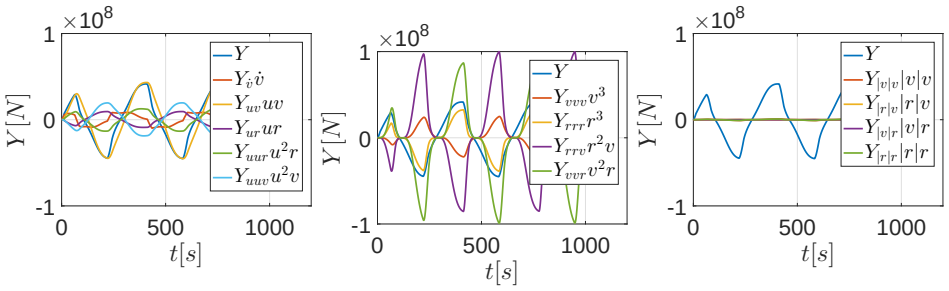

(a) (b) (c)

Figure 8.10: Comparison of lateral force components during 20°/20° zig-zag trial.

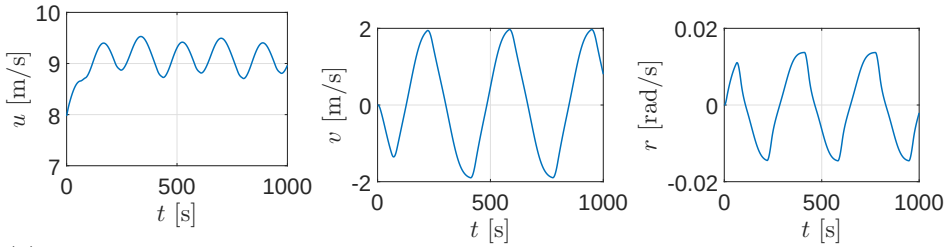

(a) Longitudinal velocity u. (b) Lateral velocity v. (c) Angular velocity r.

Figure 8.11: Velocities u, v and r during 20°/20° zig-zag trial.

The largest contribution to the total lateral hydrodynamic force is by the coefficient Y_{uv} which corresponds to part of the linear lift. Because the moment around the z-axis is very much coupled with the lateral force, the same applies for the N-coefficients for which the force contributions can be found in figure 8.12.

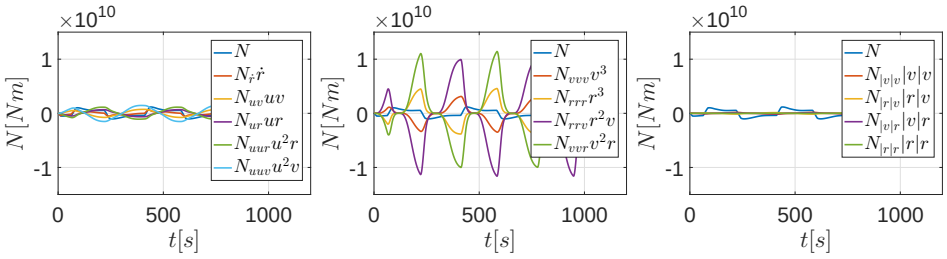

(a) (b) (c)

Figure 8.12: Comparison of vertical moment components during 20°/20° zig-zag trial.

The cancellation of components of the hydrodynamic force show that a set consisting of less coefficients could model the same behaviour.

8.2.2 Hydrodynamic force components during turning circle manoeuvre

The coefficients found using the turning circle manoeuvre where not able to reproduce the entire turning circle manoeuvre. This is caused by the exploding values of the hydrodynamic forces. Decomposing the hydrodynamic forces can give insight in the coefficients that cause the hydrodynamic forces to explode.

Longitudinal hydrodynamic force

In figure 8.13 the longitudinal force contributions are plotted. The longitudinal hydrodynamic force should be almost constant over time and close to zero. This is expected because the longitudinal velocity is almost constant during a turning circle. Due to the coefficients that represent the longitudinal force due to rotation and lateral motion the longitudinal hydrodynamic force becomes negative which results in a deceleration of the longitudinal velocity, this can be seen in figure 8.14a. The same cancelling behaviour can be seen that is explained in section 8.2.1 for these coefficients. The forces do not cancel entirely however, which results in the negative longitudinal force and the decrease in velocity.
Figure 8.15 shows the components of the lateral hydrodynamic force. It should be noted that in this case the total lateral hydrodynamic force is

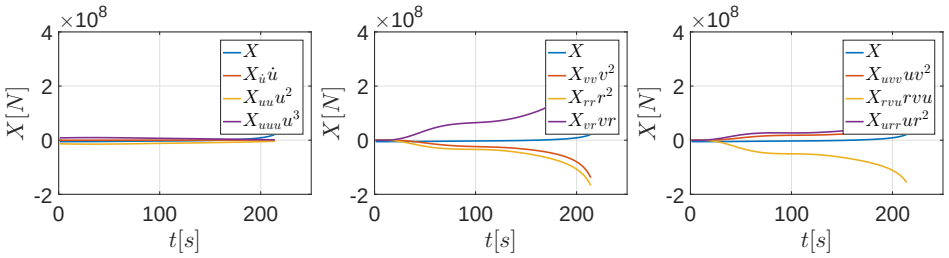

(a) (b) (c)

Figure 8.13: Comparison of lateral force components during turning circle manoeuvre.

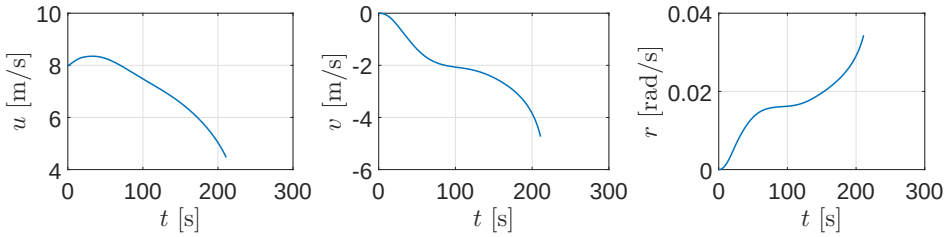

(a) Longitudinal velocity u (b) Lateral velocity v (c) Angular velocity r

Velocities u, v and r during turning circle manoeuvre.

almost an order of magnitude larger than the single components. This is mostly caused by the contributions of $Y_{|v|v}$,$Y_{|r|v}$,$Y_{|v|r}$ and $Y_{|r|r}$ which all cause a force in the same direction. This force causes a decrease in the lateral velocity, which will increase the force again. The square absolute terms are included because it is expected that the vessel shows the same behaviour when moving in opposite directions. In the case of a turning circle however, only motion in one direction of v en r is included, which makes determination of the square absolute terms unreliable. A similar behaviour happens with the moments around the z-axis which are displayed in 8.16. These moments and the lateral force are strongly coupled. The contributions of $N_{|v|v}$,$N_{|r|v}$,$N_{|v|r}$ and $N_{|r|r}$ act all in the same direction causing the angular velocity of the vessel to increase in magnitude. When a closer look is taken at 8.8 it can be seen that the path of the vessel simulated wit Low aspect ratio lift coefficient follows the original track really well till around t=150 s. This corresponds to the increase in forces and moments which can be seen in figures 8.15 and 8.16. This increase starts near t=100 s and becomes significant at t=150 s.

Because the coefficients depending on the square absolute terms determined from zig-zag manoeuvres show different signs this set is able to simulate a turning circle manoeuvre. This change in sign is caused by the fact that v and r become both positive and negative during a zig-zag manoeuvre, but

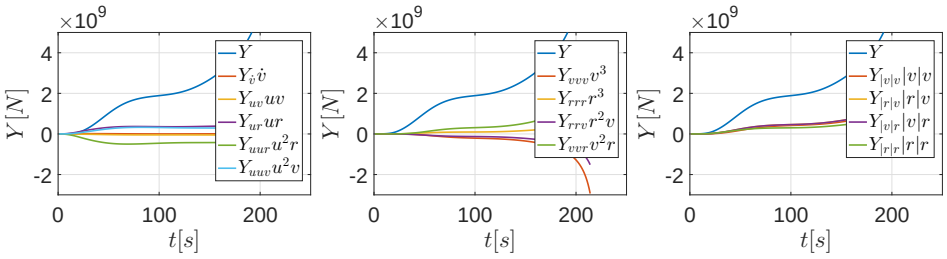

(a) (b) (c)

Figure 8.15: Comparison of lateral force components during turning circle manoeuvre.

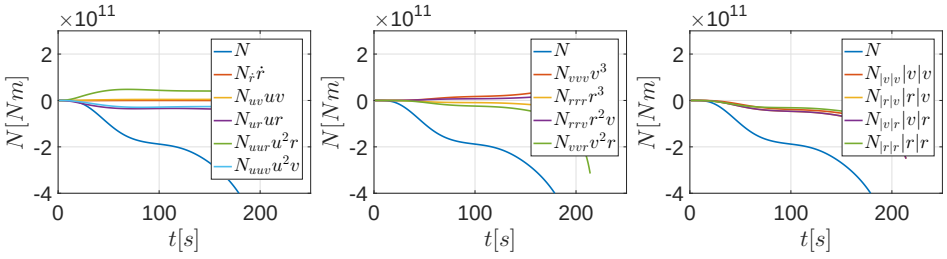

(a) (b) (c)

Figure 8.16: Comparison of lateral force components during turning circle manoeuvre.

have only positive or negative sign during the turning circle manoeuvre.

8.3 Validation using multiple manoeuvres

From the results of a single manoeuvre it is concluded that some manoeuvres do not contain enough information about the behaviour of a vessel to predict a set of coefficients. In section 7.7 it is showed that the accuracy of the prediction method can be increased by using more different manoeuvres. Two methods were tested, the first method predicts a part of the set with one manoeuvre, which can be done more accurately by selecting the right manoeuvre. In this section the second method is used where multiple manoeuvres are merged into one dataset, this dataset is then used to predict the coefficients. The second method is used because it can theoretically use an unlimited amount of manoeuvres and is therefore suitable to create information-rich datasets to determine coefficients.

8.3.1 Combining Turning circle and zig-zag manoeuvre

A few problems found during the single manoeuvre tests can already be solved by combining them in one data set. When the 20/20 zig-zag manoeuvre and turning circle are combined, this should already partly eliminate the problems with the square absolute terms found with only a turning circle, because there are positive and negative values of v and r in the dataset. The coefficients found when using both a 20/20 zig-zag manoeuvre and a turning circle manoeuvre are displayed in table 8.6.
The square absolute terms in table 8.6 show lower values than when only the turning circle manoeuvre was used to find the coefficients, also the signs have changed. The coefficients for added mass are also closer to the original values of the MMG method. In figure 8.17a the turning circle is plotted using the coefficients from table 8.6 together with the turning circle manoeuvre obtained from MMG results. Figure 8.17a shows that entire turning circle can now be modelled, which was not possible with the coefficients obtained from a turning circle only, which shows that the addition of information solves the problems that where encountered with the coefficients found with only a turning circle manoeuvre. The plot shows also better accordance with the MMG results than the turning circle simulated with coefficients obtained from a zig-zag manoeuvre. With the coefficients obtained from a zig-zag manoeuvre the tactical diameter of the turning circle manoeuvre was underestimated. In figure 8.17a it is shown that the coefficients determined with both turning circle and 20/20 zig-zag manoeuvre can model a turning circle manoeuvre that resembles the MMG results. In figure 8.18a a 20/20 zig-zag manoeuvre is plotted, simulated using the coefficients found with zig-zag and turning circle manoeuvres. This manoeuvre is also closer to

Table 8.6: Table of al the dimensionless coefficients based on low aspect ratio lift theory found from combined 20/20 zig-zag and turning circle manoeuvres.

$X'_{\dot{u}}$	$-0.025\,216$	$Y'_{\dot{v}}$	$-0.293\,555$	$N'_{\dot{r}}$	$-0.014\,254$
X'_{uu}	$-0.016\,979$	Y'_{uv}	$-1.617\,860$	N'_{uv}	$0.154\,935$
X'_{uuu}	$-1.353\,870 \cdot 10^{-05}$	Y'_{ur}	$-0.364\,788$	N'_{ur}	$0.051\,339$
X'_{vv}	$-3.158\,025$	Y'_{uur}	$0.317\,701$	N'_{uur}	$-0.078\,193$
X'_{rr}	$-0.551\,138$	Y'_{uuv}	$1.071\,340$	N'_{uuv}	$-0.254\,660$
X'_{vr}	$-2.674\,480$	Y'_{vvv}	$8.013\,291$	N'_{vvv}	$-3.262\,525$
X'_{uvv}	$2.737\,263$	Y'_{rrr}	$0.047\,259$	N'_{rrr}	$-0.110\,029$
X'_{rvu}	$2.339\,471$	Y'_{rrv}	$1.542\,482$	N'_{rrv}	$-0.917\,181$
X'_{urr}	$0.489\,609$	Y'_{vvr}	$7.116\,089$	N'_{vvr}	$-2.968\,359$
		$Y'_{v\|v\|}$	$-1.346\,012$	$N'_{v\|v\|}$	$0.341\,845$
		$Y'_{r\|v\|}$	$-0.015\,829$	$N'_{r\|v\|}$	$0.025\,292$
		$Y'_{v\|r\|}$	$-0.427\,689$	$N'_{v\|r\|}$	$0.114\,723$
		$Y'_{r\|r\|}$	$0.179\,823$	$N'_{r\|r\|}$	$-0.035\,010$

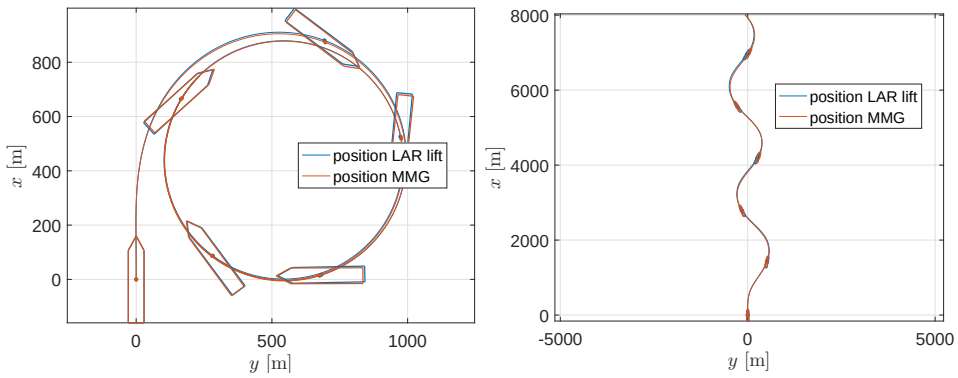

(a) Turning circle manoeuvre.

(b) 20/20 zig-zag manoeuvre.

Figure 8.17: Plot of the position of the turning circle and 20/20 zig-zag manoeuvres calculated with third order coefficients, predicted with a 20/20 zig-zag trial and turning circle manoeuvre. Every 175 seconds a contour of the ship is plotted.

the MMG results than the zig-zag manoeuvres simulated with coefficients obtained from a single manoeuvre.

It is shown that there is some improvement on the simulation of a turning circle and 20/20 zig-zag manoeuvre when the coefficients are based on these manoeuvres. When a 10/10 zig-zag manoeuvre is simulated however, the simulation becomes worse, as is shown in figure 8.18a. In figure 8.18b, the rudder angle and heading of the vessel are shown. It can be seen that the timing of the rudder is right, but the overshoot angles are very large and unrealistic. To get insight in the cause of the large overshoot angles,

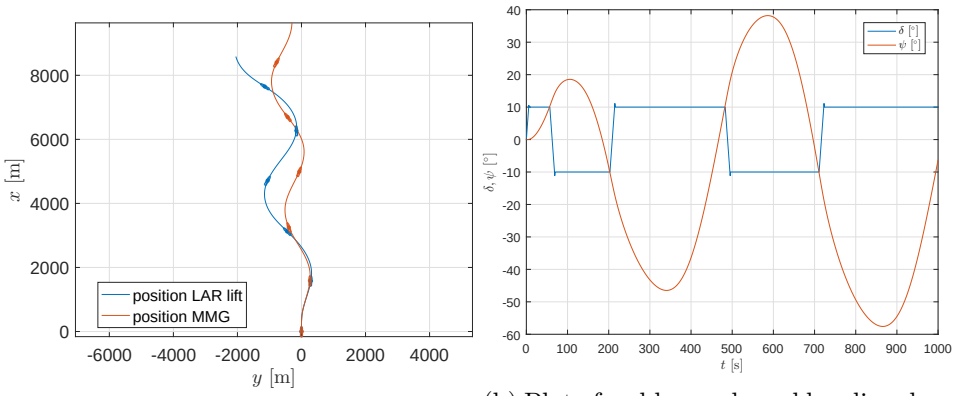

(a) 10/10 zig-zag manoeuvre.

(b) Plot of rudder angle and heading during 10/10 zig-zag manoeuvre.

Figure 8.18: Plot of the position of a 10/10 zig-zag manoeuvre calculated with third order coefficients, predicted with a 20/20 zig-zag trial and turning circle manoeuvre. Every 175 seconds a contour of the ship is plotted.

the moments around the z-axis during the manoeuvre are plotted in figure 8.19. In figure 8.19a it can be seen that the moments that involve the longitudinal component u account for the largest contribution to the total vertical moment, this is not in accordance with the behaviour found when looking at the 20/20 zig-zag test in section 8.2.1. When the coefficients are compared, it can be seen that the coefficients for N that depend on u are much larger than the coefficients found with a 20/20 zig-zag manoeuvre only, the coefficients depending on r however have much less influence which causes the rotational motion to have less damping. To improve the set of coefficients, manoeuvres witch include more information about r can be included.

8.3.2 Combining 4 different manoeuvres

The tests with coefficients based on two manoeuvres show that improvements can be made on a set of coefficients by adding more manoeuvres to

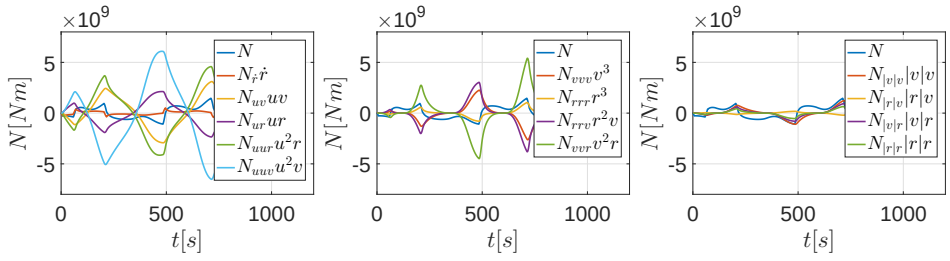

(a) (b) (c)

Figure 8.19: Comparison of vertical moment components during 10°/10° zig-zag zig-zag manoeuvre calculated with third order coefficients, predicted with a 20/20 zig-zag trial and turning circle manoeuvre.

the data set. The 10/10 zig-zag manoeuvre showed that the coefficients do not improve the simulation of every manoeuvre. Adding more manoeuvres to the dataset however could also improve the behaviour during other manouevres. During verification it was already shown that adding a track of straight acceleration could improve the determination of the longitudinal added mass. Because the coefficients determined with a 20/20 zig-zag and a turning circle manoeuvre show a less accurate value of longitudinal added mass, a straight acceleration part is added to the dataset. To be able to make a better prediction of the N coefficients dependent on u, a 10/10 zig-zag manoeuvre is added to the dataset. The total dataset now contains a turning circle manoeuvre, a 20/20 zig-zag manoeuvre, straight acceleration and a 10/10 zig-zag manoeuvre. The coefficients derived from this dataset are displayed in table 8.7.
Compared to the coefficients found with only 2 manoeuvres the values of the added mass have improved and are closer to the values given by the MMG methods. It can also be seen that the N coefficients dependent on u are smaller in comparison to the coefficients dependent on r, therefore this set of coefficients should give better results for the 10/10 zig-zag manoeuvre. In figure 8.20 the simulations of a turning circle and zig-zag manoeuvre using the coefficients found with 4 manoeuvres are displayed. The manoeuvres slow slightly more deviation from the MMG results than the manoeuvres simulated using the coefficients found with two manoeuvres. The simulation of a 10/10 zig-zag manoeuvre however, as shown in figure 8.21 shows a much better result than the manoeuvre simulated with the coefficients found with two manoeuvres. It can be concluded that a set of coefficients can be improved by carefully selecting coefficients and adding them to the data set.

Table 8.7: Table of al the dimensionless coefficients based on low aspect ratio lift theory found from combined straight acceleration, 10/10 zig-zag, 20/20 zig-zag and turning circle manoeuvres.

$X'_{\dot{u}}$	$-0.023\,980$	$Y'_{\dot{v}}$	$-0.276\,760$	$N'_{\dot{r}}$	$-0.014\,792$
X'_{uu}	$-0.021\,376$	Y'_{uv}	$-0.496\,231$	N'_{uv}	$-0.053\,891$
X'_{uuu}	$-1.327\,910 \cdot 10^{-06}$	Y'_{ur}	$0.153\,734$	N'_{ur}	$-0.048\,632$
X'_{vv}	$-0.173\,163$	Y'_{uur}	$-0.085\,963$	N'_{uur}	$0.003\,976$
X'_{rr}	$-0.056\,685$	Y'_{uuv}	$0.124\,815$	N'_{uuv}	$-0.066\,317$
X'_{vr}	$-0.263\,868$	Y'_{vvv}	$26.515\,867$	N'_{vvv}	$-9.301\,482$
X'_{uvv}	$0.054\,208$	Y'_{rrr}	$-0.096\,957$	N'_{rrr}	$-0.246\,490$
X'_{rvu}	$0.169\,259$	Y'_{rrv}	$2.325\,957$	N'_{rrv}	$-2.219\,393$
X'_{urr}	$0.043\,916$	Y'_{vvr}	$17.209\,079$	N'_{vvr}	$-7.748\,912$
		$Y'_{v\|v\|}$	$-2.777\,808$	$N'_{v\|v\|}$	$0.657\,196$
		$Y'_{r\|v\|}$	$-0.634\,247$	$N'_{r\|v\|}$	$0.180\,410$
		$Y'_{v\|r\|}$	$-1.249\,708$	$N'_{v\|r\|}$	$0.297\,708$
		$Y'_{r\|r\|}$	$-0.024\,239$	$N'_{r\|r\|}$	$0.016\,639$

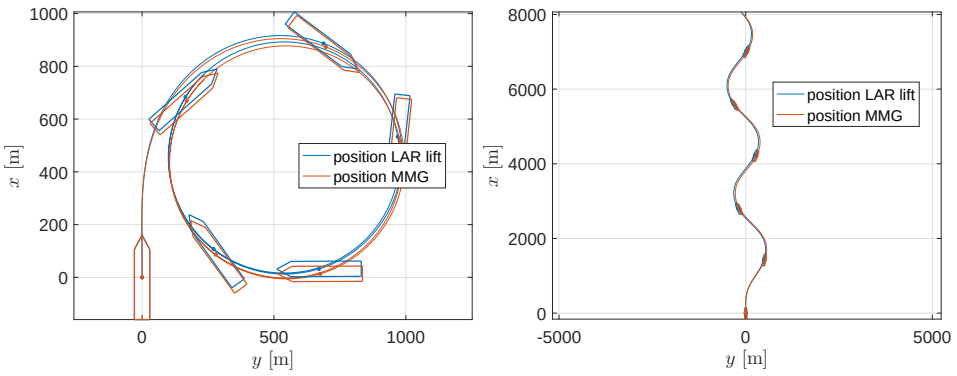

(a) Turning circle manoeuvre.

(b) 20/20 zig-zag manoeuvre.

Figure 8.20: Plot of the position of the turning circle and 20/20 zig-zag manoeuvres calculated with third order coefficients, predicted with 4 manoeuvres. Every 175 seconds a contour of the ship is plotted.

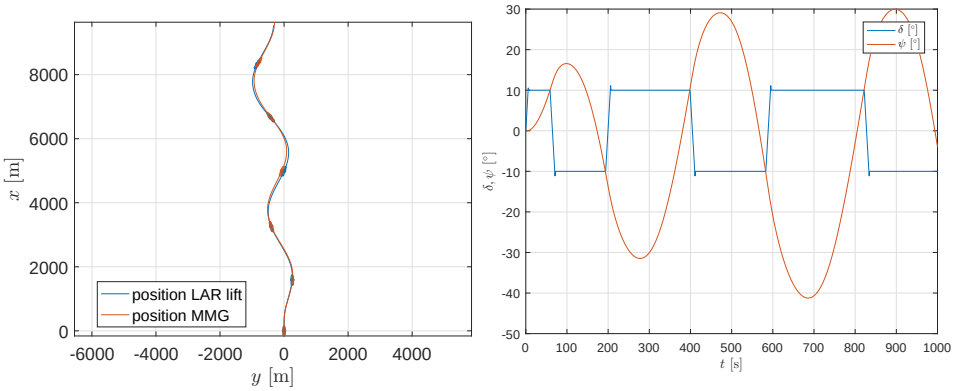

(a) 10/10 zig-zag manoeuvre.

(b) Plot of rudder angle and heading during 10/10 zig-zag manoeuvre.

Figure 8.21: Plot of the position of a 10/10 zig-zag manoeuvre calculated with third order coefficients, predicted with 4 manoeuvres. Every 175 seconds a contour of the ship is plotted.

Chapter 9

Conclusions and Recommendations

In this chapter the results of the research are summarized, also some recommendations for further research are given.

9.1 Conclusions

It is shown that a set of coefficients based on low aspect ratio is suitable for simulation of straight sailing forward, zig-zag manoeuvres and turning circle manoeuvres. This set consists of the following coefficients: $X_{\dot{u}}$, X_{uu}, X_{uuu}, X_{vv}, X_{rr}, X_{vr}, X_{uvv}, X_{rvu}, X_{urr}, $Y_{\dot{v}}$, Y_{uv}, Y_{ur}, Y_{uur}, Y_{uuv}, Y_{vvv}, Y_{rrr}, Y_{rrv}, Y_{vvr}, $Y_{|v|v}$, $Y_{|r|v}$, $Y_{|v|r}$, $Y_{|r|r}$, $N_{\dot{r}}$, N_{uv}, N_{ur}, N_{uur}, N_{uuv}, N_{vvv}, N_{rrr}, N_{rrv}, N_{vvr}, $N_{|v|v}$, $N_{|r|v}$, $N_{|v|r}$, $N_{|r|r}$.

It can be concluded that the singular value decomposition is able to find a set of hydrodynamic coefficients from a single path of a vessel that can recreate a manoeuvre of a vessel when used in simulation. Care should be taken however, because the set of coefficients is only able to recreate the behaviour that was present in the manoeuvre(s) used to determine the set of coefficients.

It is shown that coefficients can be determined more accurately when more different manoeuvres are used. Accelerating in a straight line is a good manoeuvre to determine the added mass in longitudinal direction $X_{\dot{u}}$ accurately, especially when the acceleration varies over time. It was shown that a turning circle is a bad manoeuvre for determining $Y_{|v|v}$, $Y_{|r|v}$, $Y_{|v|r}$, $Y_{|r|r}$, $N_{|v|v}$, $N_{|r|v}$, $N_{|v|r}$ and $N_{|r|r}$ because both r and v do not change sign during this manoeuvre. It is shown that problems with the usage of a single manoeuvre can be solved by using multiple manoeuvres. It can be concluded that the method works better when the used dataset contains more information, this

corresponds to more different accelerations, velocities and combinations of velocities. Including more information in the dataset can be achieved by including more different manoeuvres in the dataset.

The set of coefficients determined by a zig-zag manoeuvre was shown to be able to recreate the zig-zag manoeuvre. This set however also showed good results when used for simulation of straight sailing and turning circle manoeuvres. It could be concluded however that a part of the total set of coefficients could not be determined because the longitudinal velocity did not vary enough. This means that a manoeuvre with more change in longitudinal velocity could result in a more accurate set of coefficients. It also means that the modelling of a zig-zag manoeuvre can be done with a smaller set of coefficients. Instead of using an other manoeuvre with more change in velocity, more zig-zag manoeuvres at different velocities can be used to increase the amount of information in the data set.

9.2 Recommendations for further Research

When more research in done in the future on this subject there are a few area's in which it is recommended to look into.

The first area regards the information that is needed to find a set of coefficients using singular value decomposition. It was shown that the result of the singular valued decomposition is highly dependent on two things: the manoeuvre(s) that are used as input data and the set of coefficients that is sought after. To make better use of this method more research should be done on the set of coefficients that is needed to model a ship in a real-time ship simulator. Also more research should be done on the manoeuvres that are needed to provide enough information about the behaviour of the vessel to find these coefficients. It should be noted that both the set of coefficients and the amount of information in the manoeuvres have to be larger when the behaviour of a vessel is more complex.

The second area concerns the practical use of the developed method. In this research only theoretical cases where studied. When the method is used on real ship data, more research should be done on the effect of errors in the measuring of forces and position of the vessel on the final set of coefficients. Also the environmental forces have to be taken into account when real ship data is used in this method.

In this research some assumptions were made. Most of these assumptions had something to do with the origin of the forces acting on the vessel. In the future research could be done on expanding the method for ships that don't

have a conventional single propeller and single rudder configuration, which means that more complex rudder and propeller models are needed. Also the environmental forces where not taken into account in this research, which means that forces caused by wind, waves and current where considered to be negligible. More research could be done on including these forces in the method.

The last area that could be looked into is the used equations of motion in this method. In this research only planar motion was concerned. In the case of a very large crude carrier this assumption is valid. When smaller and faster vessels are considered it might be needed to take roll in account also and maybe even the full 3DOF equations. More research is needed to determine what the boundaries of the method are with respect to different ship types.

Bibliography

[1] M. A. Abkowitz. Lectures on ship hydrodynamics - steering and manoeuvrability. Technical report, Hydro- and Aerodynamics Laboratory, Lyngby, Denmark, 1964.

[2] M. A. Abkowitz. Measurement of hydrodynamic characteristics from ship maneuvering trials by system identification. Technical report, 1980.

[3] American Bureau of Shipping. *Guide for vessel maneuverability.* American Bureau of Shipping, 2006.

[4] C. E. Badoe, A. B. Phillips, and S. T. Turnock. Influence of drift angle on computation of hull-propeller-rudder interaction. Technical report, Fluid Structure Interactions Research Group, Faculty of Engineering and the Environment, University of Southampton, 2014.

[5] M. M. Barnitsas, D. Ray, and P. Kinley. Kt, Kq and efficiency curves for the Wageningen B-series propellers. 1981.

[6] D.A. Belsley, E. Kuh, and R.E. Welsch. *Regression Diagnostics: Identifying Influential Data and Sources of Collinearity.* Wiley Series in Probability and Statistics. Wiley, 2005. ISBN 9780471725145.

[7] V. Bertram. *Practical Ship Hydrodynamics.* Elsevier Science, 2011. ISBN 9780080971520. URL `https://books.google.nl/books?id=p9_O6abC_8AC`.

[8] N. Butt, D. Johnson, K. Pike, N. Pryce-Roberts, and N. Vigar. 15 years of shipping accidents: A review for WWF. Technical report, Southampton Solent University, 2013.

[9] E.W. Cheney and D.R. Kincaid. *Numerical Mathematics and Computing.* Cengage Learning, 2012. ISBN 9781133103714.

[10] M. S. Chislett and J. Strom-Tejsen. Planar motion mechanism tests and full scale steering and full scale steering maneuvering predictions for a mariner class vessel. Technical report, Hydro- and aerodynamics laboratory, 1965.

[11] D. Clarke, D. R. Patterson, and R. K. Wooderson. Manoeuvring trials with the 193,000 tonne deadweight tanker "Esso Bernicia". *Naval Architect*, (2), 1973.

[12] Frédéric Cohen Tenoudji. Analog and digital signal analysis. 2016.

[13] D. Conniffe and J. Stone. A critical view of ridge regression. *Journal of the Royal Statistical Society. Series D (The Statistician)*, 22(3): 181–187, 1973. ISSN 00390526, 14679884.

[14] C. L. Crane Jr. Maneuvering trials of the 278,000 DWT Esso Osaka in shallow and deep waters. Technical report, 1979.

[15] K. S. M. Davidson and L. I. Schiff. Turning and course-keeping qualities. Technical report, The Society of Navel Architects and Marine Engineers, 1946.

[16] F. M. Dekking, C. Kraaikamp, H. P. Lopuhaä, and L. E. Meester. *A Modern Introduction to Probability and Statistics: Understanding Why and How*. Springer Texts in Statistics. Springer London, 2006. ISBN 9781846281686.

[17] M. A. El-Reedy. *Offshore Structures: Design, Construction and Maintenance*. Gulf Professional Pub., 2012. ISBN 9780123854759.

[18] L. Euler. *Scientia Navalis seu Tractatus de Construendis ac Dirigendis Navibus*. Academy of scienses, 1749.

[19] H. Fuji and T. Tuda. Experimental researches on rudder performance. *Journal of the Society of Naval Architects of Japan*, pages 31–42, 1961.

[20] C. Fureby, S. L. Toxopeus, M. Johansson, M. Tormalm, and K. Petterson. A computational study of the flow around the KVLCC2 model hull at straight ahead conditions and at drift. *Ocean Engineering*, 118:1–16, 2016.

[21] Walter Gautschi. *Numerical analysis*. Springer Science & Business Media, 2011.

[22] M. Gertler and G. R. Hagen. Standard equations of motion for submarine simulation. Technical report, Naval Ship Research and Development Center, June 1967.

[23] M. Grasselli and D. Pelinovsky. *Numerical Mathematics*. Jones & Bartlett Learning, 2008. ISBN 9780763737672.

[24] R. C. Hibbeler and S. C. Fan. *Engineering Mechanics: Dynamics*. Prentice Hall, 2010. ISBN 9789810681371.

[25] A. E. Hoerl and R. W. Kennard. Ridge regression: Biased estimation for nonorthogonal problems. *Technometrics*, 42(1):80–86, 2000. ISSN 00401706.

[26] Erik Hogkamer. Inside of fmb1, 2017.

[27] L. H. Holthuijsen. *Waves in oceanic and coastal waters*. Cambridge University Press, 2010.

[28] J. P. Hooft. The cross-flow drag on a manoeuvring ship. *Ocean engineering*, 21(3):329–342, 1994.

[29] IMO. IMO standards for ship manoeuvrability, IMO MSC 76/23/Add. 1 Annex 6, 2002. URL `http://www.imo.org/blast/blastDataHelper.asp?data_id=15507&filename=137(76).pdf`.

[30] S Inoue, M Hirano, K Kijima, and J Takashina. A practical calculation method of ship maneuvering motion. *International Shipbuilding Progress*, 28(325):207–222, 1981.

[31] S. Inoue, K. Kijima, and M. Hirano. Hydrodynamic derivatives on ship manoeuvring. In *International shipbuilding progress*, volume 28, pages 112 – 125, May 1981.

[32] J. M. J. Journeé. A simple method for determining the manoeuvring indices K and T from zigzag trial data. Technical report, Delft University of Technology, 1970.

[33] J. M. J. Journée and W. W. Massie. *Offshore Hydromechanics*. Lecture notes. Delft University of Technology, 2008.

[34] G. Kempf. Manövriernorm für schiffe. Technical report, Hansa, 1944.

[35] K. Kose, A. Yumuro, and Y. Yoshimura. Concrete of mathematical model for ship manoeuvrability. *3rd S. on ship manoeuvrability, SNAJ*, pages 27–80, 1981.

[36] D. C. Lay. *Linear Algebra and Its Applications*. Addison-Wesley, 2012. ISBN 9780321623355.

[37] Sungwook Lee, Katsuro Kijima, Yoshitaka Furukawa, Yasuaki Nakiri, and Hiroshi Ibaragi. On the ship manoeuvring characteristics in shallow water. *The Western Shipbuilding Company Proceedings*, (109): 127–134, 2005.

[38] E. M. Lewandowski. *The dynamics of marine craft: Maneuvring and Seakeeping*. World Scientific, 2004.

[39] J. Liu, R. Hekkenberg, and F. Quadvlieg. Impacts of rudder profiles on ship manoeuvrability. In *International Conference on Marine Simulation and Ship Maneuverability*, 2015.

[40] G. C. McDonald. Ridge regression. *Wiley Interdisciplinary Reviews: Computational Statistics*, 1(1):93–100, 2009. ISSN 1939-0068. doi: 10.1002/wics.14. URL `http://dx.doi.org/10.1002/wics.14`.

[41] A. F. Molland and S. R. Turnock. Flow straightening effects on a ship rudder due to upstream propeller and hull. *International shipbuilding progress*, 49(3):195–214, 2002.

[42] K. Nomoto. Analysis of kempfs standard manoeuvre test and proposed steering quality indices. In *First Symposium on Ship manouevrability*, October 1960.

[43] N. H. Norrbin. Theory and observations on the use of a mathematical model for ship manoeuvring in deep and confined waters. Technical report, DTIC Document, 1971.

[44] A. Ogawa, T. Koyama, and K Kijima. On the mathematical model of manoeuvring motion of ships. In *International Shipbuilding progress*, 1978.

[45] Panel H-10 of the Society of Navel Architects and Marine Engineers. *Design workbook on Ship Maneuverability*. The Society of Navel Architects and Marine Engineers, 1993.

[46] J. Pinkster. *Bewegingen en Sturen II Manoevreren*. TUDelft, 2006.

[47] W.H. Press. *Numerical Recipes in C: The Art of Scientific Computing*. Cambridge University Press, 1992. ISBN 9780521437202. URL `https://books.google.nl/books?id=4t-sybVuoqoC`.

[48] F. H. H. A. Quadvlieg and P. van Coevorden. Manoeuvring criteria: more than IMO A751 requirements alone! In *MARSIM International Conference on Marine Simulation and Ship Manoeuvring*. The Society of Naval Architects of Japan and Japan Institute of Navigation, 2003.

[49] H. Rong and J. Mou. Predict maneuvering indices using ais data by ridge regression. Technical report, International Workshop on Next Generation Nautical Traffic Models 2013, Delft, The Netherlands, 2013.

[50] A. Ross, T. Perez, and T. I. Fossen. A novel manoeuvering model based on low-aspect-ratio lift theory and lagrangian mechanics. *IFAC Proceedings Volumes*, 40(17):229–234, 2007.

[51] H. Shiba. Model experiments about the maneuverability and turning of ships. In *First Symposium on Ship manouevrability*, October 1960.

[52] STC-Group. About the STC-Group, october 2016. `http://stc-group.nl/en/about-stc-group`.

[53] J. Stewart. *Calculus: Early Transcendentals*. Brooks/Cole, Cengage Learning, 2011. ISBN 9780538498876.

[54] A. N. Tikhonov, A. V. Goncharsky, V. V. Stepanov, and A. G. Yagola. *Numerical methods for the solution of ill-posed problems*, volume 328. Springer Science & Business Media, 2013.

[55] S. Toxopeus and S. W. Lee. Comparison of maneuvering simulation programs for simman test cases. In *Proceedings of SIMMAN 2008 workshop on verification and validation of ship maneuvering simulation methods, Lyngby, Denmark*, 2008.

[56] S. L. Toxopeus. Validation of slender-body method for prediction of linear manoeuvring coefficients using experiments and viscous-flow calculations. In *Proceedings of the seventh ICHD international conference on hydrodynamics, University of Naples Federico II, Ischia*, pages 589–598, 2006.

[57] S. L. Toxopeus, C. D. Simonsen, E. Guilmineau, M. Visonneau, T. Xing, and F. Stern. Investigation of water depth and basin wall effects on KVLCC2 in manoeuvring motion using viscous-flow calculations. *Journal of Marine Science and Technology*, 18(4): 471–496, 2013.

[58] M. S. Triantafyllou and F. S. Hover. *Maneuvering and control of marine vehicles*. Massachusetts Institute of Technology, 2003.

[59] W. P. A. van Lammeren, J. D. van Manen, and M. W. C. Oosterveld. The wageningen B-screw series. 1969.

[60] C. Vuik, F. J. Vermolen, M. B. van Gijzen, and M. J. Vuik. *Numerical methods for ordinary differential equations*. Delft Academic Press, 2015.

[61] A. M. Wang, X. Jiang, Z. Li, C. Yu, S. Zhu, J. Pinkster, et al. Virtual simulations of VLCC class FPSO-SYMS mating operation. In *The Twentieth International Offshore and Polar Engineering Conference*. International Society of Offshore and Polar Engineers, 2010.

[62] J. H. Wulder. *The implementation of a ship manoeuvring model in an integrated navigation system*. TU Delft, Delft University of Technology, 1992.

[63] H. Yasukawa and Y. Yoshimura. Introduction of MMG standard method for ship maneuvering predictions. *Journal of Marine Science and Technology*, 20(1):37–52, 2015. ISSN 1437-8213. doi: 10.1007/s00773-014-0293-y.

[64] Y. Yoshimura, M. Ueno, and Y. Tsukada. Analysis of steady hydrodynamic force component and prediction of manoeuvring ship motion with KVLCC1, KVLCC2 and KCS. In *Proceedings of Workshop on Verification and Validation of Ship Manoeuvring Simulation Methods*, 2008.

Appendix A

Derivation of Euler's equation

The acceleration of an object in a rotating moving reference fram is shown to be equal to

$$\mathbf{a_O} = \mathbf{a_A} + \boldsymbol{\Omega} \times \mathbf{v_A} + \frac{\mathrm{d}\boldsymbol{\Omega}}{\mathrm{d}t} \times \mathbf{r_G} + \boldsymbol{\Omega} \times (\boldsymbol{\Omega} \times \mathbf{r_G}). \tag{A.1}$$

The velocity vector of the moving reference frame can be defined using the velocities of the origin

$$\mathbf{v_A} = \begin{bmatrix} u \\ v \\ w \end{bmatrix}. \tag{A.2}$$

The accelerations of the origin are the derivatives of the velocities and the acceleration vector is thus equal to

$$\mathbf{a_A} = \begin{bmatrix} \dot{u} \\ \dot{v} \\ \dot{w} \end{bmatrix}. \tag{A.3}$$

The rotation vector can be defined by the three rotations around the origin p,q,r

$$\boldsymbol{\Omega} = \begin{bmatrix} p \\ q \\ r \end{bmatrix}. \tag{A.4}$$

Now the second term on the right hand side of the acceleration can be calculated

$$\boldsymbol{\Omega} \times \mathbf{v_A} = \begin{bmatrix} p \\ q \\ r \end{bmatrix} \times \begin{bmatrix} u \\ v \\ w \end{bmatrix} = \begin{bmatrix} qw - rv \\ -pw + ru \\ pv - qu \end{bmatrix}. \tag{A.5}$$

The position of the center of gravity in the body fixed frame can be described as

$$\mathbf{r_G} = \begin{bmatrix} x_G \\ y_G \\ z_G \end{bmatrix} \tag{A.6}$$

Now the third term on the right hand side can be evaluated as

$$\frac{\mathrm{d}\mathbf{\Omega}}{\mathrm{d}t} \times \mathbf{r_G} = \begin{bmatrix} \dot{p} \\ \dot{q} \\ \dot{r} \end{bmatrix} \times \begin{bmatrix} x_G \\ y_G \\ z_G \end{bmatrix} = \begin{bmatrix} \dot{q}z_G - \dot{r}y_G \\ \dot{r}x_G - \dot{p}z_G \\ \dot{p}y_G - \dot{q}x_G \end{bmatrix}. \tag{A.7}$$

The last term on the right hand side is equal to

$$\begin{aligned} \mathbf{\Omega} \times (\mathbf{\Omega} \times \mathbf{r_G}) &= \begin{bmatrix} p \\ q \\ r \end{bmatrix} \times \left(\begin{bmatrix} p \\ q \\ r \end{bmatrix} \times \begin{bmatrix} x_G \\ y_G \\ z_G \end{bmatrix} \right) = \begin{bmatrix} p \\ q \\ r \end{bmatrix} \times \begin{bmatrix} qz_G - ry_G \\ rx_G - pz_G \\ py_G - qx_G \end{bmatrix} \\ &= \begin{bmatrix} q(py_G - qx_G) - r(rx_G - pz_G) \\ r(qz_G - ry_G) - p(py_G - qx_G) \\ p(rx_G - pz_G) - q(qz_G - ry_G) \end{bmatrix} \\ &= \begin{bmatrix} pqy_G + prz_G - q^2x_G - r^2x_G \\ pqx_G + grz_G - p^2y_G - r^2y_G \\ prx_G + qry_G - p^2z_G - q^2z_G \end{bmatrix} \\ &= \begin{bmatrix} p(qy_G + rz_G) - x_G(q^2 + r^2) \\ q(px_G + rz_G) - y_G(p^2 + r^2) \\ r(px_G + qy_G) - z_G(p^2 + q^2) \end{bmatrix}. \end{aligned} \tag{A.8}$$

Substituting A.3, A.5, A.7 and A.8 in A.1 yields

$$\mathbf{a_O} = \begin{bmatrix} \dot{u} + qw - rv + \dot{q}z_G - \dot{r}y_G + p(qy_G + rz_G) - x_G(q^2 + r^2) \\ \dot{v} - pw + ru + \dot{r}x_G - \dot{p}z_G + q(px_G + rz_G) - y_G(p^2 + r^2) \\ \dot{w} + pv - qu + \dot{p}y_G - \dot{q}x_G + r(px_G + qy_G) - z_G(p^2 + q^2) \end{bmatrix} \tag{A.9}$$

Appendix B

Taylor Series Expansion

B.1 Fluid force X

When the fluid force is approximated by a Taylor series up to the second order terms this results in B.1. Because of port/starboard symmetry the center of gravity is located at $y = 0$ and the fluid force X will not be depending on $\dot{r}$.

$$\begin{aligned} X(u, \dot{u}, v, r, \delta) = {} & X_e + X_u u + X_{\dot{u}} \dot{u} + X_r r + X_\delta \delta + X_v v \\ & + X_{uu} u^2 + X_{uv} uv + X_{ur} ur + X_{u\delta} u\delta + X_{u\dot{u}} u\dot{u} \\ & + X_{\dot{u}\dot{u}} \dot{u}^2 + X_{\dot{u}u} \dot{u}u + X_{\dot{u}v} \dot{u}v + X_{\dot{u}r} \dot{u}r + X_{\dot{u}\delta} \dot{u}\delta \\ & + X_{vv} v^2 + X_{vu} vu + X_{v\dot{u}} v\dot{u} + X_{vr} vr + X_{v\delta} v\delta \\ & + X_{rr} r^2 + X_{ru} ru + X_{r\dot{u}} r\dot{u} + X_{rv} rv + X_{r\delta} r\delta \\ & + X_{\delta\delta} \delta^2 + X_{\delta u} \delta u + X_{\delta\dot{u}} \delta\dot{u} + X_{\delta v} \delta v + X_{\delta r} \delta r \end{aligned} \tag{B.1}$$

Because of three assumptions this expression can be simplified.

1. The first assumption, based on Newton's second law, is that the force is linear with acceleration. This means the second order acceleration term (coloured brown) is zero.

2. The second assumption is that there is no coupling between velocities and accelerations. So all the terms that invoke an acceleration and velocity term (coloured red) are zero.

3. The third assumption is that the ship has port-starboard symmetry. This leads to three conditions:

   (a) X is a symmetric function of v when $r = 0$ and $\delta = 0$. This implies $X_v = 0$; $X_{vu} = 0$ and $X_{uv} = 0$.

   (b) X is a symmetric function of r when $v = 0$ and $\delta = 0$. This implies $X_r = 0$; $X_{ru} = 0$ and $X_{ur} = 0$.

(c) X is a symmetric function of δ when $v = 0$ and $r = 0$. This implies $X_\delta = 0$; $X_{\delta u} = 0$ and $X_{u\delta} = 0$.

These terms are all coloured blue

This means B.1 simplifies to

$$\begin{aligned} X(u, \dot{u}, v, r, \delta) = X_e + X_u u + X_{\dot{u}}\dot{u} + X_{uu}u^2 + X_{vv}v^2 \\ + X_{vr}vr + X_{v\delta}v\delta + X_{rr}r^2 + X_{rv}rv + X_{r\delta}r\delta \\ + X_{\delta\delta}\delta^2 + X_{\delta v}\delta v + X_{\delta r}\delta r \end{aligned} \tag{B.2}$$

B.2 Fluid force Y

In the same way the Y force can be approximated by a taylor series of the second order to find B.3.

$$\begin{aligned} Y(u, v, \dot{v}, r, \dot{r}, \delta) = Y_e + Y_u u + Y_v v + Y_{\dot{v}}\dot{v} + Y_r r + Y_{\dot{r}}\dot{r} + Y_\delta \delta \\ + Y_{uu}u^2 + Y_{uv}uv + Y_{u\dot{v}}u\dot{v} + Y_{ur}ur + Y_{u\dot{r}}u\dot{r} + Y_{u\delta}u\delta \\ + Y_{vv}v^2 + Y_{vu}vu + Y_{v\dot{v}}v\dot{v} + Y_{vr}vr + Y_{v\dot{r}}v\dot{r} + Y_{v\delta}v\delta \\ + Y_{\dot{v}\dot{v}}\dot{v}^2 + Y_{\dot{v}u}\dot{v}u + Y_{\dot{v}v}\dot{v}v + Y_{\dot{v}r}\dot{v}r + Y_{\dot{v}\dot{r}}\dot{v}\dot{r} + Y_{\dot{v}\delta}\dot{v}\delta \\ + Y_{rr}r^2 + Y_{ru}ru + Y_{rv}rv + Y_{r\dot{v}}r\dot{v} + Y_{r\dot{r}}r\dot{r} + Y_{r\delta}r\delta \\ + Y_{\dot{r}\dot{r}}\dot{r}^2 + Y_{\dot{r}u}\dot{r}u + Y_{\dot{r}v}\dot{r}v + Y_{\dot{r}\dot{v}}\dot{r}\dot{v} + Y_{\dot{r}r}\dot{r}r + Y_{\dot{r}\delta}\dot{r}\delta \\ + Y_{\delta\delta}\delta^2 + Y_{\delta u}\delta u + Y_{\delta v}\delta v + Y_{\delta\dot{v}}\delta\dot{v} + Y_{\delta r}\delta r + Y_{\delta\dot{r}}\delta\dot{r} \end{aligned} \tag{B.3}$$

Because of three assumptions this expression can be simplified.

1. The first assumption, based on Newton's second law, is that the force is linear with acceleration. This means the second order acceleration term (coloured brown) is zero.

2. The second assumption is that there is no coupling between velocities and accelerations. So all the terms that invoke an acceleration and velocity term (coloured red) are zero.

3. The third assumption is that the ship has port-starboard symmetry. This leads to three conditions:

   (a) Y is an ant-symmetric function of v when $r = 0$ and $\delta = 0$. This implies $Y_{vv} = 0$.

   (b) Y is an anti-symmetric function of r when $v = 0$ and $\delta = 0$. This implies $Y_{rr} = 0$.

   (c) Y is an anti-symmetric function of δ when $v = 0$ and $r = 0$. This implies $Y_{\delta\delta} = 0$.

These terms are all coloured blue

This means B.3 simplifies to

$$\begin{aligned} Y(u,v,\dot{v},r,\dot{r},\delta) = {} & Y_e + Y_u u + Y_v v + Y_{\dot{v}}\dot{v} + Y_r r + Y_{\dot{r}}\dot{r} + Y_\delta \delta \\ & + Y_{uu}u^2 + Y_{uv}uv + Y_{ur}ur + Y_{u\delta}u\delta + Y_{vu}vu + Y_{vr}vr \\ & + Y_{ru}ru + Y_{rv}rv + Y_{r\delta}r\delta + Y_{\delta u}\delta u + Y_{\delta v}\delta v + Y_{\delta r}\delta r \end{aligned} \tag{B.4}$$

B.3 Fluid moment N

The same trick applies for the moment caused by the fluid. This taylor series up to second order yields B.5.

$$\begin{aligned} N(u,v,\dot{v},r,\dot{r},\delta) = {} & N_e + N_u u + N_v v + N_{\dot{v}}\dot{v} + N_r r + N_{\dot{r}}\dot{r} + N_\delta \delta \\ & + N_{uu}u^2 + N_{uv}uv + N_{u\dot{v}}u\dot{v} + N_{ur}ur + N_{u\dot{r}}u\dot{r} + N_{u\delta}u\delta \\ & + N_{vv}v^2 + N_{vu}vu + N_{v\dot{v}}v\dot{v} + N_{vr}vr + N_{v\dot{r}}v\dot{r} + N_{v\delta}v\delta \\ & + N_{\dot{v}\dot{v}}\dot{v}^2 + N_{\dot{v}u}\dot{v}u + N_{\dot{v}v}\dot{v}v + N_{\dot{v}r}\dot{v}r + N_{\dot{v}\dot{r}}\dot{v}\dot{r} + N_{\dot{v}\delta}\dot{v}\delta \\ & + N_{rr}r^2 + N_{ru}ru + N_{rv}rv + N_{r\dot{v}}r\dot{v} + N_{r\dot{r}}r\dot{r} + N_{r\delta}r\delta \\ & + N_{\dot{r}\dot{r}}\dot{r}^2 + N_{\dot{r}u}\dot{r}u + N_{\dot{r}v}\dot{r}v + N_{\dot{r}\dot{v}}\dot{r}\dot{v} + N_{\dot{r}r}\dot{r}r + N_{\dot{r}\delta}\dot{r}\delta \\ & + N_{\delta\delta}\delta^2 + N_{\delta u}\delta u + N_{\delta v}\delta v + N_{\delta\dot{v}}\delta\dot{v} + N_{\delta r}\delta r + N_{\delta\dot{r}}\delta\dot{r} \end{aligned} \tag{B.5}$$

Because of three assumptions this expression can be simplified.

1. The first assumption, based on Newton's second law, is that the force is linear with acceleration. This means the second order acceleration term (coloured brown) is zero.

2. The second assumption is that there is no coupling between velocities and accelerations. So all the terms that invoke an acceleration and velocity term (coloured red) are zero.

3. The third assumption is that the ship has port-starboard symmetry. This leads to three conditions:

   (a) N is an ant-symmetric function of v when $r = 0$ and $\delta = 0$. This implies $N_{vv} = 0$.

   (b) N is an anti-symmetric function of r when $v = 0$ and $\delta = 0$. This implies $N_{rr} = 0$.

   (c) N is an anti-symmetric of δ function when $v = 0$ and $r = 0$. This implies $N_{\delta\delta} = 0$.

   These terms are all coloured blue

This means B.5 simplifies to

$$\begin{aligned} N(u,v,\dot{v},r,\dot{r},\delta) = {} & N_e + N_u u + N_v v + N_{\dot{v}}\dot{v} + N_r r + N_{\dot{r}}\dot{r} + N_\delta \delta \\ & + N_{uu}u^2 + N_{uv}uv + N_{ur}ur + N_{u\delta}u\delta + N_{vu}vu + N_{vr}vr \\ & + N_{ru}ru + N_{rv}rv + N_{r\delta}r\delta + N_{\delta u}\delta u + N_{\delta v}\delta v + N_{\delta r}\delta r \end{aligned} \tag{B.6}$$

Appendix C

Derivation of equations of Motion

In this appendix the following equations are derived using classical mechanics.

$$X = m(\dot{u} - vr) \tag{C.1}$$

$$Y = m(\dot{v} + ur) \tag{C.2}$$

$$N = I_z \dot{r} \tag{C.3}$$

Equations C.1 and C.2 are derived using newton's second law. Equation C.3 is derived using angular momentum.

C.1 Applying Newton's second law

To find the equations of motion Newton's second law is applied. This law relates the forces on the center of gravity of a body to the linear momentum of the body.

$$\mathbf{F} = \frac{\mathrm{d}}{\mathrm{d}t}(m\mathbf{v}). \tag{C.4}$$

Because the mass of the ship is constant the mass can be taken outside of the differentiation

$$\mathbf{F} = m\frac{\mathrm{d}\mathbf{v}}{\mathrm{d}t} = m\mathbf{a_0} \tag{C.5}$$

where $\mathbf{v}$ is the velocity and $\mathbf{a_0}$ is the acceleration in the earth fixed reference frame. The ship fixed coordinate system however, is no inertial coordinate system, because the ship can accelerate. So an expression of the acceleration of the vessel in the earth fixed reference frame has to be found.

Consider an earth fixed inertial coordinate system x_0, y_0, z_0 and another arbitrary body fixed coordinate system x, y, z as drawn in figure C.1.

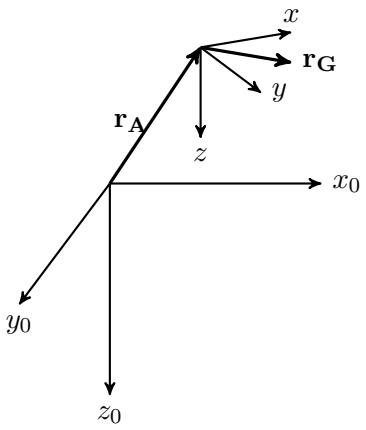

Figure C.1: Definition of the position vector of a rotating reference frame in an inertial frame.

The position of the origin of this coordinate system can be defined by the vector $\mathbf{r_A}$. The center of gravity of the body in the body fixed reference frame can be defined by the vector $\mathbf{r_G}$. The location of the center of gravity can now be determined for the inertial frame as

$$\mathbf{r_O} = \mathbf{r_G} + \mathbf{r_A}. \tag{C.6}$$

When the body fixed coordinate system also has an angular velocity $\mathbf{\Omega}$ the velocity of the center of gravity with respect to the inertial frame can be calculated as

$$\mathbf{v_O} = \frac{\mathrm{d}\mathbf{r_O}}{\mathrm{d}t} + \mathbf{\Omega} \times \mathbf{r_G} \tag{C.7}$$

Hibbeler and Fan [24]. By substituting C.6 this becomes

$$\mathbf{v_O} = \frac{\mathrm{d}\mathbf{r_G}}{\mathrm{d}t} + \frac{\mathrm{d}\mathbf{r_A}}{\mathrm{d}t} + \mathbf{\Omega} \times \mathbf{r_G}. \tag{C.8}$$

Because the center of gravity is considered to be fixed in the body fixed coordinate system $\frac{\mathrm{d}\mathbf{r_G}}{\mathrm{d}t}$ is zero which leads to

$$\mathbf{v_O} = \frac{\mathrm{d}\mathbf{r_A}}{\mathrm{d}t} + \mathbf{\Omega} \times \mathbf{r_G}. \tag{C.9}$$

The acceleration can now be found using

$$\mathbf{a_O} = \frac{\mathrm{d}\mathbf{v_O}}{\mathrm{d}t} + \mathbf{\Omega} \times \mathbf{v_G}. \tag{C.10}$$

Which is equal to

$$\mathbf{a_O} = \frac{\mathrm{d}}{\mathrm{d}t}(\mathbf{v_A} + \mathbf{\Omega} \times \mathbf{r_G}) + \mathbf{\Omega} \times (\mathbf{\Omega} \times \mathbf{r_G}). \tag{C.11}$$

$$\mathbf{a_O} = \mathbf{a_A} + \mathbf{\Omega} \times \mathbf{v_A} + \frac{\mathrm{d}\mathbf{\Omega}}{\mathrm{d}t} \times \mathbf{r_G} + \mathbf{\Omega} \times (\mathbf{\Omega} \times \mathbf{r_G}). \tag{C.12}$$

Substituting

$$\mathbf{v_A} = \begin{bmatrix} u \\ v \\ w \end{bmatrix}, \ \mathbf{a_A} = \begin{bmatrix} \dot{u} \\ \dot{v} \\ \dot{w} \end{bmatrix}, \ \mathbf{\Omega} = \begin{bmatrix} p \\ q \\ r \end{bmatrix} \text{ and } \mathbf{r_G} = \begin{bmatrix} x_G \\ y_G \\ z_G \end{bmatrix} \tag{C.13}$$

in C.12 yields

$$\mathbf{a_O} = \begin{bmatrix} \dot{u} + qw - rv + \dot{q}z_G - \dot{r}y_G + p(qy_G + rz_G) - x_G(q^2 + r^2) \\ \dot{v} - pw + ru + \dot{r}x_G - \dot{p}z_G + q(px_G + rz_G) - y_G(p^2 + r^2) \\ \dot{w} + pv - qu + \dot{p}y_G - \dot{q}x_G + r(px_G + qy_G) - z_G(p^2 + q^2) \end{bmatrix}. \tag{C.14}$$

A detailed derivation of this equation can be found in appendix A. The resultant forces X, Y and Z on the vessel are therefore equal to

$$\begin{bmatrix} X \\ Y \\ Z \end{bmatrix} = m \begin{bmatrix} \dot{u} + qw - rv + \dot{q}z_G - \dot{r}y_G + p(qy_G + rz_G) - x_G(q^2 + r^2) \\ \dot{v} - pw + ru + \dot{r}x_G - \dot{p}z_G + q(px_G + rz_G) - y_G(p^2 + r^2) \\ \dot{w} + pv - qu + \dot{p}y_G - \dot{q}x_G + r(px_G + qy_G) - z_G(p^2 + q^2) \end{bmatrix}. \tag{C.15}$$

When only motions in the horizontal plane are considered, hence the vertical velocity w is zero and the angular velocities p and q are zero, this simplifies to

$$\begin{bmatrix} X \\ Y \\ Z \end{bmatrix} = m \begin{bmatrix} \dot{u} - rv + \dot{r}y_G - x_G r^2 \\ \dot{v} + ru + \dot{r}x_G - y_G r^2 \\ 0 \end{bmatrix}. \tag{C.16}$$

When a symmetric ship is assumed y_G is zero so the equation reduces further to

$$\begin{bmatrix} X \\ Y \\ Z \end{bmatrix} = m \begin{bmatrix} \dot{u} - rv - x_G r^2 \\ \dot{v} + ru + \dot{r}x_G \\ 0 \end{bmatrix}. \tag{C.17}$$

When the coordinate system is defined to have its origin in the center of gravity of the vessel, the expression reduces even further to

$$\begin{bmatrix} X \\ Y \\ Z \end{bmatrix} = m \begin{bmatrix} \dot{u} - rv \\ \dot{v} + ru \\ 0 \end{bmatrix}. \tag{C.18}$$

C.2 Applying Angular momentum

To find information about the rotations of a body the expression of angular momentum can be used. When the body is considered to be consisting of N particles, the equation for angular momentum becomes

$$\sum_{i=1}^{N} (\mathbf{M}_i + \mathbf{r}_i \times \mathbf{F}_i) = \sum_{i=1}^{N} \mathbf{r}_i \times \frac{\mathrm{d}}{\mathrm{d}t} (m_i \mathbf{v}_i) \tag{C.19}$$

$$\sum_{i=1}^{N} (\mathbf{M}_i + \mathbf{r}_i \times \mathbf{F}_i) = \sum_{i=1}^{N} m_i \mathbf{r}_i \times \frac{\mathrm{d}\mathbf{v}_i}{\mathrm{d}t} \tag{C.20}$$

From the case where linear momentum was considered we can fill in the expression for $\frac{\mathrm{d}\mathbf{v}_i}{\mathrm{d}t}$, where it should be noted that $\mathbf{r}_i$ is the position vector of a particle relative to the point where it rotates around.

$$\begin{aligned}
&\sum_{i=1}^{N} (\mathbf{M}_i + \mathbf{r}_i \times \mathbf{F}_i) = \\
&\sum_{i=1}^{N} m_i \mathbf{r}_i \times \left(\frac{\partial \mathbf{v_O}}{\partial t} + \boldsymbol{\Omega} \times \mathbf{v_O} + \frac{\partial \boldsymbol{\Omega}}{\partial t} \times \mathbf{r}_i + \boldsymbol{\Omega} \times (\boldsymbol{\Omega} \times \mathbf{r}_i) \right) = \\
&\sum_{i=1}^{N} m_i \mathbf{r}_i \times \left(\frac{\partial \mathbf{v_O}}{\partial t} + \boldsymbol{\Omega} \times \mathbf{v_O} \right) + \sum_{i=1}^{N} m_i \mathbf{r}_i \times \left(\frac{\partial \boldsymbol{\Omega}}{\partial t} \times \mathbf{r}_i \right) \\
&+ \sum_{i=1}^{N} m_i \mathbf{r}_i \times (\boldsymbol{\Omega} \times (\boldsymbol{\Omega} \times \mathbf{r}_i))
\end{aligned} \tag{C.21}$$

For the first term on the right hand side, the definition of center of gravity can be used to get rid of the summation

$$\sum_{i=1}^{N} m_i \mathbf{r}_i \times \left(\frac{\partial \mathbf{v_O}}{\partial t} + \boldsymbol{\Omega} \times \mathbf{v_O} \right) = m \mathbf{r}_G \times \left(\frac{\partial \mathbf{v_O}}{\partial t} + \boldsymbol{\Omega} \times \mathbf{v_O} \right). \tag{C.22}$$

Substituting the position, velocity and angular velocity vectors yields

$$m \mathbf{r}_G \times \left(\frac{\partial \mathbf{v_O}}{\partial t} + \boldsymbol{\Omega} \times \mathbf{v_O} \right) = m \begin{bmatrix} y_G(\dot{w} + pv - qu) - z_G(\dot{v} - pw + ru) \\ z_G(\dot{u} + qw - rv) - x_G(\dot{w} + pv - qu) \\ x_G(\dot{v} - pw + ru) - y_G(\dot{u} + qw - rv) \end{bmatrix} \tag{C.23}$$

For the second term on the right hand side, the triple product can be used

$$\sum_{i=1}^{N} m_i \mathbf{r}_i \times \left(\frac{\partial \boldsymbol{\Omega}}{\partial t} \times \mathbf{r}_i \right) = \sum_{i=1}^{N} m_i \left((\mathbf{r}_i \cdot \mathbf{r}_i) \frac{\partial \boldsymbol{\Omega}}{\partial t} - \left(\frac{\partial \boldsymbol{\Omega}}{\partial t} \cdot \mathbf{r}_i \right) \mathbf{r}_i \right) \tag{C.24}$$

Substituting the position, velocity and angular velocity vectors yields

$$\sum_{i=1}^{N} m_i \mathbf{r}_i \times \left(\frac{\partial \boldsymbol{\Omega}}{\partial t} \times \mathbf{r}_i \right) = \sum_{i=1}^{N} m_i \begin{bmatrix} \dot{p}(y_i^2 + z_i^2) - x_i(\dot{q} y_i + \dot{r} z_i) \\ \dot{q}(x_i^2 + z_i^2) - y_i(\dot{p} x_i + \dot{r} z_i) \\ \dot{r}(x_i^2 + y_i^2) - z_i(\dot{p} x_i + \dot{q} y_i) \end{bmatrix} \tag{C.25}$$

Now the moments of inertia can be defined to be

$$I_{xx} = \sum_{i=1}^{N} m_i (y_i^2 + z_i^2) \tag{C.26}$$

$$I_{yy} = \sum_{i=1}^{N} m_i(x_i^2 + z_i^2) \tag{C.27}$$

$$I_{zz} = \sum_{i=1}^{N} m_i(x_i^2 + y_i^2) \tag{C.28}$$

$$I_{xy} = I_{yx} = -\sum_{i=1}^{N} m_i x_i y_i \tag{C.29}$$

$$I_{xz} = I_{zx} = -\sum_{i=1}^{N} m_i x_i z_i \tag{C.30}$$

$$I_{yz} = I_{zy} = -\sum_{i=1}^{N} m_i y_i z_i \tag{C.31}$$

which reduces the second term on the right hand side to

$$\begin{aligned} \sum_{i=1}^{N} m_i \mathbf{r}_i \times \left(\frac{\partial \mathbf{\Omega}}{\partial t} \times \mathbf{r}_i \right) &= \begin{bmatrix} I_{xx} & I_{xy} & I_{xz} \\ I_{yx} & I_{yy} & I_{yz} \\ I_{zx} & I_{zy} & I_{zz} \end{bmatrix} \frac{\partial \mathbf{\Omega}}{\partial t} \\ &= \begin{bmatrix} \dot{p} I_{xx} + \dot{q} I_{xy} + \dot{r} I_{xz} \\ \dot{p} I_{yx} + \dot{q} I_{yy} + \dot{r} I_{yz} \\ \dot{p} I_{zx} + \dot{q} I_{zy} + \dot{r} I_{zz} \end{bmatrix}. \end{aligned} \tag{C.32}$$

The third term can be rewritten using the triple product

$$\sum_{i=1}^{N} m_i \mathbf{r}_i \times (\mathbf{\Omega} \times (\mathbf{\Omega} \times \mathbf{r}_i)) = \sum_{i=1}^{N} m_i \mathbf{r}_i \times ((\mathbf{\Omega} \cdot \mathbf{r}_i)\mathbf{\Omega} - (\mathbf{\Omega} \cdot \mathbf{\Omega})\mathbf{r}_i) \tag{C.33}$$

Substituting the position, velocity and angular velocity vectors yields

$$\begin{aligned} &\sum_{i=1}^{N} m_i \mathbf{r}_i \times ((\mathbf{\Omega} \cdot \mathbf{r}_i)\mathbf{\Omega} - (\mathbf{\Omega} \cdot \mathbf{\Omega})\mathbf{r}_i) = \\ &\sum_{i=1}^{N} m_i \mathbf{r}_i \times \begin{bmatrix} (px_i + qy_i + rz_i)p - (p^2 + q^2 + r^2)x_i \\ (px_i + qy_i + rz_i)q - (p^2 + q^2 + r^2)y_i \\ (px_i + qy_i + rz_i)r - (p^2 + q^2 + r^2)z_i \end{bmatrix} = \\ &\sum_{i=1}^{N} m_i \begin{bmatrix} r^2 y_i z_i - q^2 y_i z_i - pg x_i z_i + pr x_i y_i + qr y_i^2 - qr z_i^2 \\ r^2 x_i z_i - p^2 x_i z_i - pg y_i z_i + qr x_i y_i + pr x_i^2 - rp z_i^2 \\ p^2 x_i y_i - q^2 x_i y_i - rq x_i z_i + pr y_i z_i + pq y_i^2 - pq x_i^2 \end{bmatrix} = \\ &\begin{bmatrix} -(r^2 - q^2) I_{yz} + pq I_{xz} - pr I_{xy} + qr(I_{zz} - I_{yy}) \\ -(r^2 - p^2) I_{xz} + qr I_{xy} - pq I_{yz} + pr(I_{zz} - I_{xx}) \\ -(p^2 - q^2) I_{xy} + pr I_{yz} - rq I_{xz} + pq(I_{xx} - I_{yy}) \end{bmatrix} \end{aligned} \tag{C.34}$$

This leads to the moment equation

$$\begin{aligned} K =& m(y_G(\dot{w} + pv - qu) - z_G(\dot{v} - pw + rv)) + \dot{p}I_{xx} + \dot{q}I_{xy} + \dot{r}I_{xz} \\ & - (r^2 - q^2)I_{yz} + pqI_{xz} - prI_{xy} + qr(I_{zz} - I_{yy}) \end{aligned} \tag{C.35}$$

$$\begin{aligned} M =& m(z_G(\dot{u} + qw - rv) - x_G(\dot{w} + pv - qu)) + \dot{p}I_{yx} + \dot{q}I_{yy} + \dot{r}I_{yz} \\ & - (r^2 - p^2)I_{xz} + qrI_{xy} - pqI_{yz} + pr(I_{zz} - I_{xx}) \end{aligned} \tag{C.36}$$

$$\begin{aligned} N =& m(x_G(\dot{v} - pw + rv) - y_G(\dot{u} + qw - rv)) + \dot{p}I_{zx} + \dot{q}I_{zy} + \dot{r}I_{zz} \\ & - (p^2 - q^2)I_{xy} + prI_{yz} - rqI_{xz} + pq(I_{xx} - I_{yy}) \end{aligned} \tag{C.37}$$

When only motions in the horizontal plane are considered, hence the vertical velocities w is zero and the angular velocities p and q are zero, this simplifies to

$$K = -mz_G(\dot{v} + ru) + \dot{r}I_{xz} - r^2 I_{yz} \tag{C.38}$$

$$M = mz_G(\dot{u} - rv) + \dot{r}I_{yz} - r^2 I_{xz} \tag{C.39}$$

$$N = m(x_G(\dot{v} + ru) - y_G(\dot{u} - rv)) + \dot{r}I_{zz}. \tag{C.40}$$

When a symmetric ship is considered, y_G is zero, and ship the because the coordinate system is placed at the height of the center of gravity z_G is zero, the equations then simplify to

$$K = -\dot{r}I_{xz} - r^2 I_{yz} \tag{C.41}$$

$$M = \dot{r}I_{yz} - r^2 I_{xz} \tag{C.42}$$

$$N = mx_G(\dot{v} + rv) + \dot{r}I_{zz}. \tag{C.43}$$

When the origin of the coordinate system is placed in the center of gravity this reduces to

$$N = \dot{r}I_{zz}. \tag{C.44}$$

The inertia terms in the equations of motion are know now, These inertia terms should be equal to the forces that are acting on the vessel. These forces are propeller thrust, the rudder forces, the resistance of the vessel and the other hydrodynamic forces. The difference between manoeuvring models arises from the way in which these forces are treated.

Appendix D

Derivation Low aspect ratio lift theory

In this appendix, a more detailed derivation of the low aspect ratio lift theory is given. The theory makes use of the assumption that a ship can be modelled as a wing with a low aspect ratio.

D.1 Lift

When the ship is modelled as a low aspect ratio wing, the lift force on a section of the vessel can be defined as

$$L = \frac{1}{2}\rho U^2 S C_L. \tag{D.1}$$

The sectional lift coefficient is assumed to behave linear with the sine of the drift angle

$$\begin{aligned} C_L(x) &= C_{L\beta} \sin\beta(x) \\ &= C_{L\beta} \frac{v + xr}{U(x)}. \end{aligned} \tag{D.2}$$

This means the lift force on every section of the vessel can be expressed as

$$\begin{aligned} L(x) &= \frac{1}{2}\rho U(x)^2 S C_L(x) \\ &= \frac{1}{2}\rho U(x)^2 S C_{L\beta} \frac{v + xr}{U(x)} \\ &= \frac{1}{2}\rho U(x) S C_{L\beta} (v + xr) \end{aligned} \tag{D.3}$$

The longitudinal component of the sectional lift force can be expressed as

$$\begin{aligned} X_L(x) &= L(x)\sin\beta(x) \\ &= \frac{1}{2}\rho U(x) S C_{L\beta}(v+xr)\frac{v+xr}{U(x)} \\ &= \frac{1}{2}\rho S C_{L\beta}(v+xr)^2 \end{aligned} \tag{D.4}$$

To get the total longitudinal force due to lift, the longitudinal component of the sectional lift force is integrated over the length of the vessel

$$\begin{aligned} X_L &= \int \frac{1}{2}\rho S C_{L\beta}(v+xr)^2 \,\mathrm{d}x \\ &= \frac{1}{2}\rho S C_{L\beta}\int v^2 + x^2r^2 + 2xvr \,\mathrm{d}x \\ &= \frac{1}{2}\rho S C_{L\beta}\left[xv^2 + \frac{1}{3}x^3r^2 + x^2vr\right]. \end{aligned} \tag{D.5}$$

Collecting all constants yields

$$X_L = X_{vv}v^2 + X_{rr}r^2 + X_{vr}vr \tag{D.6}$$

The lateral component of the sectional lift force can be expressed as

$$\begin{aligned} Y_L(x) &= -L(x)\cos\beta(x) \\ &= -\frac{1}{2}\rho U(x) S C_{L\beta}(v+xr)\frac{u}{U(x)} \\ &= -\frac{1}{2}\rho S C_{L\beta}(v+xr)u. \end{aligned} \tag{D.7}$$

The total lateral force due to lift can be found by integration

$$\begin{aligned} Y_L &= \int -\frac{1}{2}\rho S C_{L\beta}(v+xr)u \,\mathrm{d}x \\ &= -\frac{1}{2}\rho S C_{L\beta}\int uv + uxr \,\mathrm{d}x \\ &= -\frac{1}{2}\rho S C_{L\beta}\left[xuv + \frac{1}{2}x^2ur\right]. \end{aligned} \tag{D.8}$$

Collecting all constants results in

$$Y_L = Y_{uv}uv + Y_{ur}ur. \tag{D.9}$$

D.2 Drag force

The drag force can be expressed as

$$D = \frac{1}{2}\rho U^2 S C_D. \tag{D.10}$$

The drag coefficient can be expressed as a quadratic function of side-slip angle and a drag coefficient for drag at a drift angle of 0°

$$C_D(x) = C_{D0} + C_{D\beta\beta} \sin^2(\beta(x)). \tag{D.11}$$

Ross et al. [50] also include a term that is linear dependent on Reynolds number and thus linear dependent on the velocity U.

$$C_D(x) = C_{D0} + C_{DU}U(x) + C_{D\beta\beta} \sin^2(\beta(x)). \tag{D.12}$$

Now the drag force on every section can be expressed as

$$\begin{aligned} D(x) &= \frac{1}{2}\rho S U^2(x) C_D(x) \\ &= \frac{1}{2}\rho S U^2(x) \left[C_{D0} + C_{DU}U(x) + C_{D\beta\beta} \sin^2(\beta(x))\right] \\ &= \frac{1}{2}\rho S U^2(x) \left[C_{D0} + C_{DU}U(x) + C_{D\beta\beta} \left(\frac{v + xr}{U(x)}\right)^2\right] \\ &= \frac{1}{2}\rho S \left[C_{D0}U(x)^2 + C_{DU}U^3(x) + C_{D\beta\beta} (v + xr)^2\right]. \end{aligned} \tag{D.13}$$

The longitudinal component of the drag force can be found by decomposing the drag using the drift angle

$$\begin{aligned} X_D(x) &= -D(x) \cos\beta(x) \\ &= -\frac{1}{2}\rho S \left[C_{D0}U(x)^2 + C_{DU}U^3(x) + C_{D\beta\beta} (v + xr)^2\right] \cos\beta(x) \\ &= -\frac{1}{2}\rho S \left[C_{D0}U(x)^2 + C_{DU}U^3(x) + C_{D\beta\beta} (v + xr)^2\right] \frac{u}{U(x)} \\ &= -\frac{1}{2}\rho S \left[C_{D0}U(x)u + C_{DU}U^2(x)u + C_{D\beta\beta} (v + xr)^2 \frac{u}{U(x)}\right]. \end{aligned} \tag{D.14}$$

Now the assumption is made that $U(x)u \approx u^2$. This assumption is valid when $u \gg (v + xr)$.

$$U(x)u = \sqrt{u^2 + (v + xr)^2}u \approx u^2. \tag{D.15}$$

Now the longitudinal component of the drag force can be simplified to

$$\begin{aligned} X_D(x) &= -\frac{1}{2}\rho S \left[C_{D0}u^2 + C_{DU}U^2(x)u + C_{D\beta\beta} (v + xr)^2\right]. \\ &= -\frac{1}{2}\rho S[C_{D0}u^2 + C_{DU}(u^2 + (v + xr)^2) \\ &+ C_{D\beta\beta}(v^2 + x^2r^2 + 2xvr)]. \\ &= -\frac{1}{2}\rho S[C_{D0}u^2 + C_{DU}(u^3 + uv^2 + x^2ur^2 + 2xuvr) \\ &+ C_{D\beta\beta}(v^2 + x^2r^2 + 2xvr)]. \end{aligned} \tag{D.16}$$

The total longitudinal force caused by drag can now be found by integrating the longitudinal component of the sectional drag force.

$$\begin{aligned} X_D &= \int -\frac{1}{2}\rho S[C_{D0}u^2 + C_{DU}(u^3 + uv^2 + x^2ur^2 + 2xuvr) \\ &\quad + C_{D\beta\beta}(v^2 + x^2r^2 + 2xvr)]\,\mathrm{d}x \\ &= -\frac{1}{2}\rho S[C_{D0}xu^2 + C_{DU}(xu^3 + xuv^2 + \frac{1}{3}x^3ur^2 + x^2uvr) \\ &\quad + C_{D\beta\beta}(xv^2 + \frac{1}{3}x^3r^2 + x^2vr)]. \end{aligned} \tag{D.17}$$

Collecting all constants yields

$$\begin{aligned} X_D =& X_{uu}u^2 + X_{uuu}u^3 X_{uvv}uv^2 + X_{urr}ur^2 + X_{rvu}rvu \\ &+ X_{vv}v^2 + X_{rr}r^2 + X_{vr}vr \end{aligned} \tag{D.18}$$

The lateral component of the drag force can be calculated with

$$Y_D = -D\sin\beta \tag{D.19}$$

$$\begin{aligned} Y_D(x) &= -\frac{1}{2}\rho S\left[C_{D0}U(x)^2 + C_{DU}U^3(x) + C_{D\beta\beta}\left(v + xr\right)^2\right]\sin\beta(x) \\ &= -\frac{1}{2}\rho S\left[C_{D0}U(x)^2 + C_{DU}U^3(x) + C_{D\beta\beta}\left(v + xr\right)^2\right]\frac{v + xr}{U(x)} \\ &= -\frac{1}{2}\rho S\left[C_{D0}U(x)(v + xr) + C_{DU}U^2(x)(v + xr) + C_{D\beta\beta}\frac{(v + xr)^3}{U(x)}\right] \end{aligned} \tag{D.20}$$

When $U(x) \gg (v + xr)$, it can be assumed that $U(x) \approx u$. When $U(x) \gg (v + xr)^3$ the term with $C_{D\beta\beta}$ can be neglected. Using these assumptions we find

$$\begin{aligned} Y_D(x) &= -\frac{1}{2}\rho S\left[C_{D0}u(v + xr) + C_{DU}(u^2 + (v + xr)^2)(v + xr)\right] \\ &= -\frac{1}{2}\rho S\left[C_{D0}(uv + uxr) + C_{DU}(u^2 + v^2 + x^2r^2 + 2xrv)(v + xr)\right] \\ &= -\frac{1}{2}\rho S[C_{D0}(uv + uxr) + C_{DU}(vu^2 + v^3 + vx^2r^2 + 2xrv^2 + \\ &\quad xru^2 + xrv^2 + x^3r^3 + 2x^2r^2v)] \\ &= -\frac{1}{2}\rho S[C_{D0}(uv + uxr) + C_{DU}(vu^2 + v^3 + 3vx^2r^2 + 3xrv^2 + \\ &\quad xru^2 + x^3r^3)]. \end{aligned} \tag{D.21}$$

Total lateral component of drag force can be found by integrating

$$\begin{aligned} Y_D = &\int -\frac{1}{2}\rho S[C_{D0}(uv + uxr) + C_{DU}(vu^2 + v^3 + 3vx^2r^2 + 3xrv^2 + \\ &xru^2 + x^3r^3)]\,\mathrm{d}x \\ &= -\frac{1}{2}\rho S[C_{D0}(xuv + \frac{1}{2}u^2xr) + C_{DU}(xvu^2 + xv^3 + vx^3r^2 + \frac{3}{2}x^2rv^2 + \\ &\frac{1}{2}x^2ru^2 + \frac{1}{4}x^4r^3)]. \end{aligned} \tag{D.22}$$

Combining al constants results in

$$\begin{aligned} Y_D = &X_{uv}uv + X_{uur}u^2r + X_{uuv}u^2v + X_{vvv}v^3 \\ &+X_{vrr}vr^2 + X_{vvr}v^2r + X_{uur}u^2r + X_{rrr}r^3. \end{aligned} \tag{D.23}$$

Appendix E

Derivation of pseudo-inverse using SVD

It was mentioned earlier that the calculation of the pseudo-inverse

$$A^+ = (A^T A)^{-1} A^T \tag{E.1}$$

can be done faster and more accurate by using Singular Value Decomposition. In this Appendix it will be shown that

$$A^+ = V\Sigma^+ U^T. \tag{E.2}$$

The Singular Value Decomposition for a $m \times n$ matrix A is defined as

$$A = U\Sigma V^T, \tag{E.3}$$

where U is a $m \times m$ orthogonal matrix, V is a $n \times n$ orthogonal matrix and Σ is a $m \times n$ "diagonal" matrix. The orthogonality of U and V yields the properties

$$UU^T = I = U^T U \tag{E.4}$$

and

$$VV^T = I = V^T V. \tag{E.5}$$

This is the same statement as: The inverse of U and V are the same as the transpose of U and V. Using the Singular Value Decomposition of A we can derive the transpose of A to be equal to

$$A^T = (U(\Sigma V^T))^T = (\Sigma V^T)^T U^T = V\Sigma^T U^T. \tag{E.6}$$

Using the property of orthogonality from U we can now find $A^T A$ to be equal to

$$A^T A = V\Sigma^T U^T U\Sigma V^T = V\Sigma^T \Sigma V^T \tag{E.7}$$

Then this can be inverted using orthogonality of V to get

$$(A^T A)^{-1} = (V\Sigma^T \Sigma V^T)^{-1} = V(\Sigma^T \Sigma)^{-1} V^T. \tag{E.8}$$

Multiplying by A now gives

$$(A^T A)^{-1} A^T = V(\Sigma^T \Sigma)^{-1} V^T V \Sigma^T U^T = V(\Sigma^T \Sigma)^{-1} \Sigma^T U^T. \tag{E.9}$$

And by substituting the definition of the pseudo-inverse this can be written as

$$A^+ = V\Sigma^+ U^T. \tag{E.10}$$

The pseudo-inverse of the matrix Σ can be found by transposing Σ and replacing all non-zero entries of Σ with there reciprocals.

Appendix F

Actuator Disk

Assume that the propeller is a disk that delivers a thrust force in the water. Also assume a laminar flow around the disk, then the streamlines touching the disk can be drawn, see Figure F.1.

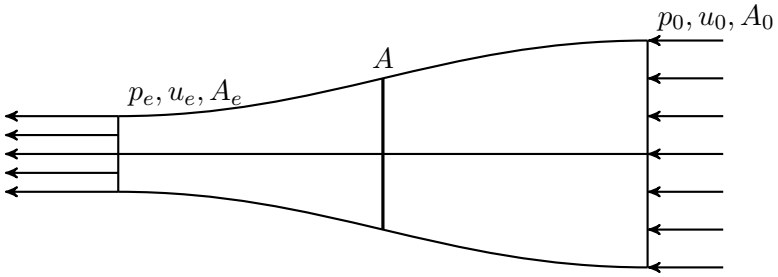

Figure F.1: Schematic drawing of an actuator disk and the streamlines of the flow around it.

Around the actuator disk a control volume V with an infinitesimal width can be drawn which is bounded in height by both streamlines. A control volume like this is drawn in figure F.2. Now conservation of mass can be

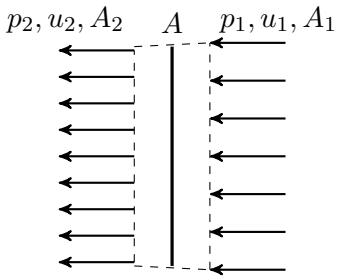

Figure F.2: Drawing of a control volume around the actuator disk.

applied

$$\frac{\partial}{\partial t}\iiint_V \rho \, \mathrm{d}V = -\iint_S .\rho \mathbf{u} \cdot \mathbf{n} \, \mathrm{d}S \tag{F.1}$$

When the assumption that water is incompressible is made this reduces to

$$0 = -\iint_S .\rho \mathbf{u} \cdot \mathbf{n} \, \mathrm{d}S \tag{F.2}$$

Evaluating this equation for the control volume yields

$$\rho u_1 A_1 = \rho u_2 A_2. \tag{F.3}$$

When the width of the control volume goes to zero A_1, A_2 are equal to A, which implies

$$u_1 = u_2. \tag{F.4}$$

Now also conservation of momentum can be applied

$$\frac{\partial}{\partial t}\iiint_V \rho \mathbf{u} \, \mathrm{d}V = -\iint \rho \mathbf{u} \cdot \mathbf{u} \cdot \mathbf{n} \, \mathrm{d}S + \iint_S \underline{\underline{T}} \mathbf{n} \, \mathrm{d}S + \iiint_V \mathbf{f} \, \mathrm{d}V. \tag{F.5}$$

Because the flow is assumed to be steady, the left hand side of the equation becomes 0.

$$0 = -\iint \rho \mathbf{u} \cdot \mathbf{u} \cdot \mathbf{n} \, \mathrm{d}S + \iint_S \underline{\underline{T}} \mathbf{n} \, \mathrm{d}S + \iiint_V \mathbf{f} \, \mathrm{d}V. \tag{F.6}$$

Carrying out the integrals yields

$$0 = -\rho A u_1^2 + \rho A u_2^2 + p_1 A - p_2 A + T. \tag{F.7}$$

Because u_1 and u_2 are equal we find

$$T = (p_2 - p_1)A. \tag{F.8}$$

Between the two streamlines Bernoulli's principle can be applied. For the suction side of the actuator disk this results in

$$\frac{1}{2}\rho u_1^2 + p_1 = \frac{1}{2}\rho u_0^2 + p_0. \tag{F.9}$$

For the pressure side of the actuator disk

$$\frac{1}{2}\rho u_2^2 + p_2 = \frac{1}{2}\rho u_e^2 + p_0 \tag{F.10}$$

is found. To find the difference in pressure over the actuator disk, equation F.9 can be subtracted from equation F.10, which yields

$$p_2 - p_1 = \frac{1}{2}\rho(u_e^2 - u_0^2). \tag{F.11}$$

Substituting this expression in equation F.8 results in the following expression for the thrust.

$$T = \frac{1}{2}\rho(u_e^2 - u_0^2)A \tag{F.12}$$

This expression can be made non-dimensional by dividing by $\rho n_P^2 D^4$.

$$\frac{T}{\rho n_P^2 D^4} = \frac{\rho(u_e^2 - u_0^2)A}{2\rho n_P^2 D^4} \tag{F.13}$$

$$K_T = \frac{(u_e^2 - u_0^2)A}{2n_P^2 D^4}. \tag{F.14}$$

Substituting $A = \frac{\pi}{4}D^2$ yields

$$K_T = \frac{(u_e^2 - u_0^2)\frac{\pi}{4}D^2}{2n_P^2 D^4}. \tag{F.15}$$

$$K_T = \frac{(u_e^2 - u_0^2)\pi}{8n_P^2 D^2}. \tag{F.16}$$

The exit velocity can be expressed as

$$u_e = \eta u_0. \tag{F.17}$$

Substitution in F.16 yields

$$K_T = \frac{(\eta^2 u_0^2 - u_0^2)\pi}{8n_P^2 D^2} \tag{F.18}$$

$$K_T = \frac{\pi(\eta^2 - 1)u_0^2}{8n_P^2 D^2}. \tag{F.19}$$

Substituting the definition of advance ratio results in

$$K_T = \frac{\pi}{8}(\eta^2 - 1)J_P^2. \tag{F.20}$$

Solving for η gives

$$\eta = \sqrt{1 + \frac{8K_T}{\pi J_P^2}}. \tag{F.21}$$

Appendix G

Wageningen B-series coefficients

G.1 Thrust coefficient polynomials

Barnitsas et al. [5] used regression analysis to find polynomials for the K_T-curves of the Wageningen B-series propellers. These polynomials can be found using

$$K_T = \sum_{s,t,u,v} C^T_{s,t,u,v} J^s \left(\frac{P}{D}\right)^t \left(\frac{A_E}{A_0}\right)^u Z^v. \tag{G.1}$$

The coefficients and powers that define these polynomials can be found in table G.1.

Table G.1: Coefficients and exponents of polynomial of K_T for Wageningen B-series propellers. Taken from Barnitsas et al. [5].

$C^T_{s,t,u,v}$	s	t	u	v
0.008 804 96	0	0	0	0
−0.204 554	1	0	0	0
0.166 351	0	1	0	0
0.158 114	0	2	0	0
−0.147 581	2	0	1	0
−0.481 497	1	1	1	0
0.415 437	0	2	1	0
0.014 404 3	0	0	0	1
−0.053 005 4	2	0	0	1
0.014 348 1	0	1	0	1
0.060 682 6	1	1	0	1
−0.012 589 4	0	0	1	1
0.010 968 9	1	0	1	1
−0.133 698	0	3	0	0

Table G.1: (continued)

$C^T_{s,t,u,v}$	s	t	u	v
0.006 384 07	0	6	0	0
−0.001 327 18	2	6	0	0
0.168 496	3	0	1	0
−0.050 721 4	0	0	2	0
0.085 455 9	2	0	2	0
−0.050 447 5	3	0	2	0
0.010 465	1	6	2	0
−0.006 482 72	2	6	2	0
−0.008 417 28	0	3	0	1
0.168 424	1	3	0	1
−0.001 022 96	3	3	0	1
−0.031 779 1	0	3	1	1
0.018 604	1	0	2	1
−0.004 107 98	0	2	2	1
−0.000 606 848	0	0	0	2
−0.004 981 9	1	0	0	2
0.002 598 3	2	0	0	2
−0.000 560 528	3	0	0	2
0.001 636 52	1	2	0	2
−0.000 328 787	1	6	0	2
0.000 116 502	2	6	0	2
0.000 690 904	0	0	1	2
0.004 217 49	0	3	1	2
$5.652\,29 \times 10^{-5}$	3	6	1	2
−0.001 465 64	0	3	2	2

G.2 Torque coefficient polynomials

In a similar manner as for the trust coefficients, Barnitsas et al. [5] defined polynomials for the K_Q-curves of the Wageningen B-series propellers. These polynomials are defined as

$$K_Q = \sum_{s,t,u,v} C^Q_{s,t,u,v} J^s \left(\frac{P}{D}\right)^t \left(\frac{A_E}{A_0}\right)^u Z^v. \tag{G.2}$$

The coefficients and powers that define these polynomials can be found in table G.2.

Table G.2: Coefficients and exponents of polynomial of K_Q for Wageningen B-series propellers. Taken from Barnitsas et al. [5].

$C^Q_{s,t,u,v}$	s	t	u	v
0.003 793 68	0	0	0	0
0.008 865 23	2	0	0	0
−0.032 241	1	1	0	0
0.003 447 78	0	2	0	0
−0.040 881 1	0	1	1	0
−0.108 009	1	1	1	0
−0.088 538 1	2	1	1	0
0.188 561	0	2	1	0
−0.003 708 71	1	0	0	1
0.005 136 96	0	1	0	1
0.020 944 9	1	1	0	1
0.004 743 19	2	1	0	1
−0.007 234 08	2	0	1	1
0.004 383 88	1	1	1	1
−0.026 940 3	0	2	1	1
0.055 808 2	3	0	1	0
0.016 188 6	0	3	1	0
0.003 180 86	1	3	1	0
0.015 896	0	0	2	0
0.047 172 9	1	0	2	0
0.019 628 3	3	0	2	0
−0.050 278 2	0	1	2	0
−0.030 055	3	1	2	0
0.041 712 2	2	2	2	0
−0.039 772 2	0	3	2	0
−0.003 500 24	0	6	2	0
−0.010 685 4	3	0	0	1
0.001 109 03	3	3	0	1
−0.000 313 912	0	6	0	1
0.003 598 5	3	0	1	1
−0.001 421 21	0	6	1	1
−0.003 836 37	1	0	2	1
0.012 680 3	0	2	2	1
−0.003 182 78	2	3	2	1
0.003 342 68	0	6	2	1
−0.001 834 91	1	1	0	2
0.000 112 451	3	2	0	2
$-2.972\,28 \times 10^{-5}$	3	6	0	2
0.000 269 551	1	0	1	2
0.000 832 65	2	0	1	2

Table G.2: (continued)

$C^Q_{s,t,u,v}$	s	t	u	v
0.001 553 34	0	2	1	2
0.000 302 683	0	6	1	2
−0.000 184 3	0	0	2	2
−0.000 425 399	0	3	2	2
$8.692\,43 \times 10^{-5}$	3	3	2	2
−0.000 465 9	0	6	2	2
$5.541\,94 \times 10^{-5}$	1	6	2	2

Appendix H

Solution to Differential equation

For verification purposes the equation of motion in x-direction was considered to be

$$(m - X_{\dot{u}})\dot{u} - X_u u = F_0 + F_A \sin \omega t. \tag{H.1}$$

This is a first order linear differential equation which can be solved analytically. To find the solutions to this equation, first homogeneous differential equation is considered

$$\dot{u} - \frac{X_u}{m - X_{\dot{u}}} u = 0. \tag{H.2}$$

It is known that $u = ce^{rt}$ satisfies this equation.

$$cre^{rt} - ce^{rt} \frac{X_u}{m - X_{\dot{u}}} = 0 \tag{H.3}$$

$$r = \frac{X_u}{m - X_{\dot{u}}}. \tag{H.4}$$

So the homogeneous solution to the differential equation is

$$u_h(t) = c_1 e^{\frac{X_u}{m - X_{\dot{u}}} t}. \tag{H.5}$$

To find the particular solution a solution of the form

$$u = A + B \sin \omega t + C \cos \omega t \tag{H.6}$$

is assumed. Substitution in the equation of motion yields

$$\begin{aligned} &(B\omega \cos \omega t - C\omega \sin \omega t) - \frac{X_u}{m - X_{\dot{u}}}(A + B \sin \omega t + C \cos \omega t) \\ &= \frac{F_0}{m - X_{\dot{u}}} + \frac{F_A}{m - X_{\dot{u}}} \sin \omega t. \end{aligned} \tag{H.7}$$

$$\begin{aligned}&\left(B\omega - \frac{X_u}{m - X_{\dot{u}}}C\right)\cos\omega t + \left(-C\omega - \frac{X_u}{m - X_{\dot{u}}}B\right)\sin\omega t - X_u A \\ &= \frac{F_0}{m - X_{\dot{u}}} + \frac{F_A}{m - X_{\dot{u}}}\sin\omega t.\end{aligned} \tag{H.8}$$

This leads to equations

$$-\frac{X_u}{m - X_{\dot{u}}}A = \frac{F_0}{m - X_{\dot{u}}}, \tag{H.9}$$

$$B\omega - \frac{X_u}{m - X_{\dot{u}}}C = 0, \tag{H.10}$$

$$-C\omega - \frac{X_u}{m - X_{\dot{u}}}B = \frac{F_A}{m - X_{\dot{u}}}. \tag{H.11}$$

These equations can be solved to find

$$A = -\frac{F_0}{X_u} \tag{H.12}$$

$$B = -\frac{F_A X_u}{(m - X_{\dot{u}})^2\omega^2 + X_u^2} \tag{H.13}$$

$$C = -\frac{(m - X_{\dot{u}})\omega F_A}{(m - X_{\dot{u}})^2\omega^2 + X_u^2}. \tag{H.14}$$

Together with the homogeneous solution, the total solution to the differential equation becomes

$$\begin{aligned}u(t) = c_1 e^{\frac{X_u}{m - X_{\dot{u}}}t} &- \frac{F_A X_u}{(m - X_{\dot{u}})^2\omega^2 + X_u^2}\sin\omega t \\ &- \frac{(m - X_{\dot{u}})\omega F_A}{(m - X_{\dot{u}})^2\omega^2 + X_u^2}\cos\omega t - \frac{F_0}{X_u}.\end{aligned} \tag{H.15}$$

The boundary condition is $u(0) = u_0$, which yields

$$c_1 = u_0 + \frac{(m - X_{\dot{u}})\omega F_A}{(m - X_{\dot{u}})^2\omega^2 + X_u^2} + \frac{F_0}{X_u}. \tag{H.16}$$

Differentiation of $u(t)$ gives the expression for the acceleration:

$$\begin{aligned}\dot{u}(t) = c_1 \frac{X_u}{m - X_{\dot{u}}} e^{\frac{X_u}{m - X_{\dot{u}}}t} &- \frac{F_A X_u \omega}{(m - X_{\dot{u}})^2\omega^2 + X_u^2}\cos\omega t \\ &+ \frac{(m - X_{\dot{u}})\omega^2 F_A}{(m - X_{\dot{u}})^2\omega^2 + X_u^2}\sin\omega t.\end{aligned} \tag{H.17}$$

Integration of $u(t)$ gives the expression for location:

$$\begin{aligned}x(t) = c_1 \frac{m - X_{\dot{u}}}{X_u} e^{\frac{X_u}{m - X_{\dot{u}}}t} &+ \frac{F_A X_u}{\omega((m - X_{\dot{u}})^2\omega^2 + X_u^2)}\cos\omega t \\ &- \frac{(m - X_{\dot{u}})F_A}{(m - X_{\dot{u}})^2\omega^2 + X_u^2}\sin\omega t - \frac{F_0}{X_u}t + c_2.\end{aligned} \tag{H.18}$$

The boundary condition is $x(0) = x_0$, which yields

$$c_2 = x_0 - c_1 \frac{m - X_{\dot{u}}}{X_u} - \frac{F_A X_u}{\omega((m - X_{\dot{u}})^2 \omega^2 + X_u^2)}. \tag{H.19}$$

Appendix I

Richardson Extrapolation

I.1 Right end of interval

De basis of the method is the backwards difference method:

$$R_1(h) = \frac{y(x) - y(x-h)}{h} \tag{I.1}$$

$$R_1(2h) = \frac{y(x) - y(x-2h)}{2h} \tag{I.2}$$

Now a Taylor series expansion can be used to approximate $y(x-h)$ and $y(x-2h)$

$$y(x-h) = y(x) - hf'(x_0) + \frac{1}{2}h^2 f''(x_0) - \frac{1}{6}h^3 f'''(x_0) + O(h^4) \tag{I.3}$$

$$y(x-2h) = y(x) - 2hf'(x_0) + 2h^2 f''(x_0) - \frac{8}{6}h^3 f'''(x_0) + O(h^4). \tag{I.4}$$

substitution in I.1 and I.2 yields

$$\begin{aligned} R_1(h) &= \frac{hf'(x_0) - \frac{1}{2}h^2 f''(x_0) + O(h^3)}{h} \\ &= f'(x_0) - \frac{1}{2}hf''(x_0) + O(h^2) \end{aligned} \tag{I.5}$$

$$\begin{aligned} R_1(2h) &= \frac{2hf'(x_0) - 2h^2 f''(x_0) + O(h^3)}{2h} \\ &= f'(x_0) - hf''(x_0) + O(h^2) \end{aligned} \tag{I.6}$$

To cancel the second term a combination of these solutions can be used

$$\begin{aligned} R_2(h) = 2R_1(h) - R_1(2h) &= 2\frac{y(x) - y(x-h)}{h} - \frac{y(x) - y(x-2h)}{2h} \\ &= \frac{3y(x) - 4y(x-h) + y(x-2h)}{2h}. \end{aligned} \tag{I.7}$$

This approximation now can be use to do the same thing

$$R_2(2h) = \frac{3y(x) - 4y(x-2h) + y(x-4h)}{4h}. \tag{I.8}$$

Now also a tailor series expansion for $y(x-4h)$ is needed

$$y(x-4h) = y(x) - 4hf'(x_0) + 8h^2 f''(x_0) - \frac{64}{6}h^3 f'''(x_0) + O(h^4). \tag{I.9}$$

substitution of the Taylor series expansions in I.7 and I.8 yields

$$\begin{aligned} R_2(h) &= \frac{-2hf'(x_0) - \frac{2}{3}h^3 f'''(x_0) + O(h^4)}{2h} \\ &= hf'(x_0) - \frac{1}{3}h^2 f'''(x_0) + O(h^3) \end{aligned} \tag{I.10}$$

$$\begin{aligned} R_2(2h) &= \frac{4hf'(x_0) - \frac{16}{3}h^3 f'''(x_0) + O(h^4)}{4h} \\ &= f'(x_0) - \frac{4}{3}h^2 f'''(x_0) + O(h^3). \end{aligned} \tag{I.11}$$

To cancel the second term a combination of these solutions can be used

$$\begin{aligned} R_3(h) &= \frac{4R_2(h) - R_2(2h)}{3} \\ &= \frac{21y(x) - 32y(x-h) + 12y(x-2h) - y(x-4h)}{12h} \end{aligned} \tag{I.12}$$

Appendix J

Verification single motions

In section 7.4 the prediction method is verificated for sailing straight forward. For other uncoupled 1 DOF motions the verification can be done in exactly the same way. The results for the motions sway and yaw are discussed in this appendix.

J.1 Testing pure sway

The motion will be simulated by applying a known sinusoidal force

$$Y_{known} = Y_0 + Y_A \sin \omega t. \tag{J.1}$$

Together with the inertial forces,they make up the 'known'forces in the prediction method. The input values for these known forces can be found in table J.1. The initial conditions of the simulation are displayed in table J.2. The coefficient sets that are used in testing pure sway motion resemble the

Table J.1: Input values for known lateral forces

Y_0 [N]	Y_A [N]	ω [rad/s]	m [kg]
100000	7000000	0.01	320415000

Table J.2: Initial conditions used in the simulation for testing sway.

u_0 [m/s]	$\dot{u}_0$ [m/s^2]	v_0 [m/s]	$\dot{v}_0$ [m/s^2]	r_0 [rad/s]	$\dot{r}_0$ [rad/s^2]
0	0	5	0	0	0

sets used in straight sailing and are displayed in table J.3
First the coefficients are determined using the prediction method with a differentiation time step of d$t = 1$ s. The coefficients found are displayed in table J.4

Table J.3: Coefficients that are used for testing pure sway motion.

Set	$Y_{\dot{v}}$ [kg]	Y_v [kg/s]	Y_{vv} [kg/m]	Y_{vvv} [kg s/m^2]
1	-100000	-20000	-	-
2	-100000	-20000	-8000	-
3	-100000	-20000	-8000	-500

Table J.4: Predicted coefficients for differentiation time step d$t = 1$.

Set	$Y_{\dot{v}}$ [kg]	Y_v [kg/s]	Y_{vv} [kg/m]	Y_{vvv} [kg s/m^2]
1	−99 980.53	−19 999.95	-	-
2	−99 980.75	−19 999.82	−8 000.02	-
3	−99 980.64	−20 000.18	−7 999.88	−500.01

In table J.5 the relative errors of the found coefficients are displayed. It can be seen that the found coefficients approximate the original coefficients very well. It should be noticed that the error for the inertial coefficient $Y_{\dot{v}}$ are of higher order than the other coefficients. This is due to smaller size of $\dot{v}$ compared to v. Because $\dot{v}$ is smaller, the round-off error is a larger part of the total error. To show what the influence of the differentiation time step is, the same tests are done for a differentiation time step d$t = 10$ s. The results of the prediction are displayed in table J.6. It can be seen that these coefficients are less accurate than with a differentiation time step of 1 second. This is due to the truncation error in the differentiation method. This can also be conclude from the size of the errors, which are displayed in table J.7.

J.2 Testing pure yaw

The last 1 DOF motion that needs testing is yaw. The input for the known moments can be found in J.8. The initial conditions of the simulation are displayed in table J.9. The coefficients that are used in the simulation of pure yaw are displayed in J.10. For these test larger coefficients and are used because the mass moment of inertia I_{zG} is much larger than the mass and because the values for r are in reality much smaller than the values of

Table J.5: Relative error of predicted coefficients for differentiation time step d$t = 1$.

Set	$\epsilon_{Y_{\dot{v}}}$ [%]	ϵ_{Y_v} [%]	$\epsilon_{Y_{vv}}$ [%]	$\epsilon_{Y_{vvv}}$ [%]
1	−0.019 5	−0.000 2	-	-
2	−0.019 2	−0.000 9	0.000 2	-
3	−0.019 4	0.000 9	−0.001 5	0.002 6

Table J.6: Predicted coefficients for differentiation time step d$t = 10$.

Set	$Y_{\dot{v}}$ [kg]	Y_v [kg/s]	Y_{vv} [kg/m]	Y_{vvv} [kg s/m^2]
1	−76 960.77	−19 939.23	-	-
2	−77 032.18	−19 739.30	−8 029.42	-
3	−76 775.90	−20 195.63	−7 851.42	−515.86

Table J.7: Relative error of predicted coefficients for differentiation time step d$t = 10$.

Set	$\epsilon_{Y_{\dot{v}}}$ [%]	ϵ_{Y_v} [%]	$\epsilon_{Y_{vv}}$ [%]	$\epsilon_{Y_{vvv}}$ [%]
1	−0.019 5	−0.000 2	-	-
2	−0.019 2	−0.000 9	0.000 2	-
3	−0.019 4	0.000 9	−0.001 5	0.002 6

Table J.8: Input values for known moments

N_0 [N]	N_A [N]	ω [rad/s]	I_{zG} [kg m^2]
100000000	700000	0.01	2.0507E+12

Table J.9: Initial conditions used in the simulation for testing yaw

u_0 [m/s]	$\dot{u}_0$ [m/s^2]	v_0 [m/s]	$\dot{v}_0$ [m/s^2]	r_0 [rad/s]	$\dot{r}_0$ [rad/s^2]
0	0	0	0	0.01	0

u and v.

Table J.10: Coefficients that are used for testing pure yaw motion.

Set	$N_{\dot{r}}$ [kg m^2]	N_r [kg m^2/s]	N_{rr} [kg m^2]	N_{rrr} [kg m^2 s]
1	$-1.00 \cdot 10^{+12}$	$-10\,000\,000.00$	-	-
2	$-1.00 \cdot 10^{+12}$	$-10\,000\,000.00$	$-8\,000\,000.00$	-
3	$-1.00 \cdot 10^{+12}$	$-10\,000\,000.00$	$-8\,000\,000.00$	$-7\,000\,000.00$

Table J.11: Predicted coefficients for yaw motion with differentiation time step d$t = 1$.

Set	$N_{\dot{r}}$ [kg m^2]	N_r [kg m^2/s]	N_{rr} [kg m^2]	N_{rrr} [kg m^2 s]
1	$-1\,0.00 \cdot 10^{+11}$	$-9\,999\,992.70$	-	-
2	$-1\,0.00 \cdot 10^{+11}$	$-10\,000\,000.32$	$-8\,000\,137.09$	-
3	$-1\,0.00 \cdot 10^{+11}$	$-10\,001\,157.87$	$-7\,980\,274.76$	$-7\,096\,090.51$

Table J.12: Relative error of predicted coefficients for differentiation time step d$t = 1$.

Set	$\epsilon_{N_{\dot{r}}}$ [%]	ϵ_{N_r} [%]	$\epsilon_{N_{rr}}$ [%]	$\epsilon_{N_{rrr}}$ [%]
1	$-3.589\,7 \cdot 10^{-06}$	$-7.297\,7 \cdot 10^{-05}$	-	-
2	$-2.703\,4 \cdot 10^{-06}$	$3.248\,2 \cdot 10^{-06}$	0.001 7	-
3	$-5.534\,1 \cdot 10^{-05}$	0.011 6	$-0.246\,6$	1.372 7

Table J.13: Predicted coefficients for yaw motion with differentiation time step $\mathrm{d}t = 10$.

1	$-1.00 \cdot 10^{+12}$	$-9\,998\,775.05$	-	-
2	$-1\,0.00 \cdot 10^{+11}$	$-10\,009\,683.27$	$-7\,927\,103.95$	-
3	$-1.00 \cdot 10^{+12}$	$-9\,985\,986.00$	$-8\,299\,292.12$	$-5\,348\,112.72$

Table J.14: Relative error of predicted coefficients for differentiation time step $\mathrm{d}t = 10$.

Set	$\epsilon_{N_{\dot{r}}}$ [%]	ϵ_{N_r} [%]	$\epsilon_{N_{rr}}$ [%]	$\epsilon_{N_{rrr}}$ [%]
1	0.000 2	$-0.012\,2$	-	-
2	$-0.000\,8$	0.096 8	$-0.911\,2$	-
3	0.000 4	$-0.140\,1$	3.741 2	$-23.598\,4$

Appendix K

Non-dimensionalize coefficients

In this report, non-dimensional coefficients are denoted by putting a prime $'$ above a symbol. Forces are non-dimensionalized by $\frac{1}{2}\rho L_{pp} d U^2$, moments are non-dimensionalized by $\frac{1}{2}\rho L_{pp}^2 d U^2$, velocities are non-dimensionalized by characteristic velocity U, accelerations are non-dimensionalized by $\frac{U^2}{L}$ and angular velocity is non-dimensionalized by $\frac{U}{L}$. Using these definitions, the non-dimensional hydrodynamic coefficients in the following sections are derived. The values used for non-dimensionalization can be found in table K.1.

Table K.1: Values used for non-dimensionalization.

U	7.97382	m/s
L_{pp}	320	m
d	20.8	m
ρ	1025	kg/m^3

K.1 Non-dimensional X coeffcients

$$X'_{\dot{u}} = \frac{X_{\dot{u}}}{\frac{1}{2}\rho L_{pp}^2 d} \qquad X_{\dot{u}} \sim [\text{kg}] \tag{K.1}$$

$$X'_{uu} = \frac{X_{uu}}{\frac{1}{2}\rho L_{pp} d} \qquad X_{uu} \sim \left[\frac{\text{kg}}{\text{m}}\right] \tag{K.2}$$

$$X'_{uuu} = \frac{X_{uuu} U}{\frac{1}{2}\rho L_{pp} d} \qquad X_{uuu} \sim \left[\frac{\text{kg s}}{\text{m}^2}\right] \tag{K.3}$$

$$X'_{vv} = \frac{X_{vv}}{\frac{1}{2}\rho L_{pp} d} \qquad X_{vv} \sim \left[\frac{\text{kg}}{\text{m}}\right] \tag{K.4}$$

$$X'_{rr} = \frac{X_{rr}}{\frac{1}{2}\rho L_{pp}^3 d} \qquad X_{rr} \sim [\text{kg m}] \tag{K.5}$$

$$X'_{vr} = \frac{X_{vr}}{\frac{1}{2}\rho L_{pp}^2 d} \qquad X_{vr} \sim [\text{kg}] \tag{K.6}$$

$$X'_{uvv} = \frac{X_{uvv}U}{\frac{1}{2}\rho L_{pp} d} \qquad X_{uvv} \sim \left[\frac{\text{kg s}}{\text{m}^2}\right] \tag{K.7}$$

$$X'_{rvu} = \frac{X_{rvu}U}{\frac{1}{2}\rho L_{pp}^2 d} \qquad X_{rvu} \sim \left[\frac{\text{kg s}}{\text{m}}\right] \tag{K.8}$$

$$X'_{urr} = \frac{X_{urr}U}{\frac{1}{2}\rho L_{pp}^3 d} \qquad X_{urr} \sim [\text{kg s}] \tag{K.9}$$

K.2 Non-dimensional Y coeffcients

$$Y'_{\dot{v}} = \frac{Y_{\dot{v}}}{\frac{1}{2}\rho L_{pp}^2 d} \qquad Y_{\dot{v}} \sim [\text{kg}] \tag{K.10}$$

$$Y'_{uv} = \frac{Y_{uv}}{\frac{1}{2}\rho L_{pp} d} \qquad Y_{uv} \sim \left[\frac{\text{kg}}{\text{m}}\right] \tag{K.11}$$

$$Y'_{ur} = \frac{Y_{ur}}{\frac{1}{2}\rho L_{pp}^2 d} \qquad Y_{ur} \sim [\text{kg}] \tag{K.12}$$

$$Y'_{uur} = \frac{Y_{uur}U}{\frac{1}{2}\rho L_{pp}^2 d} \qquad Y_{uur} \sim \left[\frac{\text{kg s}}{\text{m}}\right] \tag{K.13}$$

$$Y'_{uuv} = \frac{Y_{uuv}U}{\frac{1}{2}\rho L_{pp} d} \qquad Y_{uuv} \sim \left[\frac{\text{kg s}}{\text{m}^2}\right] \tag{K.14}$$

$$Y'_{vvv} = \frac{Y_{vvv}U}{\frac{1}{2}\rho L_{pp} d} \qquad Y_{vvv} \sim \left[\frac{\text{kg s}}{\text{m}^2}\right] \tag{K.15}$$

$$Y'_{rrr} = \frac{Y_{rrr}U}{\frac{1}{2}\rho L_{pp}^4 d} \qquad Y_{rrr} \sim [\text{kg m s}] \tag{K.16}$$

$$Y'_{rrv} = \frac{Y_{rrv}U}{\frac{1}{2}\rho L_{pp}^3 d} \qquad Y_{rrv} \sim [\text{kg s}] \tag{K.17}$$

$$Y'_{vvr} = \frac{Y_{vvr}U}{\frac{1}{2}\rho L_{pp}^2 d} \qquad Y_{vvr} \sim \left[\frac{\text{kg s}}{\text{m}}\right] \tag{K.18}$$

$$Y'_{|v|v} = \frac{Y_{|v|v}}{\frac{1}{2}\rho L_{pp} d} \qquad Y_{|v|v} \sim \left[\frac{\text{kg}}{\text{m}}\right] \tag{K.19}$$

$$Y'_{|r|v} = \frac{Y_{|r|v}}{\frac{1}{2}\rho L_{pp}^2 d} \qquad Y_{|r|v} \sim [\text{kg}] \tag{K.20}$$

$$Y'_{|v|r} = \frac{Y_{|v|r}}{\frac{1}{2}\rho L_{pp}^2 d} \qquad Y_{|v|r} \sim [\text{kg}] \tag{K.21}$$

$$Y'_{|r|r} = \frac{Y_{|r|r}}{\frac{1}{2}\rho L_{pp}^3 d} \qquad Y_{|r|r} \sim [\text{kg m}] \tag{K.22}$$

K.3 Non-dimensional N coeffcients

$$N'_{\dot{r}} = \frac{N_{\dot{r}}}{\frac{1}{2}\rho L_{pp}^4 d} \qquad N_{\dot{r}} \sim [\text{kg m}^2] \tag{K.23}$$

$$N'_{uv} = \frac{N_{uv}}{\frac{1}{2}\rho L_{pp}^2 d} \qquad N_{uv} \sim [\text{kg}] \tag{K.24}$$

$$N'_{ur} = \frac{N_{ur}}{\frac{1}{2}\rho L_{pp}^3 d} \qquad N_{ur} \sim [\text{kg m}] \tag{K.25}$$

$$N'_{uur} = \frac{N_{uur}U}{\frac{1}{2}\rho L_{pp}^3 d} \qquad N_{uur} \sim [\text{kg s}] \tag{K.26}$$

$$N'_{uuv} = \frac{N_{uuv}U}{\frac{1}{2}\rho L_{pp}^2 d} \qquad N_{uuv} \sim \left[\frac{\text{kg s}}{\text{m}}\right] \tag{K.27}$$

$$N'_{vvv} = \frac{N_{vvv}U}{\frac{1}{2}\rho L_{pp}^2 d} \qquad N_{vvv} \sim \left[\frac{\text{kg s}}{\text{m}}\right] \tag{K.28}$$

$$N'_{rrr} = \frac{N_{rrr}U}{\frac{1}{2}\rho L_{pp}^5 d} \qquad N_{rrr} \sim \left[\text{kg m}^2 \text{ s}\right] \tag{K.29}$$

$$N'_{rrv} = \frac{N_{rrv}U}{\frac{1}{2}\rho L_{pp}^4 d} \qquad N_{rrv} \sim [\text{kg m s}] \tag{K.30}$$

$$N'_{vvr} = \frac{N_{vvr}U}{\frac{1}{2}\rho L_{pp}^3 d} \qquad N_{vvr} \sim [\text{kg s}] \tag{K.31}$$

$$N'_{|v|v} = \frac{N_{|v|v}}{\frac{1}{2}\rho L_{pp}^2 d} \qquad N_{|v|v} \sim [\text{kg}] \tag{K.32}$$

$$N'_{|r|v} = \frac{N_{|r|v}}{\frac{1}{2}\rho L_{pp}^3 d} \qquad N_{|r|v} \sim [\text{kg}] \tag{K.33}$$

$$N'_{|v|r} = \frac{N_{|v|r}}{\frac{1}{2}\rho L_{pp}^3 d} \qquad N_{|v|r} \sim [\text{kg}] \tag{K.34}$$

$$N'_{|r|r} = \frac{N_{|r|r}}{\frac{1}{2}\rho L_{pp}^4 d} \qquad N_{|r|r} \sim [\text{kg m}^2] \tag{K.35}$$

Appendix L

Dimension-full coefficients

Table L.1: Table of al the coefficients based on low aspect ratio lift theory found in straight sailing.

$X_{\dot{u}}$	$-2.401\,6 \cdot 10^{+07}$	$Y_{\dot{v}}$	$0.000\,0$	$N_{\dot{r}}$	$0.000\,0$
X_{uu}	$-7.504\,6 \cdot 10^{+04}$	Y_{uv}	$0.000\,0$	N_{uv}	$0.000\,0$
X_{uuu}	$-6.840\,0 \cdot 10^{-02}$	Y_{ur}	$0.000\,0$	N_{ur}	$0.000\,0$
X_{vv}	$0.000\,0$	Y_{uur}	$0.000\,0$	N_{uur}	$0.000\,0$
X_{rr}	$0.000\,0$	Y_{uuv}	$0.000\,0$	N_{uuv}	$0.000\,0$
X_{vr}	$0.000\,0$	Y_{vvv}	$0.000\,0$	N_{vvv}	$0.000\,0$
X_{uvv}	$0.000\,0$	Y_{rrr}	$0.000\,0$	N_{rrr}	$0.000\,0$
X_{rvu}	$0.000\,0$	Y_{rrv}	$0.000\,0$	N_{rrv}	$0.000\,0$
X_{urr}	$0.000\,0$	Y_{vvr}	$0.000\,0$	N_{vvr}	$0.000\,0$
		$Y_{\|v\|v}$	$0.000\,0$	$N_{\|v\|v}$	$0.000\,0$
		$Y_{\|r\|v}$	$0.000\,0$	$N_{\|r\|v}$	$0.000\,0$
		$Y_{\|v\|r}$	$0.000\,0$	$N_{\|v\|r}$	$0.000\,0$
		$Y_{\|r\|r}$	$0.000\,0$	$N_{\|r\|r}$	$0.000\,0$

Table L.2: Table of al the coefficients based on low aspect ratio lift theory found with 10/10 zig-zag manoeuvre.

$X_{\dot{u}}$	$-2.217\,4 \cdot 10^{+07}$	$Y_{\dot{v}}$	$-2.776\,2 \cdot 10^{+08}$	$N_{\dot{r}}$	$-1.432\,1 \cdot 10^{+12}$
X_{uu}	$-7.627\,7 \cdot 10^{+04}$	Y_{uv}	$-1.656\,8 \cdot 10^{+06}$	N_{uv}	$-1.025\,3 \cdot 10^{+08}$
X_{uuu}	$1.228\,4 \cdot 10^{+02}$	Y_{ur}	$8.952\,9 \cdot 10^{+06}$	N_{ur}	$-1.018\,5 \cdot 10^{+10}$
X_{vv}	$-1.723\,2 \cdot 10^{+06}$	Y_{uur}	$3.767\,8 \cdot 10^{+06}$	N_{uur}	$-4.345\,2 \cdot 10^{+08}$
X_{rr}	$-1.923\,8 \cdot 10^{+10}$	Y_{uuv}	$3.336\,0 \cdot 10^{+04}$	N_{uuv}	$-3.355\,1 \cdot 10^{+06}$
X_{vr}	$-3.913\,6 \cdot 10^{+08}$	Y_{vvv}	$7.882\,0 \cdot 10^{+06}$	N_{vvv}	$-1.042\,9 \cdot 10^{+09}$
X_{uvv}	$1.087\,0 \cdot 10^{+05}$	Y_{rrr}	$2.908\,9 \cdot 10^{+13}$	N_{rrr}	$-3.623\,3 \cdot 10^{+15}$
X_{rvu}	$2.452\,0 \cdot 10^{+07}$	Y_{rrv}	$5.726\,8 \cdot 10^{+11}$	N_{rrv}	$-7.114\,6 \cdot 10^{+13}$
X_{urr}	$1.170\,8 \cdot 10^{+09}$	Y_{vvr}	$3.880\,1 \cdot 10^{+09}$	N_{vvr}	$-4.790\,6 \cdot 10^{+11}$
		$Y_{\|v\|v}$	$-8.519\,4 \cdot 10^{+05}$	$N_{\|v\|v}$	$8.718\,5 \cdot 10^{+07}$
		$Y_{\|r\|v}$	$7.844\,6 \cdot 10^{+07}$	$N_{\|r\|v}$	$-7.251\,1 \cdot 10^{+09}$
		$Y_{\|v\|r}$	$-6.138\,7 \cdot 10^{+07}$	$N_{\|v\|r}$	$5.858\,1 \cdot 10^{+09}$
		$Y_{\|r\|r}$	$1.917\,5 \cdot 10^{+10}$	$N_{\|r\|r}$	$-1.826\,5 \cdot 10^{+12}$

Table L.3: Table of al the coefficients based on low aspect ratio lift theory found with 20/20 zig-zag manoeuvre.

$X_{\dot{u}}$	$-1.870\,2 \cdot 10^{+07}$	$Y_{\dot{v}}$	$-2.895\,7 \cdot 10^{+08}$	$N_{\dot{r}}$	$-1.485\,6 \cdot 10^{+12}$
X_{uu}	$-7.684\,0 \cdot 10^{+04}$	Y_{uv}	$-2.563\,7 \cdot 10^{+06}$	N_{uv}	$-4.334\,6 \cdot 10^{+07}$
X_{uuu}	$1.405\,3 \cdot 10^{+02}$	Y_{ur}	$-7.236\,4 \cdot 10^{+07}$	N_{ur}	$-5.131\,4 \cdot 10^{+09}$
X_{vv}	$-7.029\,5 \cdot 10^{+06}$	Y_{uur}	$1.120\,4 \cdot 10^{+07}$	N_{uur}	$-9.581\,1 \cdot 10^{+08}$
X_{rr}	$-1.189\,2 \cdot 10^{+11}$	Y_{uuv}	$1.237\,6 \cdot 10^{+05}$	N_{uuv}	$-9.590\,1 \cdot 10^{+06}$
X_{vr}	$-1.877\,3 \cdot 10^{+09}$	Y_{vvv}	$3.234\,4 \cdot 10^{+06}$	N_{vvv}	$-4.557\,5 \cdot 10^{+08}$
X_{uvv}	$7.458\,4 \cdot 10^{+05}$	Y_{rrr}	$1.257\,7 \cdot 10^{+13}$	N_{rrr}	$-1.485\,5 \cdot 10^{+15}$
X_{rvu}	$2.000\,6 \cdot 10^{+08}$	Y_{rrv}	$2.396\,4 \cdot 10^{+11}$	N_{rrv}	$-2.788\,1 \cdot 10^{+13}$
X_{urr}	$1.293\,6 \cdot 10^{+10}$	Y_{vvr}	$1.758\,1 \cdot 10^{+09}$	N_{vvr}	$-2.025\,5 \cdot 10^{+11}$
		$Y_{\|v\|v}$	$-2.446\,8 \cdot 10^{+05}$	$N_{\|v\|v}$	$4.572\,9 \cdot 10^{+07}$
		$Y_{\|r\|v}$	$-7.929\,3 \cdot 10^{+06}$	$N_{\|r\|v}$	$5.058\,6 \cdot 10^{+09}$
		$Y_{\|v\|r}$	$4.172\,2 \cdot 10^{+06}$	$N_{\|v\|r}$	$3.680\,4 \cdot 10^{+09}$
		$Y_{\|r\|r}$	$4.068\,3 \cdot 10^{+09}$	$N_{\|r\|r}$	$9.237\,4 \cdot 10^{+10}$

Table L.4: Table of al the coefficients based on low aspect ratio lift theory found with turning circle manoeuvre.

$X_{\dot{u}}$	-1.4612E+07	$Y_{\dot{v}}$	-3.8379E+08	$N_{\dot{r}}$	-2.0162E+12
X_{uu}	-2.0936E+05	Y_{uv}	3.0439E+06	N_{uv}	-2.8260E+08
X_{uuu}	1.6392E+04	Y_{ur}	2.9488E+09	N_{ur}	-2.8573E+11
X_{vv}	-5.5480E+06	Y_{uur}	-5.0197E+08	N_{uur}	4.8034E+10
X_{rr}	-1.2994E+11	Y_{uuv}	-2.7444E+06	N_{uuv}	2.4750E+08
X_{vr}	-1.9385E+09	Y_{vvv}	2.3503E+07	N_{vvv}	-1.9338E+09
X_{uvv}	5.6639E+05	Y_{rrr}	2.2680E+13	N_{rrr}	-2.2065E+15
X_{rvu}	2.0131E+08	Y_{rrv}	2.3569E+11	N_{rrv}	-1.3638E+13
X_{urr}	1.3670E+10	Y_{vvr}	4.5026E+09	N_{vvr}	-3.5160E+11
		$Y_{\|v\|v}$	-9.8272E+07	$N_{\|v\|v}$	9.0904E+09
		$Y_{\|r\|v}$	1.3781E+10	$N_{\|r\|v}$	-1.4003E+12
		$Y_{\|v\|r}$	-1.3781E+10	$N_{\|v\|r}$	1.4003E+12
		$Y_{\|r\|r}$	1.1541E+12	$N_{\|r\|r}$	-1.1973E+14

Table L.5: Table of al the dimensionless coefficients based on low aspect ratio lift theory found from combined 20/20 zig-zag and turning circle manoeuvres.

$X_{\dot{u}}$	-2.7525E+07	$Y_{\dot{v}}$	-3.2044E+08	$N_{\dot{r}}$	-1.5933E+12
X_{uu}	-5.7918E+04	Y_{uv}	-5.5188E+06	N_{uv}	1.6912E+08
X_{uuu}	-1.8534E+03	Y_{ur}	-3.9820E+08	N_{ur}	1.7933E+10
X_{vv}	-1.0773E+07	Y_{uur}	4.3492E+07	N_{uur}	-3.4254E+09
X_{rr}	-1.9252E+11	Y_{uuv}	4.5832E+05	N_{uuv}	-3.4862E+07
X_{vr}	-2.9194E+09	Y_{vvv}	3.4281E+06	N_{vvv}	-4.4663E+08
X_{uvv}	1.1710E+06	Y_{rrr}	6.6249E+11	N_{rrr}	-4.9357E+14
X_{rvu}	3.2026E+08	Y_{rrv}	6.7571E+10	N_{rrv}	-1.2857E+13
X_{urr}	2.1448E+10	Y_{vvr}	9.7416E+08	N_{vvr}	-1.3003E+11
		$Y_{v\|v\|}$	-4.5915E+06	$N_{v\|v\|}$	3.7315E+08
		$Y_{r\|v\|}$	-1.7279E+07	$N_{r\|v\|}$	8.8348E+09
		$Y_{v\|r\|}$	-4.6686E+08	$N_{v\|r\|}$	4.0074E+10
		$Y_{r\|r\|}$	6.2813E+10	$N_{r\|r\|}$	-3.9133E+12

Table L.6: Table of al the dimensionless coefficients based on low aspect ratio lift theory found from combined straight acceleration, 10/10 zig-zag, 20/20 zig-zag and turning circle manoeuvres.

$X_{\dot{u}}$	-2.6176E+07	$Y_{\dot{v}}$	-3.0211E+08	$N_{\dot{r}}$	-1.6534E+12
X_{uu}	-7.2916E+04	Y_{uv}	-1.6927E+06	N_{uv}	-5.8827E+07
X_{uuu}	-1.8179E+02	Y_{ur}	1.6781E+08	N_{ur}	-1.6987E+10
X_{vv}	-5.9069E+05	Y_{uur}	-1.1768E+07	N_{uur}	1.7418E+08
X_{rr}	-1.9800E+10	Y_{uuv}	5.3396E+04	N_{uuv}	-9.0786E+06
X_{vr}	-2.8803E+08	Y_{vvv}	1.1343E+07	N_{vvv}	-1.2733E+09
X_{uvv}	2.3190E+04	Y_{rrr}	-1.3592E+12	N_{rrr}	-1.1057E+15
X_{rvu}	2.3171E+07	Y_{rrv}	1.0189E+11	N_{rrv}	-3.1112E+13
X_{urr}	1.9238E+09	Y_{vvr}	2.3559E+09	N_{vvr}	-3.3945E+11
		$Y_{v\|v\|}$	-9.4757E+06	$N_{v\|v\|}$	7.1738E+08
		$Y_{r\|v\|}$	-6.9233E+08	$N_{r\|v\|}$	6.3018E+10
		$Y_{v\|r\|}$	-1.3642E+09	$N_{v\|r\|}$	1.0399E+11
		$Y_{r\|r\|}$	-8.4668E+09	$N_{r\|r\|}$	1.8599E+12